

Smoke Flow through Exterior Assembly Construction Gaps

A Major Qualifying Project Report
Submitted to the Faculty
of the
WORCESTER POLYTECHNIC INSTITUTE
in partial fulfillment of the requirements for the
Degree of Bachelor of Science
By:

Jared Harbold

Brendan Kerrigan

Camille Levy

Sarah Meehan

April 2014

Project: NAD FO13

Professor Nicholas A. Dembsey, Advisor

Professor Umberto Berardi, Co-Advisor

Abstract

Rainscreen cladding systems are becoming popular in building façades due to their ability to protect the building from extreme weather conditions. These systems are generally composed of several pieces assembled leaving horizontal and vertical gaps, allowing for thermal dilatation. In these kinds of façades, air may flow through the gaps into the space behind the façade, allowing for thermal, ventilation, and moisture control advantages. However, scarce knowledge is available about the fire behavior of these façade systems, and the effect of these gaps. The project aimed to characterize the fraction of the fire plume which may flow through gaps under external fire attack. Through temperature, velocity, and heat flux measurements in an *ad-hoc* designed gap assembly, the characterization of the plume fraction flowing through the gap is provided. How this gap flow effects design rules for preventing the possibility of exterior fire propagation behind rainscreen cladding will be explored.

Acknowledgements

We would like to thank the following individuals/companies, without whom, we would not have been able to execute this project:

Professor Dembsey – for providing us with the resources necessary for this project and advising us on all topics encountered along the way

Professor Berardi – for providing us with a Civil Engineering perspective and co-advising us

Randy Harris – for his help in the WPI Fire Lab, helpful advice, and coordinating the various MQP groups within the WPI Fire Lab

Keysler and Associates – for supplying the idea for this project based on real world applications

Authorship

Abstract - All

Introduction – Harbold & Meehan

Background – Meehan (façades), Levy (IBC), & Harbold (NFPA 285)

Experimental Set-Up – Harbold (Geometry) & Levy (Instrumentation)

Results and Characterization – Levy (Velocity), Kerrigan (Plume Characterization), Meehan (COE)

Conclusion – Harbold

Future Research - Levy

Table of Contents

Abstract.....	ii
Acknowledgements.....	ii
Authorship	ii
1.0 Introduction	1
2.0 Background	1
2.1 Exterior Façades.....	1
2.2 International Building Code	3
2.3 NFPA 285.....	4
3.0 Experimental Set-Up	5
3.1 Assembly Geometry.....	6
4.0 Results and Characterization	8
4.1 Velocity Results.....	8
4.2 Temperature Distribution across the Front Face.....	9
4.3 Fire Plume Characterization.....	10
4.4 Temperature and Velocity Profiles in the Gap.....	12
4.5 Enthalpy Flow and Energy Conservation in the Gap.....	14
4.6 Characterization of Flow from the Gap Exiting into the Chimney	16
5.0 Conclusions	18
6.0 Future Research	19
References	20
Appendix A: Exterior Facades and Functions.....	A-1
Appendix B: The Green Building Movement and International Building Code	B-1
Appendix C: IBC Requirements for External Facades	C-1
Appendix D: NFPA 285 Details	D-1
Appendix E: Assembly Details	E-1
Appendix F: Instrumentation	F-1
Appendix G: Raw Data (Bidirectional Probe/Thin Skin Calorimeter).....	G-1
Appendix H: Time Averaging of Front Face Temperature Results.....	H-1
Appendix I: Yuan & Cox Theory Applied to Front Face	I-1
Appendix J: Velocity Profile Formulation.....	J-1
Appendix K: Yuan & Cox Theory Applied to Thermal Plume up the Back Face	K-1
Appendix L: TEMPERATURE DISTRIBUTIONS – 75KW (X)	L-1
Appendix M: Enthalpy Calculations	M-1
Appendix N: Verification of Bidirectional Probe.....	N-1
Appendix O: Calculation Procedure to obtain Velocities.....	O-1

List of Figures

Figure 1 - Examples of Rainscreens on Completed Structures [4]	2
Figure 2 - Rainscreen Cladding System Schematic (Not to Scale).....	3
Figure 3 - NFPA 285 Test Diagram	5
Figure 4 - Assembly Cross View (Not to Scale).....	6
Figure 5 - Front Face below the Gap Instrumentation Overview	7
Figure 6 - Thermocouples of Varying Height	7
Figure 7 - Velocity Measurements at Various Locations	8
Figure 8 - Temperature Distribution across the Front Face of the Assembly during the 75 kW Tests.....	9
Figure 9 - Compilation of Front Face 75 kW Test Results Compared to the Yuan & Cox Theory	11
Figure 10 - Comparison of all Heat Release Rate Temperature vs $z/QI^{(2/3)}$ Ratio	12
Figure 11 – Width Temperature Profiles in the Gap.....	13
Figure 12 - Height Temperature Profiles in the Gap.....	13
Figure 13 - Depth Temperature Profiles in the Gap.....	13
Figure 14 – Y-Distribution Velocity Profiles in the Gap.....	14
Figure 15: Thin Skinned Calorimeter Set-Up.....	15
Figure 16 - 75 kW Back Face Temperature Map Theoretical Fit.....	17
Figure 17 - Comparison of Back Face Heat Release Rate Temperatures vs. $z/QI^{(2/3)}$	18

List of Tables

Table 1 - Average velocities at each probe location, 75kW test.....	9
Table 2 - Variables Related to Flow in the Return Flange.....	14
Table 3 - Variables Related to Enthalpy in the Return Flange/	15
Table 4 - Enthalpy in the Gap.....	16

1.0 Introduction

A rainscreen cladding system is a type of non-load bearing building envelope which is recently becoming more popular due to its ability to wick moisture away from a building's exterior [1]. The design for a rainscreen cladding system utilizes panels which are assembled off of the face of the exterior of the building to provide for an air channel in between the panels and the exterior of the building. Additionally, between individual panels, there is a gap in order to allow for building movement without having a physical failure of the rainscreen cladding system. This gap between panels joins with the air channel behind all of the panels. The effect that these gaps in between individual panels have on fire propagation during an exterior fire is unknown.

The goal of this project is to be able to characterize the flow through a horizontal gap during a fire. If proper characterization is developed, rainscreen manufacturers, including our sponsor, will be able to make insightful decisions regarding whether or not sealing the gaps between panels is essential. If it is shown that during fire scenarios that a minimal amount of enthalpy flow enters the gap, the prospect of not sealing gaps between panels will be recognized. This confirmation would allow for saved material and labor costs associated with sealing the gaps around every panel in a rainscreen cladding system.

2.0 Background

In order to understand why gaps between panels in rainscreen cladding systems are potentially important in relation to fire propagation, complete understanding of various design and code requirements must be explained. In this chapter, insight will be given towards exterior façades, specifically rainscreens, the International Building Code (IBC)[2], and the NFPA 285 test.[3]

2.1 Exterior Façades

An exterior façade is a building envelope that is generally used as a complementary system to a building. Rather than having a structural component, an exterior façade should be non-load bearing. Every façade is different in regards to the materials used and their properties and function. As the final layer to a building, façades acts as a protective barrier and are often used for aesthetic reasons as seen in Figure 1. More specifically, façades can have additive features such as acting as a solar panel to harness energy, increasing ventilation, reducing external noise, etc. The durability of a façade should be less than the building structure itself but greater than the internal building system.

Façades are beneficial but can lead to additional problems which are not encountered with a traditional building system. Some problems which are unique to façades are issues with building expansion/contraction and establishing proper air barriers. In order to allow for building expansion and contractions façade systems generally utilize panelized designs or specific panel elements meant for expansion and contraction are used with either gaps or special expansion joints. To make sure there is a proper air barrier good construction practices must be carried out to ensure continuity [1].



Figure 1 - Examples of Rainscreens on Completed Structures [4]

Façades can be manufactured out of acrylic, glass, metal, and/or composite materials. Major types of façade configurations include Exterior Insulation Finishing System (EIFS), Double-Skinned Façade (DSF), and Rainscreens. EIFS are composed of layers of different materials including woven glass fiber and expanded polystyrene which are generally used as a barrier wall system or a wall drainage system. DSFs are composed of glazing units and solar control devices. This unique system allows for daylight to enter a building without compromising thermal performance during all seasons. Rainscreens can be made of many different materials and are generally designed in panel form. This façade's main function is to protect building exteriors from rainwater [1].

Rainscreen cladding systems allow for ventilation behind the individual rainscreen panels in order to keep moisture away from a building's exterior. In Figure 2, a basic rainscreen cladding system is shown with two panels and an exterior wall separated by ventilation gaps. The arrows in the ventilation gaps represent the air flow through the system. In normal scenarios, the ventilation gaps between the individual panels provide for additional ventilation of the exterior wall: a benefit of the rainscreen cladding system (see Appendix A (Exterior façades and functions) for more information on rainscreens and façades). However, in fire scenarios it is feared (but not previously researched) that these same gaps will contribute to fire propagation and heating of the interior of the rainscreen system. This is an unacceptable aspect of the design as the rainscreen cladding system must pass the NFPA 285 test according to the International Building Code.

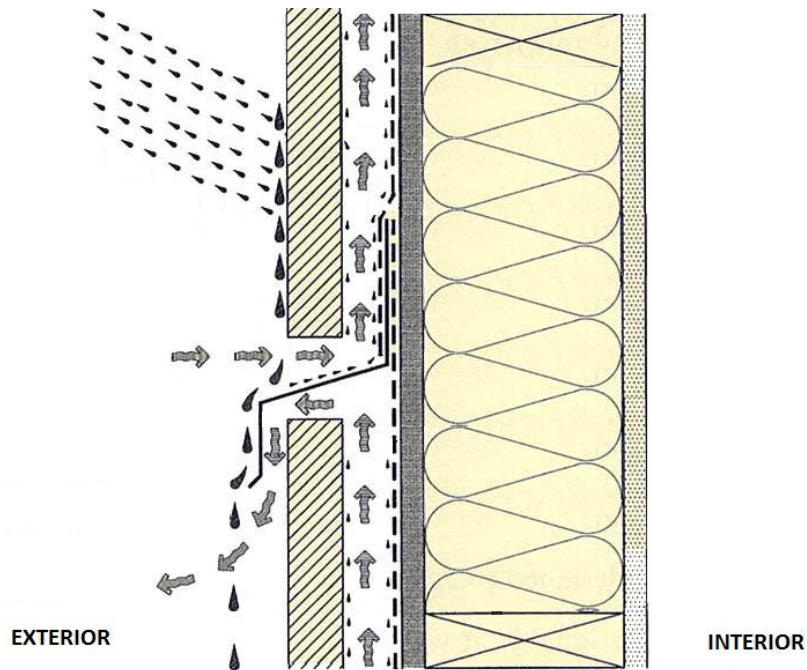


Figure 2 - Rainscreen Cladding System Schematic (Not to Scale)

2.2 International Building Code

The International Building Code (IBC)[2] is the primary international standard relating to building construction. The scope of the code is intended to protect the public's health and safety; therefore it is constantly revised every three years to allow for the use of new materials and design approaches [2].

When a building is in the design stage, it is important to determine what type of construction the building falls under according to the IBC. Chapter six defines five types of building constructions that have specific requirements based on each type. Section 602 lays out the construction classifications and section 603 states requirements for combustible materials in construction types I and II. Types I and II can have exterior and interior load bearing and nonbearing walls made of noncombustible materials. Section 603 details the exceptions to this noncombustible requirement for types I and II because under specified circumstances combustible materials are permitted. Type III construction is defined as having noncombustible exterior walls and any code approved material for interior walls. Type IV construction uses noncombustible materials for the exterior walls and solid or laminated wood for interior surfaces. Type V construction is considered to be the miscellaneous classification because both exterior and interior walls can be made of any acceptable material [2].

There are various specifications regarding the use of combustible materials such as the acceptable use of foam plastics. According to Chapter 26 of the IBC for example, foam plastics are an acceptable material. Fiber reinforced polymers (a material often used in rainscreens) used in exterior walls are discussed in Section 2612 of the IBC. However, general specifications are given in section 2603.5 for the use of plastics for exterior walls of buildings of any height [2].

The scope of this project is concerned with vertical and lateral flame propagation, which is addressed in section 2603.5.5. Regarding this type of flame propagation, the IBC states that the exterior wall assembly must be tested according to the standard NFPA 285. While there are certain exceptions

put forth in the IBC, generally speaking, combustible materials for exterior walls may be used if the assembly is in compliance with NFPA 285. Chapter 26 of the IBC also mentions the other NFPA standards that exterior plastic assemblies must comply with in order to be IBC compliant. Section 2603.5.7 refers to ignition of the assembly, stating that exterior walls must comply with NFPA 268 [2]. For more information on the IBC and the green building movement see Appendix B (The Green Building Movement and International Building Code). For more information on the IBC's requirements of external façades see Appendix C (IBC Requirements for External Façades).

2.3 NFPA 285

NFPA 285[3] provides a large obstacle for rainscreen manufacturers. NFPA 285, Standard Fire Test Method for Evaluation of Fire Propagation Characteristics of Exterior Non-Load-Bearing Wall Assemblies Containing Combustible Components, is the fire testing procedure which rainscreen cladding systems, among many other exterior assemblies, are subjected to due to the IBC's material fire testing requirements. The basic setup of a NFPA 285 test requires a 15 ft. 8 in. tall section of the assembly to be installed as it would be during construction. This assembly is then exposed to 5 minutes of indirect flame contact followed by 25 minutes of indirect and direct flame contact as seen in Figure 3. As the test is performed, the fire intensities are increased until a maximum heat release rate is reached of 904 kW for the indirect fire (room burner) and 398 kW for the direct fire (window burner). In order to be considered a "Pass" for this test, the assembly may not have flames emit from the specimen at a height greater than 10 feet above the window and no greater than 5 feet horizontally from the window centerline. Additionally, various temperature requirements must be met throughout the assembly.

In the case of panelized construction, the air space behind the exterior panels are also subjected to maximum temperature constraints in order to pass the test. It is understood that the material on the exterior of the building must be extremely durable in a fire scenario to resist vertical and horizontal surface fire propagation. However, the design of the assembly itself could possibly influence the way that fire is spread. In a rainscreen assembly, there is an air gap behind the exterior panel, as seen in Figure 3. Additionally, there are air gaps between individual panels. This raises a serious concern for rainscreen manufacturers when NFPA 285 is in mind. If the assembly is going to pass the test, not only does the exterior surface need to not allow for fire spread, but the interior air channels need to stay below 500 degrees Fahrenheit throughout the entire test. If the air behind the panel is hot, it will reduce the cooling ability of the panel as the difference between the air temperatures at the front and

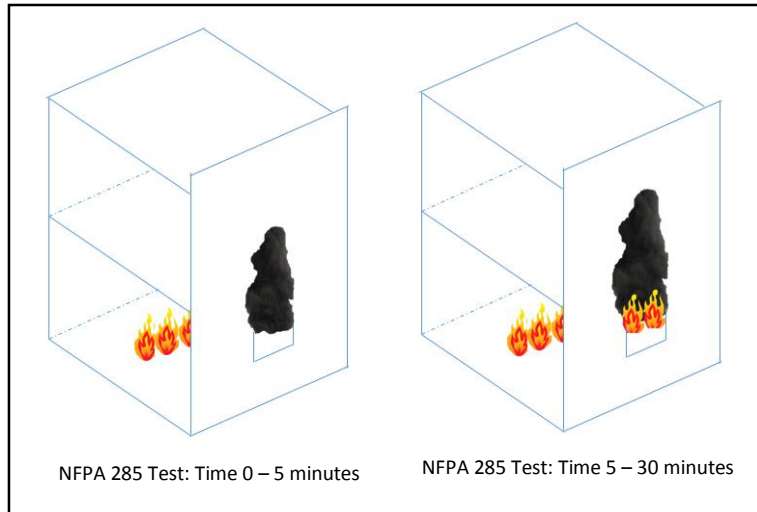


Figure 3 - NFPA 285 Test Diagram

back will be reduced. This could lead to either the panel heating faster or the interior air channel exceeding 500 degrees Fahrenheit during the test. It is unknown exactly what effect gaps in between exterior surface panels have during a fire scenario [3].

In order to pass NFPA 285, gaps between panels are generally sealed to prevent air movement to the area behind the exterior panels during a fire scenario. It is obvious that this adds labor and material expenses, but it is the current solution for passing NFPA 285. Since the cost of the NFPA 285 test alone is approximately \$60,000 for the test alone, designers are not willing to risk failing due to not sealing the gaps in between the panels [7]. If the role which gaps play during a fire scenario is better understood, a decision on whether or not sealing the gaps is essential could be made. For more information on NFPA 285 and how it effects this particular project see Appendix D (NFPA 285 Notes).

3.0 Experimental Set-Up

In order to understand how horizontal gaps effect flow up a face, an assembly was designed to focus on a single horizontal gap during a fire scenario. Within this section, the assembly's geometry will be described in detail along with instrumentation locations and descriptions.

3.1 Assembly Geometry

In order to understand how a horizontal gap effects smoke flow, an assembly was created which, with appropriate instrumentation, will allow for the analysis and conclusion regarding this topic. To begin, a 2 foot by 1 foot vaporized propane burner was used as the fire source for the assembly. The burner, which can be seen in Figure 4, was used to create fires of constant heat release rates for each of the runs. The heat release rates which were used for testing were 75 kW, 150 kW, and 200 kW. The 75 kW fire resulted in a fire height below the gap, the 150 kW fire resulted in flames reaching the bottom of the gap opening, and the 200 kW fire resulted in flame heights exceeding the gap. The burner is enclosed by walls on three sides. These walls were constructed of $\frac{1}{2}$ " thick calcium silicate board in order to provide durability throughout many fire tests. The two walls on the sides of the burner were installed to channel the fire and create a quasi-2D fire flow. The wall opposite of the non-enclosed side is where the gap is located. For the assembly tested, the opening is 2" tall while the return flange is 1' deep. It should be noted that a typical gap size is generally smaller than 2" with 2" being the maximum that one is likely to see.

It is expected that with the presence of a horizontal gap, most of the smoke flow will flow up the front face as it would without a gap present. However, some smoke is expected to flow into the gap and then out into the back (which will be referred to as the chimney area). Exactly how much smoke enters the gap, and the characteristics of the flow (such as temperature and velocity) will be calculated by analyzing data produced from the instrumentation installed on the assembly.

On the front face below the gap (as seen in Figure 5), there are 5 rows of thermocouples located 1" off the surface of the front face. 3 of these rows have a centerline thermocouple as well as two off-center thermocouples to verify a quasi-2D flame spread. In addition to the thermocouples, a bidirectional probe [5] is located on the front face in order to measure the velocity of the upward flow before it comes in contact with the gap. The data from the bidirectional probe will be essential in confirming that energy is conserved. The thermocouples located directly below the gap and directly above the gap will give excellent insight into understanding the enthalpy flow into the gap. Further information on instrumentation can be found in Appendix F.

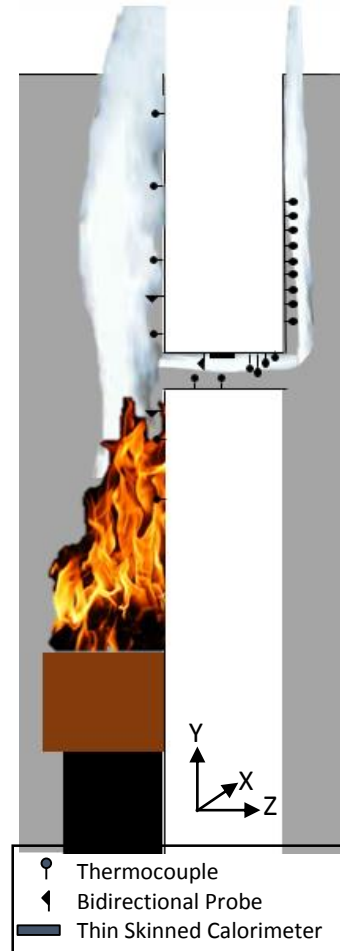


Figure 4 - Assembly Cross View
(Not to Scale)

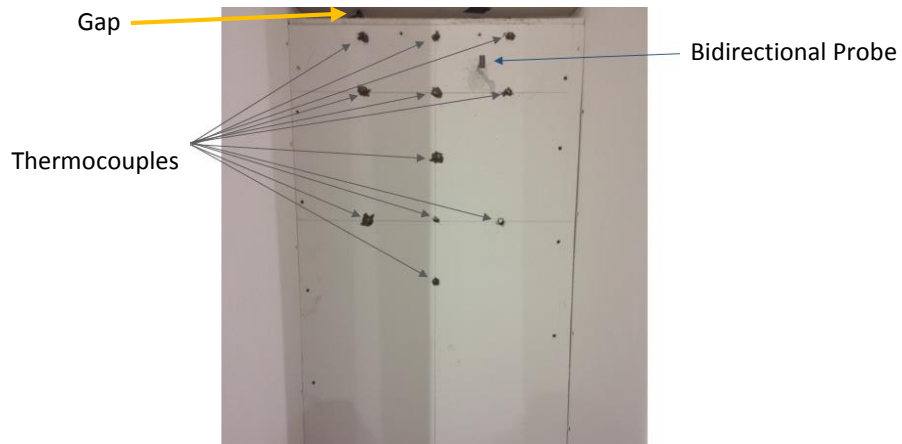


Figure 5 - Front Face below the Gap
Instrumentation Overview

Above the gap, the instrumentation setup is very similar. There are 7 rows of thermocouples above the gap, only 2 of which contain additional thermocouples to confirm the 2D flow. Like the thermocouple placement below the gap, directly above the gap there is a row of thermocouples. Additionally, there is a bidirectional probe above the gap as well. As previously mentioned, the bidirectional probe will give a direct indication of conservation of energy when compared with the bidirectional probe below the gap. Additional Figures depicting the assembly and instrumentation placement can be seen in Appendix E (Assembly Sketches).

There are thermocouples, thin skinned calorimeters[6], and a bidirectional probe located within the gap. Thermocouples are spaced evenly throughout the bottom of the gap located 1" off of the bottom face to measure flow temperature in the gap. These laterally placed thermocouples will help to confirm that 2D flow is achieved. A thin skinned calorimeter is shown on the top face of the gap, as seen in Figure 6. This instrument will record the temperature history of the metal plate. Additionally, a grouping of thermocouples at varying heights is located in the back of the gap hanging from the top face. These thermocouples are expected to give valuable insight into the temperature difference at

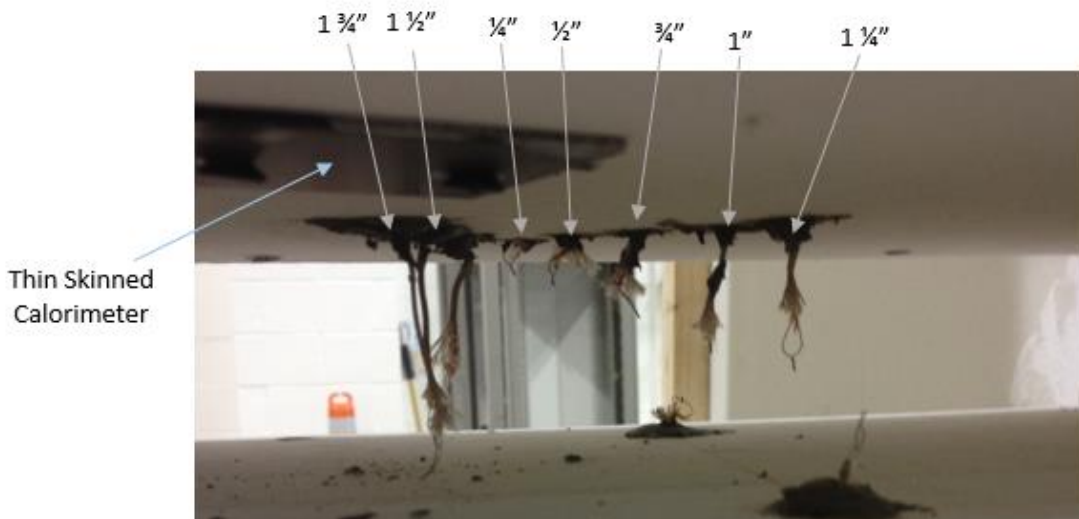


Figure 6 - Thermocouples of Varying Height

different heights in the gap. These thermocouples are spaced (vertically) at $\frac{1}{4}$ " increments from $\frac{1}{4}$ " to $1\frac{3}{4}$ ". The data produced will give a clear indication of the characteristic flow through the gap. This information is incremental to our final conclusions and our ability to characterize the flow.

As the flow leaves the gap, it will enter the chimney area which is essentially an open air area which is separate from the exterior. With the assembly in this test, many thermocouples were installed along the face above the gap in order to characterize the flow out of the gap. These thermocouples were placed in three columns and each had varying heights off of the face of either $\frac{1}{2}$ ", 1 ", or $1\frac{1}{2}$ ". By understanding which set of thermocouples off of the back face are recording the highest temperatures, proper understanding of the flow leaving the gap will take place. For more information on how the aforementioned information operates, or how it was calibrated, please see Appendix F (Instrumentation).

4.0 Results and Characterization

In order to understand what effect the horizontal gap is having on flow up the face of the assembly, proper characterization needs to take place. This includes the velocity data from various points on the assembly, initial fire plume characterization and the chimney flow characterization.

4.1 Velocity Results

Velocity data for a single 75 kW size fire test can be seen in Figure 7. The three curves represent the three bidirectional probes located below the gap, above the gap, and inside the gap. It should be noted that ambient data was recorded for roughly the first 70 seconds in this test.

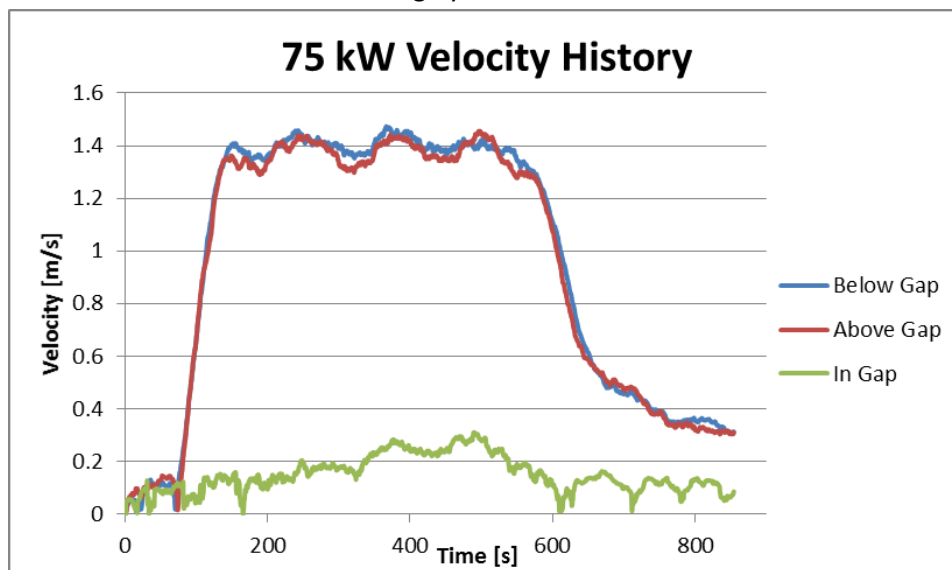


Figure 7 - Velocity Measurements at Various Locations

Additionally, the points used to chart Figure 7 represent a 10 second running average to eliminate some noise from the data.

The air velocities along the front face of the assembly were quite close in value as can be seen in the above figure. The maximum velocity recorded at these locations was 1.47 m/s below the gap and 1.46 above the gap. The maximum velocity recorded inside the gap was 0.31 m/s, which is significantly lower than the velocities along the front face. It is important to note that this peak velocity inside the gap is one order of magnitude lower than the front face peak velocities.

Table 1 - Average velocities at each probe location, 75kW test

Average Velocity [m/s]	
Below Gap	0.96
Above Gap	0.94
In Gap	0.15

Table 1 presents further indication that the air flow inside the gap is substantially lower than along the front face. The average velocities for above and below the gap are extremely close at 0.94 and 0.96 m/s. Additional velocity data is provided in Appendix G (Raw Data TSC and BDP).

4.2 Temperature Distribution across the Front Face

To assess the viability of characterizing the fire flow on the front face of the assembly as quasi-two-dimensional the temperature variation across the front face was analyzed. To do this the average temperatures were gathered at varying heights above the burner on both the centerline and with a plus or minus .17145 m offset from the centerline. The points closest with no corresponding thermocouple data from each side were omitted from this analysis. The compiled temperature profile for the 75 kW tests can be seen in Figure 8 below:

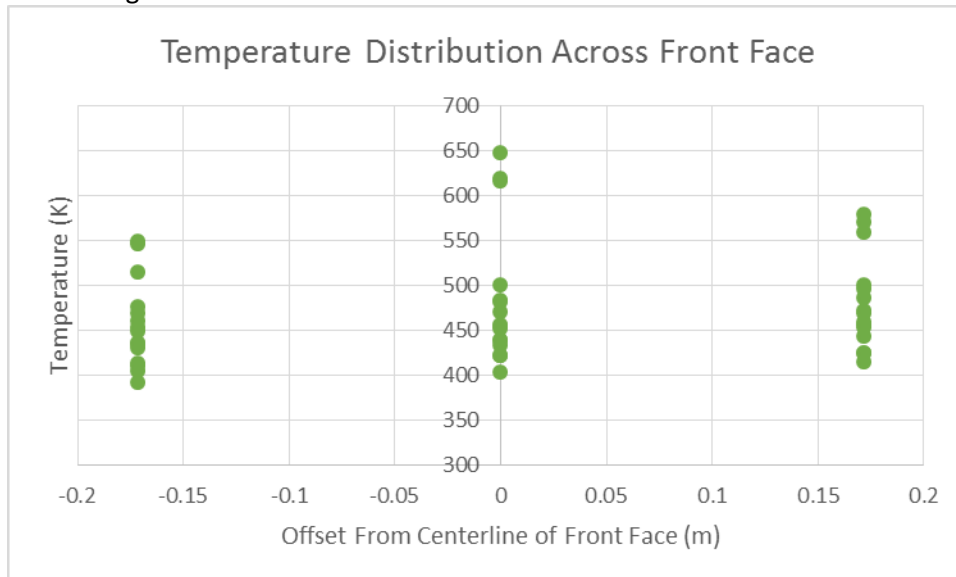


Figure 8 - Temperature Distribution across the Front Face of the Assembly during the 75 kW Tests

A noticeable trend is observed where the hottest temperatures are encountered close to the centerline of the burner. During the experimental runs, a trend of flame having the tendency to flow up the right corner of the front face and a relative absence of flame in the left corner was also observed at varying times. This can be observed in the temperature distribution graph above which compares average temperatures at each location across the front face. This indicates that the theories utilized for calculating temperatures corresponding with two-dimensional flows will correspond best with the centerline results. This variation across the face can be primarily attributed to the use of a rectangular burner as opposed to a line burner, and to inconsistency in the distribution of material used in the burner to distribute the propane flow.

4.3 Fire Plume Characterization

In order to understand how much energy actually enters the gap, it was essential to characterize the thermal plume flowing up the front face of the assembly. Physical characterization of the plume was possible through thermocouple temperature data. However, further analysis was desired in the form of applying existing theory to show that the plume in the experiments were in fact quasi-two-dimensional and to enable individuals to calculate reasonable temperature estimations for heat release rates at heights above the burner other than those that were tested. To characterize the plume, work done by Li-Ming Yuan and G. Cox [8] was utilized. Yuan and Cox performed a number of tests with a methane line burner in the open to gather temperature and velocity data up the centerline of the plume. Their results were then used to come up with a correlation for calculating a temperature change and velocity in the plume centerline. While the burner used in the gap assembly is not considered a line burner, it was decided that this theory was still a reasonable way to characterize the temperature plume due to the assumption, and confirmation, of a quasi-two-dimensional fire. The Yuan and Cox theory was not expected to correlate perfectly with the experimental results due to the differences in geometry and the fact that propane was used as a fuel source instead of methane. With three enclosed sides as opposed to a burner in the open (as was used in the development of their correlation), higher temperatures were expected in the channel up the front face of the assembly than those gathered in Yuan and Cox's testing. In order to account for this and any other variations between the gap assembly experiments and those conducted by Yuan and Cox, an adjustment to the leading constant of the theory was determined. For calculating the theoretical temperature change the following equation was used:

$$\Delta T = \beta * \left(z / Q_l^{2/3} \right)^{2n-1}$$

With this equation, ΔT is the temperature change in degrees Celsius, β is a coefficient based on correlations with the physical test results and has the units of degrees Celsius, z is the height above the burner (in meters), Q_l is a heat release rate per unit length (kW/m), and n is a unit-less variable. Both β and n vary depending on the location within the fire plume (continuous flame region, intermittent flame region, or thermal plume region). The location in the plume is determined through a ratio of the height above the burner divided by the height of the flames [8]. For the gap assembly tests, a majority of the temperature data was recorded in the thermal plume region. Some of the thermocouples closest to the burner were in the intermittent flame region for some tests, but a decision was made to simplify the

adjustment factor by utilizing a single coefficient for both the intermittent and thermal plume region. Justification was given to this decision due to the reasonably close correlation between physical data and theory with just the single adjustment made. It is however acknowledged that when dealing with temperatures in the $\frac{1}{2} \leq z/L \leq 1$ range the theoretical temperature generally will be lower than experimental results. The adjustment for β was determined by utilizing one of the 150 kW tests and adjusting the constant until a good correlation was obtained. Once this was established, the new constant, which was determined to be 8.7, was applied to all subsequent data analysis. The temperature data for the front face was determined by averaging the temperature results over the time period where each test was approximately steady state. More information regarding this topic can be found in Appendix H (Time Averaging of Front Face Temperature Results).

$$\Delta T = 7.2 * \left(\frac{z}{Q_t^{2/3}} \right)^{2n-1} \longrightarrow \Delta T = 8.7 * \left(\frac{z}{Q_t^{2/3}} \right)^{2n-1}$$

The equation above shows the adjustment from the thermal plume coefficient Yuan & Cox came up with, 7.2, to the corrected coefficient for the gap assembly of 8.7 [8]. Whether dealing with the intermittent flame region or the thermal plume region, the variable n will become 0. Comparison between the two coefficients can be seen in Figure 9.

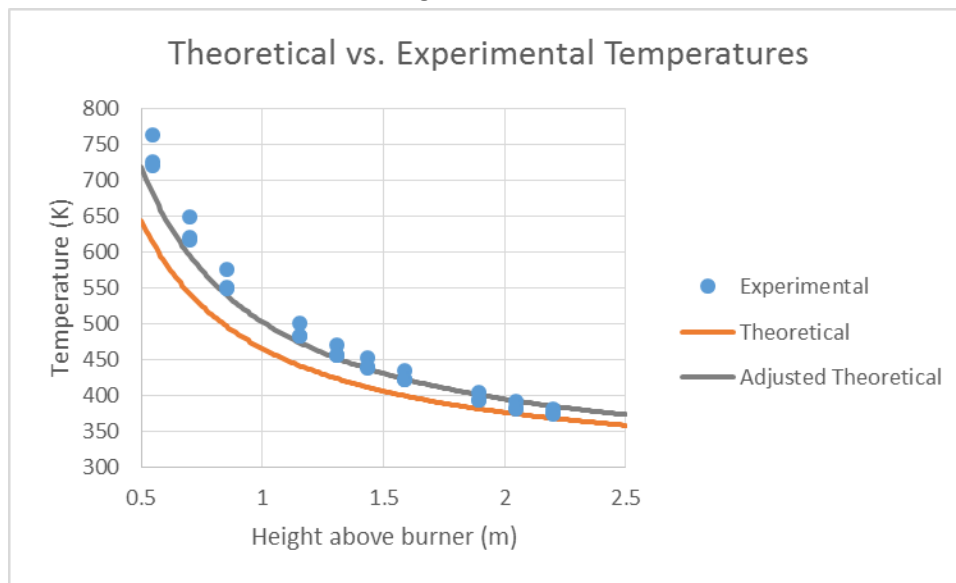


Figure 9 - Compilation of Front Face 75 kW Test Results Compared to the Yuan & Cox Theory

This figure depicts the temperature data gathered from all of the runs performed at 75 kW compared to the Yuan & Cox temperature equation with both the normal and adjusted coefficient. The blue dots each indicate a time averaged temperature at their corresponding height above the burner for each run. The orange 'Theoretical' line depicts the Yuan & Cox equation with a constant of 7.2, and the grey 'Adjusted Theoretical' line depicts the Yuan & Cox equation with the corrected constant of 8.7. A good correlation can be observed with the adjusted equation, and as mentioned previously, notice should be given to the lower theoretical temperature values when compared to the corresponding measured temperatures as the location above the burner gets closer to the intermittent flame region. Each individual test's correlation for the 75 kW, 150 kW, and 200 kW runs, as well as the compilations

for each, can be seen in Appendix I (Yuan & Cox Theory Applied to Front Face). To further compare theory and the experimental data recorded, temperature results from all three heat release rates were able to be combined by comparing the temperature at each height to its corresponding $z/Q_t^{2/3}$ calculation as can be seen in Figure 10.

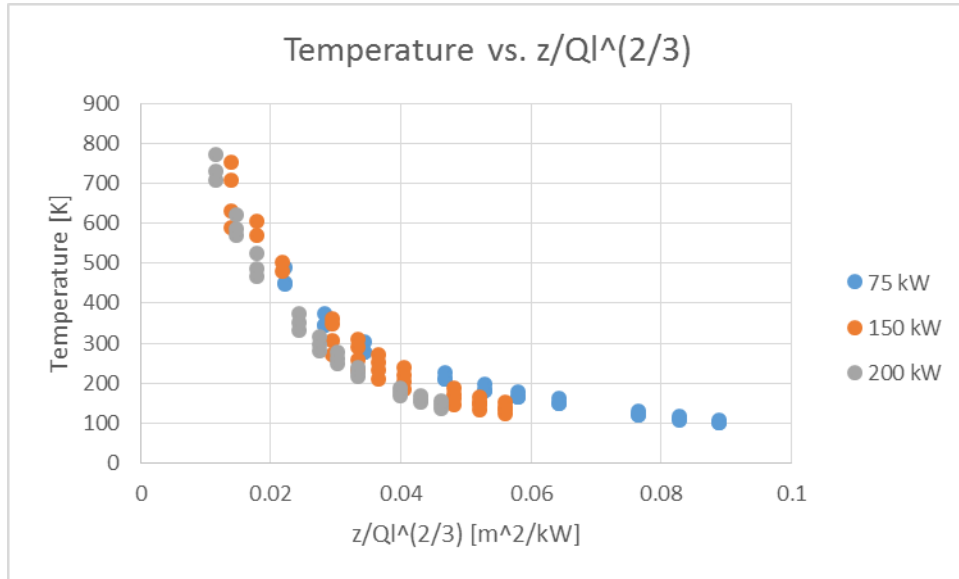


Figure 10 - Comparison of all Heat Release Rate Temperature vs $z/Q_t^{2/3}$ Ratio

With this comparison a noticeable trend can be seen when comparing the data and theory. The close grouping seen in Figure 10, which excludes our adjustment to the leading coefficient, indicates that the application of Yuan & Cox’s two-dimensional flame distribution theory and the use of $z/Q_t^{2/3}$ is a reasonable way to approximate temperature distribution up the front face of the gap assembly.

4.4 Temperature and Velocity Profiles in the Gap

To analyze temperature in the return flange temperature profiles were determined in the directions of the width and height. For the x-direction (across the width) the temperature was relatively constant as expected for a quasi-2D flow as can be seen in Figure 11. An average value for the x-direction was determined by averaging the specific data points which were used to determine the profile, excluding the outliers, which can be seen in Temperature Distribution graphs in Appendix L. For the y-direction (across the height) the temperature was not constant, but followed a parabolic trend as expected due to buoyant forces as well as an established boundary layer due to laminar flow through the gap. The temperature profiles all follow the same pattern but are adjusted based on the applied fire size as can be seen in Figure 12. The temperatures in the Z direction drop as the flow reaches further back into the gap as would be expected due to the heating of the gap wall material as can be seen in Figure 13. It should be noted that there is a large jump in temperature from the 150 kW fire to the 200 kW fire due to the gap being in the near-field for the 200 kW fire. At this distance, flame sheets were visible entering the gap.

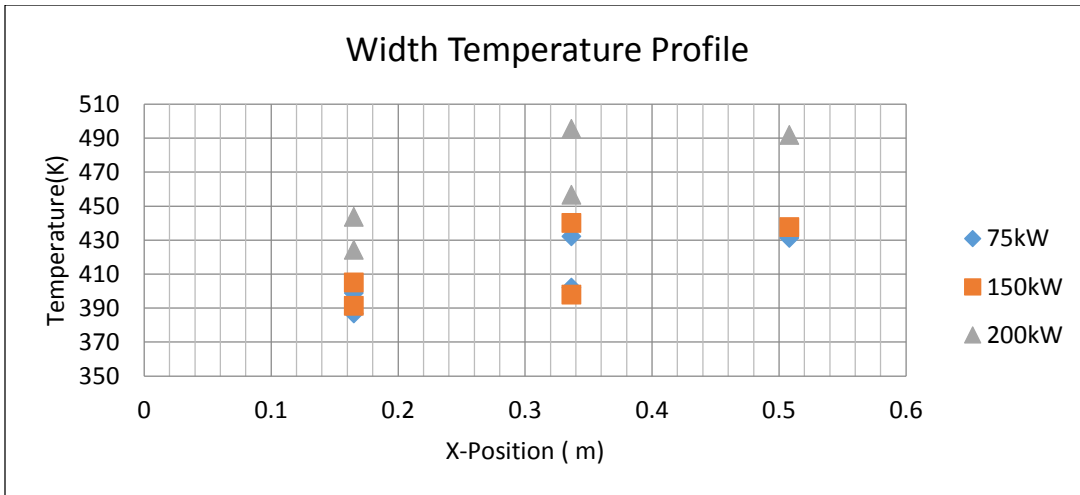


Figure 11 – Width Temperature Profiles in the Gap

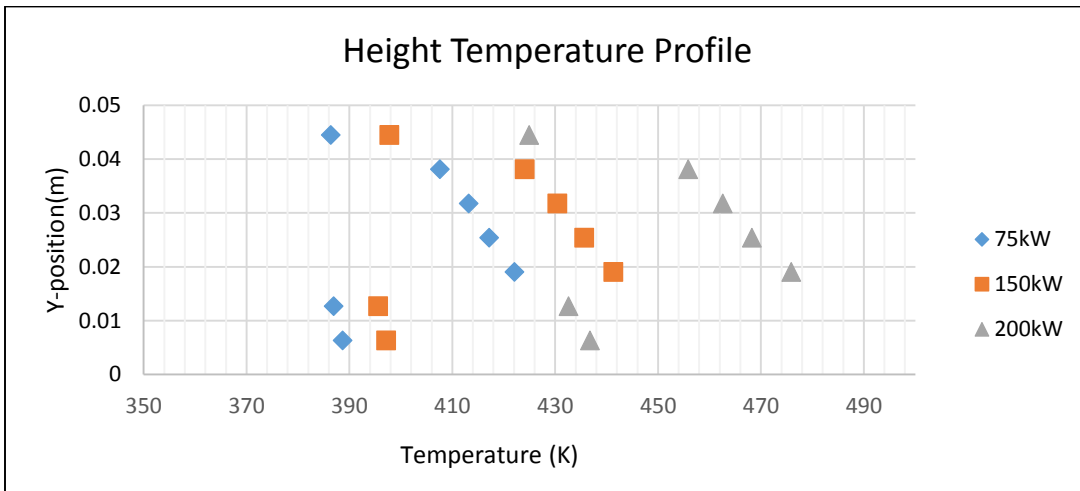


Figure 12 - Height Temperature Profiles in the Gap

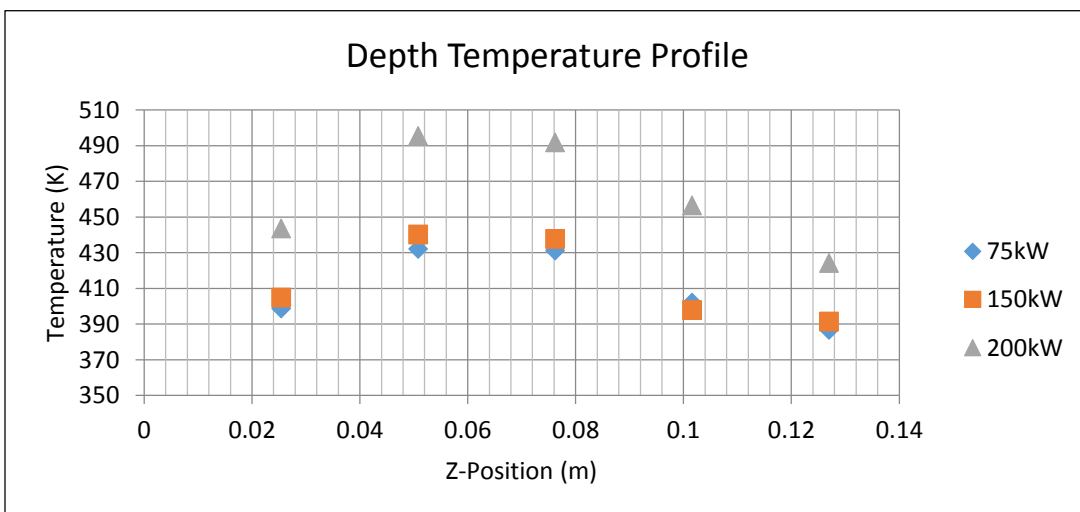


Figure 13 - Depth Temperature Profiles in the Gap

To analyze velocity in the return flange, experimental results from the bidirectional probe located in the middle of the gap were used. With an assumption of 2-dimensional flow in the gap, it can be assumed that the velocity profile is constant across the width of the gap (x-direction). For the velocity along the height of the gap, (y-direction) a velocity profile equation was generated for each fire size as shown in Table 2 which is graphically represented in Figure 14. The formulation of the velocity profiles can be seen in Appendix J (Velocity Profile Formulation). It is important to note that within the gap, there is a fully-developed laminar flow, as shown by the Reynolds numbers specific to each fire size shown in Table 2. Having these velocity equations will allow for the determination of the enthalpy flow through the return flange.

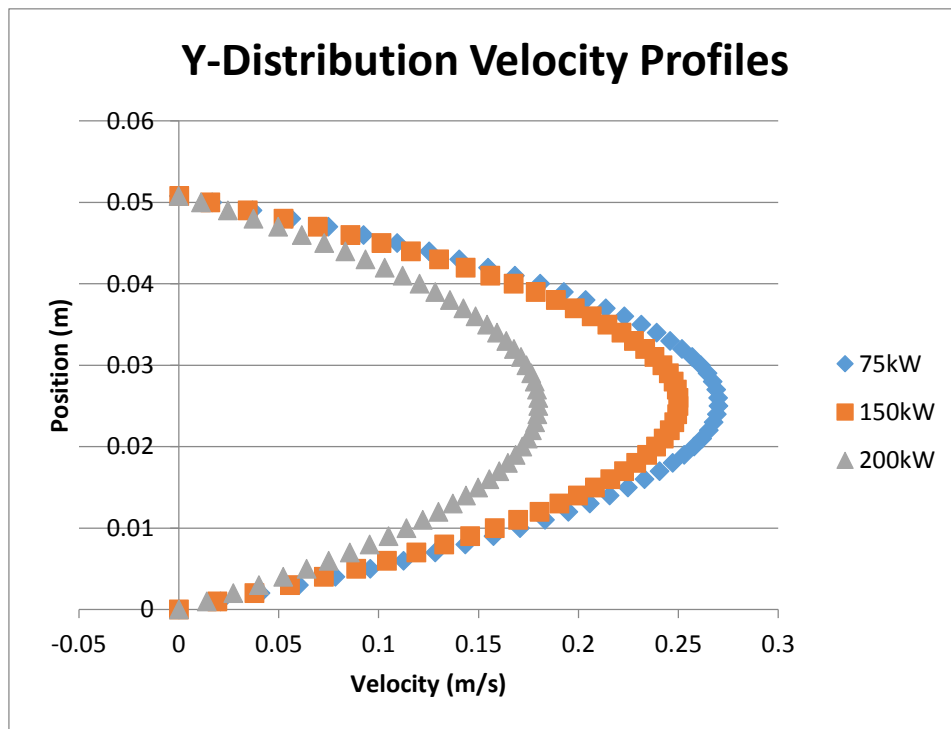


Figure 14 – Y-Distribution Velocity Profiles in the Gap

Table 2 - Variables Related to Flow in the Return Flange

Fire Size	Maximum Velocity	Average Velocity	Reynolds Number	Velocity Profile
75kW	0.27 m/s	0.18 m/s	650.77	$v(x) = -418.50x^2 + 21.26x$
150kW	0.25 m/s	0.17 m/s	580.04	$v(x) = -387.50x^2 + 19.69x$
200kW	0.18 m/s	0.12 m/s	352.50	$v(x) = -279.00x^2 + 14.17x$

4.5 Enthalpy Flow and Energy Conservation in the Gap

To determine the magnitude of energy flowing through the return flange, the values in Table 3 are used specific to each fire size with the exception of Area and T_{ambient} , which remain constant for each different

fire size. Due to the small variance in temperature across the width of the gap, the average air property values for C_p (specific heat capacity) and ρ (density) were used, based on the average temperature for each fire size. Enthalpy Flow was calculated by the following equation:

$$\text{total enthalpy} = \int_{T_{\text{ambient}}}^{T_{\text{average}}} c_p dT \int_0^A \rho v dA \quad [9]$$

Where c_p , and ρ are constant, allowing for them to be placed outside the integral. The velocity component of this equation was calculated with the velocity profiles in Table 2 and the correction factors explained in Appendix M.

Table 3 - Variables Related to Enthalpy in the Return Flange/

Fire Size	T _{average}	V _{average}	C _p average	ρ average	Area	T _{ambient}	Enthalpy Flow
75kW	403 K	0.18 m/s	1.01 kJ/kg K	0.88 kg/m ³	0.03 m ²	285 K	0.6 kJ/s
150kW	417 K	0.17 m/s	1.01 kJ/kg K	0.85 kg/m ³	0.03 m ²	285 K	0.6 kJ/s
200kW	451 K	0.12 m/s	1.02 kJ/kg K	0.78 kg/m ³	0.03 m ²	285 K	0.5 kJ/s

In order to properly confirm that conservation of energy is taking place within the gap, q_{loss} is required to be calculated. Q_{loss} is the calculation for the amount of heat which is lost to the surfaces that make up the gap. For our experiments, as previously mentioned, ½" calcium silicate board was used. The instrument which is used to collect data in order to do this calculation is the thin skinned calorimeter. The full assembly of a proper thin skinned calorimeter setup can be seen in Figure 15. On the surface of the calcium silicate board, a 2"x2" the thin skinned calorimeter's steel plate is mounted to face in towards the gap. On the other side of the calcium silicate board, a thermocouple is installed to the back surface of this same board. Then, the thermocouple is secured in place by mounting another piece of ½" thick calcium silicate board to the other side of the thermocouple. It is important to note that in the following calculations, a space between the thin skinned calorimeter plate and the surface of the calcium silicate board will be recognized to show that the plate is not perfectly in contact with the calcium silicate board throughout the entire surface.

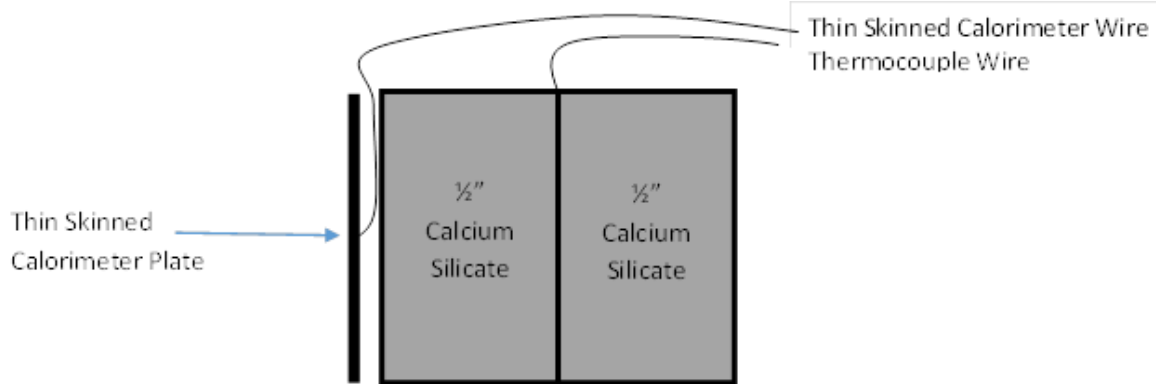


Figure 15: Thin Skinned Calorimeter Set-Up

As the thin skinned calorimeter begins to heat up, it will transfer heat to the calcium silicate board behind it. As more heat is transferred, the board will begin to heat up thicker and thicker into its surface until eventually, the thermocouple in between the two boards will begin to recognize a temperature change. As the heating continues, eventually the heat will conduct through both boards and be cooled by the ambient air behind the second board. If tests were run for long enough time, the

temperature of the thin skinned calorimeter would be the same temperature as both calcium silicate boards assuming that the ambient air behind the second board is unable to sufficiently cool the thin skinned calorimeter assembly. In order to calculate the temperature distribution through the board, and eventually calculate how much energy is lost to the boards, the following equation is used:

$$\dot{q}''_{loss} = k * \frac{\Delta T}{\Delta x}$$

In the above equation, k is the thermal conductivity of the calcium silicate board, ΔT is the change in temperature between the thermocouple and the calcium silicate board exposed to the thin skinned calorimeter, and Δx is the distance into the board which is being calculated for, in this scenario, ½". In order to determine what the temperature of the calcium silicate board exposed to the thin skinned calorimeter will be while taking into account for the temperature lost to the imperfect connection between the plate and board, the following equation is used:

$$\dot{q}''_{loss} = (T_{pl} - T_{CSB}) * h_c$$

In the above equation, T_{pl} is the temperature of the thin skinned calorimeter plate, T_{CSB} is the temperature of the calcium silicate board exposed to the thin skinned calorimeter plate, and h_c is the heat transfer coefficient between the plate and the board. These two equations are then used to calculate the total amount of heat which is lost into the calcium silicate board. The confirmation of the Qloss calculations can be seen in Appendix M.

Cross-checking the enthalpy loss in the gap between the thin skinned calorimeter readings and a simple conservation of energy balance allows for confirmation of the enthalpy results. Although an assumption is made regarding 2-dimensional flow in the gap when in reality, the gap experiences a quasi-2-dimensional flow, some small differences between Qloss (kW) and Change in Enthalpy Flow (kW) can be seen in Table 4. Qloss was determined with the use of thin skinned calorimeters whereas Change in Enthalpy Flow was determined by taking the product of the percentage temperature loss in the gap and the total enthalpy flow in the gap. This Change in Enthalpy Flow should follow a similar trend as the change in temperature from the front of the return flange to the back face (z-direction). The percent temperature change in the gap can be seen in Table 4.

Table 4 - Enthalpy in the Gap

Fire Size	% Temperature Change In Gap	Total Enthalpy Through Gap	Qloss	Change In Enthalpy Flow
75kW	7.7%	0.6 kW	0.2 kW	0.1 kW
150kW	11.1%	0.6 kW	0.2 kW	0.1 kW
200kW	14.4%	0.5 kW	0.3 kW	0.1 kW

4.6 Characterization of Flow from the Gap Exiting into the Chimney

Another area of importance for characterization is the thermal plume that exits the back of the gap and then continues up the back face (chimney) of the assembly. The array of thermocouples above the exit of the gap was utilized along with visual observations to obtain a good idea of the severity and geometry of the plume going up the back face. Through placement of thermocouples at varying distances off of the back face (½", 1", and 1 ½") it was determined that the characteristic temperature, which can roughly equate to the centerline temperature calculated in most theories, is approximately one inch from the back face. This can be observed in the back face temperature maps in Appendix K (Application of Yuan & Cox to Thermal Plume up Back Face). A decision was made to apply the Yuan &

Cox [8] flame distribution theory again as a way to estimate the amount of energy exiting the back of the assembly. To apply this theory, the bottom flange at the back of the gap was considered to be a ‘burner’ for calculation purposes. The visual observations of the plume indicated that the entirety of the plume exiting the gap would be part of the theory’s definition of the thermal plume range. Additional observations showed that there was relatively little interference from the assembly’s geometry in contrast to the front face (it is believed that relatively the same plume would have occurred regardless of the presence of the walls within the chimney). To reflect this, it was decided to utilize the default value for β in the thermal plume, 7.2, rather than apply the previously determined adjusted constant from the front face:

$$\Delta T = 7.2 * \left(z / Q_l^{2/3} \right)^{2n-1}$$

Unlike the front burner, a heat release rate leaving the gap was not physically measured. In order to account for this, the first characteristic temperature average from the back face was utilized to calculate the heat release rate per unit length, Q_l , for each run. Once this was calculated from the first data point, we applied that same heat release rate to the theory for every other height. The back face temperature average was determined by using the same method and time frame as the front face temperature averages mentioned earlier. The result of this method being applied to one of the 75 kW runs can be seen in Figure 16.

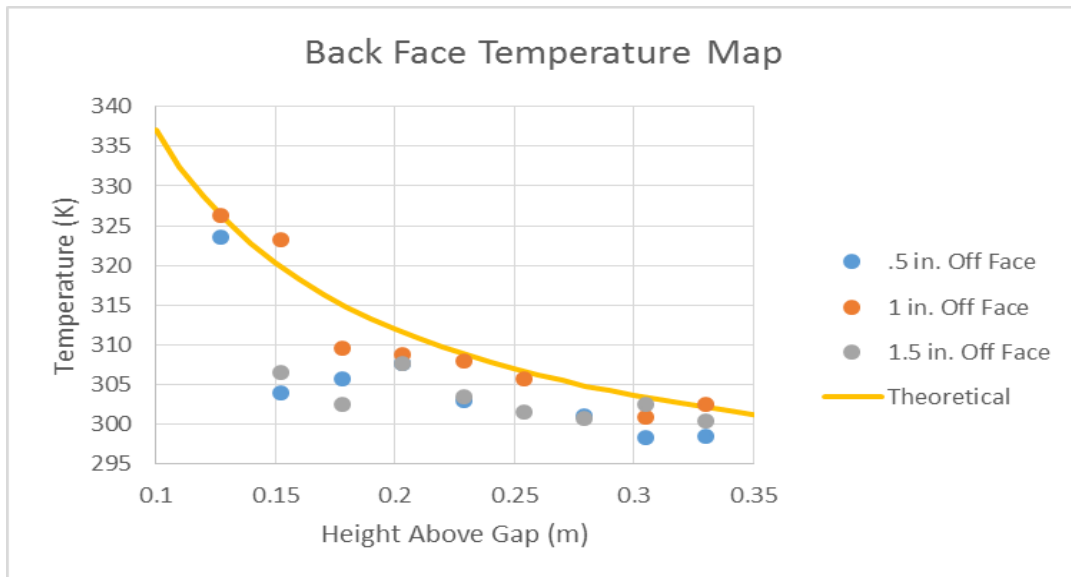


Figure 16 - 75 kW Back Face Temperature Map Theoretical Fit

In Figure 16, the blue, orange, and grey dots represent the average temperatures from ½”, 1”, and 1 ½” off the back face respectively. The yellow line is the theoretical line applied with the calculated heat release rate per unit length determined from the first point. As expected, there is a good correlation between the characteristic temperatures at the 1” location off of the back face, and those from ½” and 1 ½” are noticeably lower as would be expected considering gradients of thermal plumes. Similar correlations were achieved when applying this method to the other runs, although some of the theoretical lines appear more representative of an average temperature between the three distances

from the back face rather than solely corresponding with the 1" data. This can most likely be attributed to an overall hotter thermal plume exiting the gap in the more intense runs at 150 and 200 kW. The compilation of a similar graph to the one from the front face was done to compare the theoretical ratio $z/Q_l^{2/3}$ and the corresponding temperature data which can be seen in Figure 17.

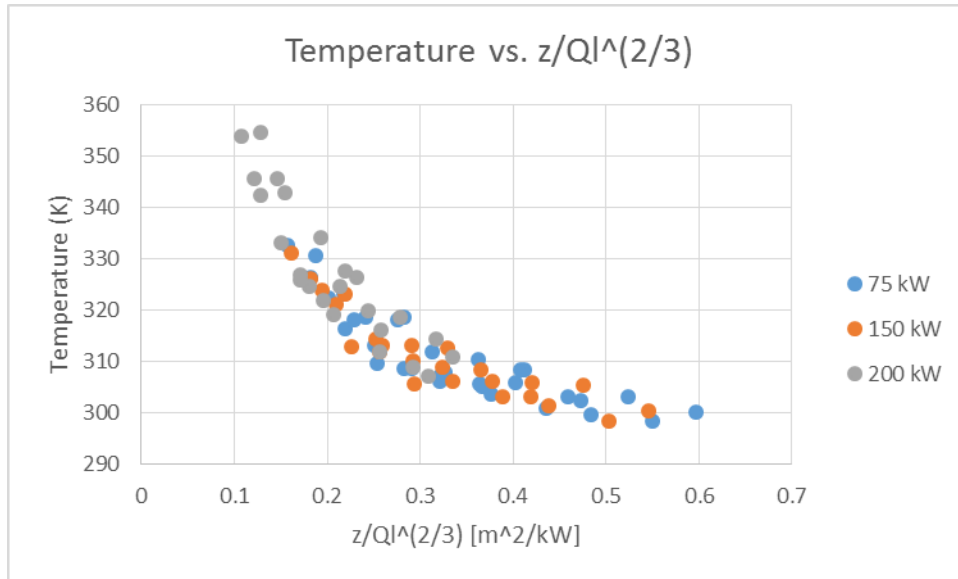


Figure 17 - Comparison of Back Face Heat Release Rate Temperatures vs. $z/Q_l^{2/3}$

With this graph, notice should be given to the fact that the data trend of the $z/Q_l^{2/3}$ ratio is a reasonable way to represent the temperatures up the back face of the assembly. If this same comparison is done with an averaged heat release rate per unit length a similar trend is formed, but without as close of a grouping between data points. Overall, the theoretical characterization of the back face indicates that for all three of the heat release rates, it is expected that the amount of energy exiting the back of the gap to be around 1 kW; two orders of magnitude less than the burner's heat release rate.

5.0 Conclusions

Based on the calculations used to characterize the temperatures on the back face, it was determined that the enthalpy flow rate exiting the gap is in the range of <1-2 kW depending on the varying heat release rates. This is a difference of two orders of magnitude which indicates a relatively small amount of the total energy from the fire actually enters the gap. Additionally, conservation of energy calculations show that some of the energy which enters the gap is absorbed by the material. This confirms why temperatures are lower when they exit the gap as opposed to entering the gap.

6.0 Future Research

It is recommended that further experimental studies be done relative to smoke flow through exterior construction gaps. This project successfully quantified the enthalpy and energy flows through the gap, however there are several other aspects to be studied. In the future, this project should be used as a baseline assembly, for which key parameters are varied, including: gap height, gap depth, and gap orientation. This project used a constant gap height of 2", which is quite large for external facades. It would be beneficial to examine the change in enthalpy flow into the gap when this height is decreased in increments down to ¼". Similarly, the effects of decreasing gap depth should be studied as this project used a 1' gap depth. Finally, this project used a horizontal gap, however there are several gap orientations used by designers that should be looked into. This could include vertical, angled, and even curved gaps.

References

- [1] Agbasi, Anumba, Gibb, Watson. (2001) Review of Specifications for Rainscreen Cladding. CIMclad, pp. 3-13. Retrieved from <http://www.engineering.leeds.ac.uk/civil/research/cae/current/cimclad/Report%203.pdf>
- [2] IBC, ICC. (2006) "International building code." International Code Council, Inc 4051: 60478-5795.
- [3] NFPA. (2012). *NFPA 285: Standard Fire Test Method for Evaluation of Fire Propagation Characteristics of Exterior Non-Load-Bearing Wall Assemblies Containing Combustible Components*. Quincy, MA
- [4] "Manufacturer of Rainscreen Cladding Systems." *Rainscreen Systems, Exterior Wall Cladding, Aluminum Composite Panels, Dry-Design Reveal Aluminum Panels*. NorthClad.
- [5] McCaffrey, B. J., G. Heskestad. (1976) "A robust bidirectional low-velocity probe for flame and fire application." *Combustion and Flame* 26: 125-127.
- [6] American Society for Testing and Materials. Philadelphia. (2005). "Standard Test Method for Measuring Heat Transfer Rate Using a Thin-Skin Calorimeter."
- [7] Wolff, D. L.. (2012) "Understanding NFPA 285: A Consultant's Perspective on the Code." *Journal of Building Enclosure Design*: 17-18
- [8] Yuan, L.-M., Cox, G. (1996). An experimental study of some line fires. *Fire Safety Journal*, 27(2), 123-139.
- [9] Martin, M. (1986). *Elements Of Thermodynamics*. Prentice-Hall, Eaglewood Cliffs, NJ. 66-68

Appendix A: Exterior Facades and Functions

Author: Sarah Meehan

Exterior Facades & Functions

Functions of a Facade

An exterior façade/building envelope is generally used as a complementary system to the building. Rather than having a structural component the exterior façade should be non-load bearing. Every façade is different in regards to the materials used and their properties. This final layer to a building acts as a protective barrier and is often used for aesthetic reasons. More specifically facades can have extra features as well including solar panels to harness energy, ventilation, noise reduction, etc. The durability of a façade should be less than the building structure itself but greater than the internal building system. [1]

Façade Features – Gaps & Air Barriers

Horizontal and vertical gaps allow for air movement in between the panels and building. These gaps also allow for building movement due to expansion or contraction of different elements of the building and panel system. “An air barrier in a wall section is dependent on continuity. Any failure or disruption in this continuity will cause an air pressure differential, leading to the passage of air, and potential water vapor, through the assembly.” Good construction practices will ensure the proper air barrier continuity. [2]

Rainscreens

The purpose of a rainscreen is to protect a building against rainwater. The conditions in which the rainscreen façade protects are the presence of water, openings in the assembly that permit water to enter, and forces that can move water through the assembly. This façade is used for drainage and ventilation with an air cavity between cladding and the wall structure. Rainscreens are comprised of a visible outer skin, an air gap, and a backing wall. [3]

There are two different types of air gaps associated with rainscreen cladding. First is continuous air gaps with either unsealed or open joints but with only unsealed joints at the top and bottom of the assembly. Second is compartmentalized air gaps consisting of air cavities behind each panel with at least one edge joint left unsealed. [4]

Exterior Facades & Materials

Exterior facades are used for aesthetics, fire protection, rain shielding, and even to harness solar energy. These facades are attached to the building structure whether they are made of aluminum, stainless steel, or concrete. Some types of exterior facades are cement plaster, metal panels, glass fiber reinforced concrete, rainscreen wall systems, stucco, wood, masonry, etc. [5]

Metal Facade

Metal façade panels can be made of different metals depending on the purpose. For example Hunter Douglas Contract makes a product called QuadroClad™ which is composed of aluminum. The way this product is designed allows for it to act as an open-joint rainscreen façade system. With these features the product allows for ventilation and thermal insulation. [6]

Terracotta Facade

Hunter Douglas Contract also manufactures a terracotta façade which also acts as a rainscreen. This façade, similar to most uses either a side attachment or back fixing method for support. [7]

Glass Rainscreen

Glass rainscreens can be comprised of laminated glass, glass interlayers, polyvinyl butyral, etc. Most glass rainscreens include plastic layers to resist impact and stop the glass from breaking into sharp pieces with impact. These glass facades can improve safety, sound control, and energy control. [8]

Solar Harnessing Facade

Some façades are made to acquire solar energy. The solar facades made by Schletter can be attached to vertical walls or facades with simple clamps or anchors. These facades use aluminum and stainless steel as part of the assembly. [9]

Exterior Insulation and Finish System (EIFS)

EIFS are commonly composed of a few layers of different materials including woven glass fiber, expanded polystyrene, etc. There are two different types of EIFS, a barrier wall system and a wall drainage system. Both types can be either a polymer based system or a polymer modified system. The barrier wall system works to resist water penetration whereas the wall drainage system works to be a secondary drainage plane. These systems must be assembled and installed correctly for moisture protection. EIFS has insulating qualities that reduce thermal loads to the exterior of the building wall. Also, EIFS is a lightweight & low cost option. [10]

Ventilation Wood Facade

This type can be used as a ventilated façade. Wood facades are generally used for aesthetics but they are also a lightweight option. The wood facades manufactured by Hunter Douglas Contract have concealed mounting on the back to maintain the look of the wood. [11]

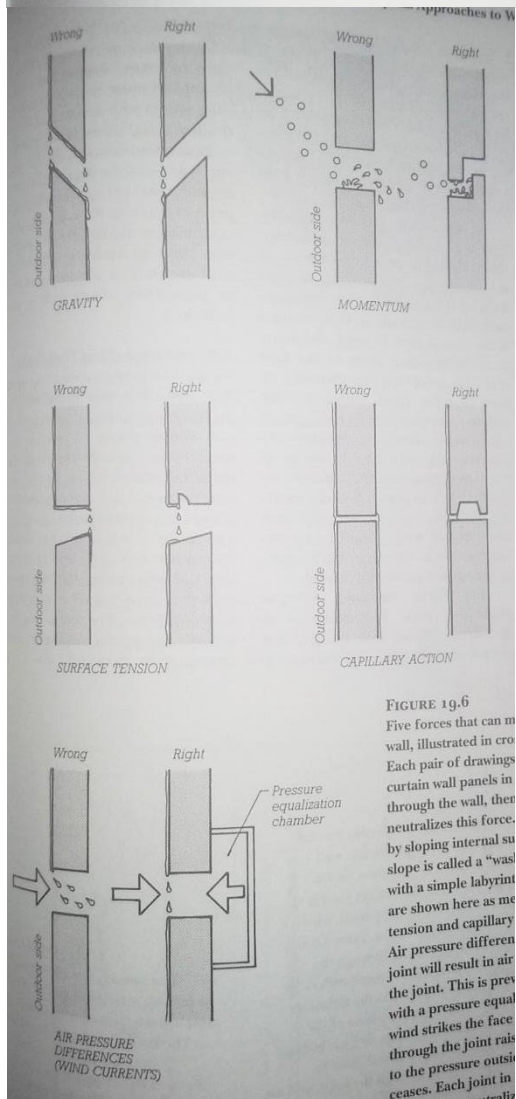
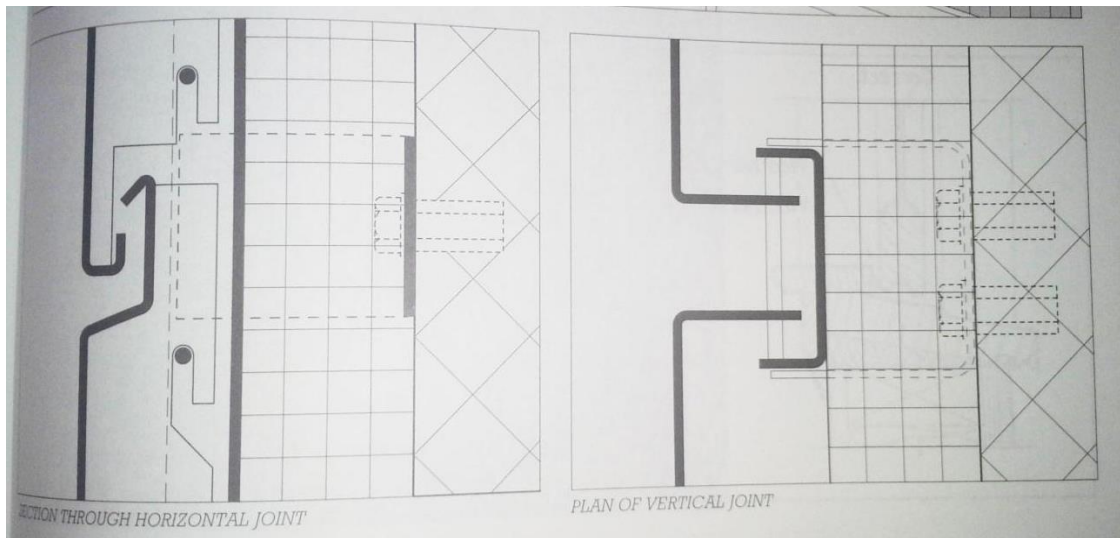


FIGURE 19.6
 Five forces that can make water infiltrate a curtain wall, illustrated in cross-section. Each pair of drawings shows a curtain wall panel in cross-section. In the 'Wrong' drawings, water enters the joint through the wall, then through the joint. In the 'Right' drawings, the water is neutralized by sloping internal surfaces. The sloped surface is called a "wash" and the sloped surface with a simple labyrinthine pattern are shown here as membranes. The forces of surface tension and capillary action are shown here as membranes. Air pressure differences in a joint will result in air entering the joint. This is prevented with a pressure equalization chamber. Each joint in a curtain wall should be designed to neutralize these forces.

Allen, E., Iano, J. (2009) Fundamentals of Building Construction Materials & Methods: Fifth Edition.

Works Cited:

1. Brookes, Alan. (1998). Cladding of Buildings. Retrieved from <http://site.ebrary.com/lib/wpi/docDetail.action?docID=10055920>
2. Lovell, J. (2010). Building Envelopes: An Integrated Approach. pp. 1-12. Retrieved from: <http://issuu.com/papress/docs/building-envelopes/12>
3. Agbasi, Anumba, Gibb, Kalian, Watson. (2001). CIMclad: Review of Specifications for Rainscreen Cladding. Loughborough University. pp. 3-10. Retrieved from: <http://www.engineering.leeds.ac.uk/civil/research/cae/current/cimclad/Report%203.pdf>
4. Knaack, U., Klein, T. (2010). The Future Envelope 3: Facades – The Making Of. Volume 10. IOS Press
5. Façades/Exteriors. (2006). Buildings, 100(3), 104. Retrieved from <http://ezproxy.wpi.edu/login?url=http://search.proquest.com/docview/210299374?accountid=29120>
6. Hunter Douglas Contract. (2013). QuadroClad™ Metal Façade Panels. Retrieved from http://www.hunterdouglascontract.com/facades/metal_facade.jsp
7. Hunter Douglas Contract. (2013). NBK™ Terracotta Façade Panels. Retrieved from http://www.hunterdouglascontract.com/facades/terracotta_facade.jsp
8. Aliva. (2009). Aliva Glass Rainscreen Systems. Retrieved from http://www.alivauk.com/sp_fs_alivaglass-detail.htm
9. Schletter. Professional Solar Mounting Systems Roof and Façade. Retrieved from <http://www.schletter.us/support/l400110%20Roof%20Mount%20System%20Overview.pdf>
10. Zwyer, Gary L. (2010, June 4). Building Envelope Design Guide – Exterior Insulation and Finish System (EIFS). Retrieved from http://www.wbdg.org/design/env_wall_eifs.php
11. Hunter Douglas Contract. (2013). Wood Linear. Retrieved from <http://www2.hunterdouglascontract.com/en-GB/facades/open/linear/wood/index.jsp>

Appendix B: The Green Building Movement and International Building Code

Author: Camille Levy

The construction industry is increasingly under pressure to be more environmentally friendly and have less of a negative impact on the Earth's atmosphere. Along with this, building designs are likewise being pushed towards greater energy efficiency and sustainability. These two campaigns along with an increase in environmental awareness and minimization of impact are a part of the 'green movement' [1]. The need for energy efficient buildings has led to unconventional building designs and materials. These materials aim to be more lightweight and environmentally resourceful, however their effects on fire performance often aren't considered before their use in buildings.

Recently there has been an increase in the literature addressing the problem that new 'green' designs pose to fire safety. FM Global's report "The Influence of Risk Factors on Sustainable Development" examines the lifecycle carbon emissions of buildings when important hazards such as fires are involved. They found that fire hazards contribute up to 14% of the carbon emissions of a building in its lifecycle often exposed to substantial fire hazards [2]. It's important that along with advances in the 'green' movement, parallel advances with relative fire codes and enforcement of these codes are put into place.

One key example of this is the guide that the National Association of State Fire Marshals produced in 2010; "Bridging the Gap: Fire Safety and Green Buildings", which discusses the importance of this issue. Relative to building exteriors and facades, the guide discusses the impacts of 'green' insulation materials in section IIIA. The NASFM brings up an important point in this section; the energy efficient facades most often use foam as insulation. This poses a risk to firefighters when they need to move up the exterior of a building using these foam insulated facades. There can be difficulty identifying what type of insulation is used for these facades, which is important for the fire service because these lightweight foam materials can't hold heavy loads such as firefighters [1]. The guide notes that foam insulation should be installed strictly following the manufacturer's instructions. Any mistakes with the installation can lead to greater fire hazards [1].

Along with input from the fire service industry, building codes for the 'green' energy efficiency movement have been produced in recent years. The International Code Council put out the International green Construction Code [3] in 2012. This provides a small but necessary guide to 'green' building requirements and their construction. Section 507.1 addresses exterior wall coverings and says they must comply with chapter 14 of the IBC [3].

International Building Code

The International Building Code is the primary standard international code relating to building construction. The scope of the code is intended to protect the public's health & safety and it is constantly revised every three years to allow for the use of new materials [4].

When a building is initially being constructed, it's important to determine what type of construction the building falls under in the IBC. Chapter six defines five types of building constructions

that have certain requirements based on each type. Section 602 lays out the construction classifications and section 603 states requirements for combustible materials in construction types I and II [4]. Types I and II are said to have exterior and interior load bearing and nonbearing walls made of noncombustible materials. Section 603 details the exceptions to this noncombustible requirement for types I and II because under specified circumstances combustible materials are permitted. Type III construction is defined as having noncombustible exterior walls and any code approved material for interior walls. Type IV construction uses noncombustible materials for the exterior walls and solid or laminated wood for interior surfaces. Type V construction is considered to be the miscellaneous classification because both exterior and interior walls can be made of any acceptable material.

Section 603 outlines the exceptions for type I and II buildings regarding the use of combustible materials. The code states that foam plastics may be used according to the specifications in chapter 26. This is relevant to our research because we are specifically looking into Fiber Reinforced Polymers used for exterior walls, which is discussed in section 2612, however general specifications are given in section 2603.5 for the use of plastics for exterior walls of buildings of any height.

The scope of this project is concerned with vertical and lateral flame propagation, which is addressed in section 2603.5.5. The IBC says that regarding this type of flame propagation, the exterior wall assembly must be tested according to the standard NFPA 285. While there are certain exceptions put forth in the IBC, generally speaking, combustible materials for exterior walls may be used if the assembly is in compliance with NFPA 285 [4].

Chapter 26 of the code also states the other NFPA standards that exterior plastic assemblies must comply with in order to be IBC compliant. Section 2603.5.7 is about ignition of the assembly, stating that exterior walls must comply with NFPA 268 [4]. While these topics are not the primary focus of our project, they must still be met in order to comply with the Code.

Works Cited:

[1] National Association of State Fire Marshals. (2010). Bridging the Gap: Fire Safety and Green Buildings [Guide]. Retrieved from <http://www.firemarshals.org/pdf/FireSafetyGreenBuildingHiResFINALv3sec.pdf>

[2] Gritz, L., Doerr, W., Bill, R., Ali, H., Nong, S., & Krasner, L. (2009). *The influence of risk factors on sustainable development*. (Technical). FM Global.

[3] IgCC, ICC. "International green construction code." *International Code Council, Inc. (formerly BOCA, ICBO and SBCCI)* (2012): 60983-0598.

[4] IBC, ICC. "International building code." *International Code Council, Inc. (formerly BOCA, ICBO and SBCCI)* 4051 (2006): 60478-5795.

Appendix C: IBC Requirements for External Facades

Author: Camille Levy

The 2012 IBC requirements relative to external facades can primarily be found in three chapters:

- Chapter 7, Fire & Smoke Protection Features
- Chapter 14, Exterior Walls
- Chapter 26, Plastic

Fire & Smoke Protection Features (Chapter 7)

Section 705.5 discusses the fire resistance ratings for exterior walls [1]. If the exterior wall is less than 10 feet from the property line or another building on the same property (fire separation distance), then the wall must be rated for both the inside and outside surfaces of the wall. If the fire separation distance is greater than 10 feet, the wall only needs to be rated for the interior.

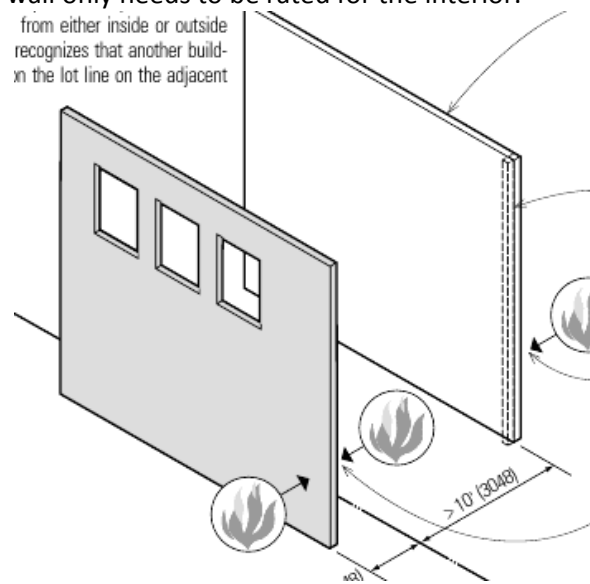


Figure 18: Fire Separation Distance shown with two buildings on one property [2]

Exterior Walls (Chapter 14)

Section 1408 of the IBC specifies the requirements for EIFS. The EIFS must be designed to meet the requirements of ASTM E2568 relative to the wall's performance (ASTM- American Society for Testing and Materials). EIFS are required to have an exterior wall envelope, which provides protection from condensation and the collection of water inside the assembly. A drainage system for behind the EIFS is also required from the standard. The system must have at least an average efficiency of 90% when tested according to ASTM E2273. Most of the performance requirements for EIFS in this section pertain to their resistance to harsh weather such as wind and rain.

Plastic (Chapter 26)

Section 2612 lays out the requirements for the usage of fiber reinforced polymer (FRP's) in building construction. This pertains to EIFS because sometimes fire reinforced polymer materials are used for the facades. Section 2603.5 states that "Exterior walls of buildings of Type I, II, III or IV construction of any height shall comply with Sections 2603.5.1 through 2603.5.7." [1] The referenced sections pertain to the

fire rating, thermal barrier, flame spread, fire propagation, and labeling of the exterior wall. If the building is 40 feet or less above grade, than it is exempt from section 2612.5. Buildings are also exempt if the following criteria from section 2612.5 are met:

“1.1. The fiber-reinforced polymer shall not exceed an aggregate total of 20 percent of the area of the specific wall to which it is attached, and no single architectural element shall exceed 10 percent of the area of the specific wall to which it is attached, and no contiguous set of architectural elements shall exceed 10 percent of the area of the specific wall to which they are attached.

1.2. The fiber-reinforced polymer shall have a flame spread index of 25 or less. The flame spread index requirement shall not be required for coatings or paints having a thickness of less than 0.036 inch (0.9 mm) that are applied directly to the surface of the fiber-reinforced polymer.

1.3. Fireblocking complying with Section 718.2.6 shall be installed.

1.4. The fiber-reinforced polymer shall be installed directly to a noncombustible substrate or be separated from the exterior wall by one of the following materials: corrosion-resistant steel having a minimum base metal thickness of 0.016 inch (0.41 mm) at any point, aluminum having a minimum thickness of 0.019 inch (0.5 mm) or other approved noncombustible material.” [1]

Works Cited

[1] IBC, ICC. "International building code." *International Code Council, Inc. (formerly BOCA, ICBO and SBCCI)* 4051 (2006): 60478-5795.

[2] Ching, Francis D. K., and Steven R. Winkel. *Building Codes Illustrated, Volume 6 : Building Codes Illustrated : A Guide to Understanding the 2012 International Building Code (4th Edition)*. Somerset, NJ, USA: Wiley, 2012. Web.

Appendix D: NFPA 285 Details

Author: Jared Harbold

The following is a list of specific information within NFPA 285 which may prove useful to us in design of our full scale fire test.

Burners 4.4:

- The window gas burner shall consist of a 60 inch length of nominal 2 inch outside diameter pipe having a .5 inch wide x 44 inch long slot
- Burner shall be supplied gas at both ends through nominal 1 inch outside diameter pipe
- Burner shall be wrapped with a layer of nominal 1 inch thick nominal 8lb/ft³ density ceramic fiber blanket
- Burner shall be placed so it is centered horizontally in the first-story test room window opening
- The horizontal centerline shall be located 9 inches below the bottom surface of the window opening header
- The vertical centerline shall be placed between 0 and 5 inches from the exterior face of the wall
- The final position of the burner from the exterior wall shall be determined by calibration procedure
- Burners must be in accordance of Table 4.4.13 and attain each prescribed gas flow rate within 15 seconds

The burners are an integral part of the success of the experiment. In order to make sure that the burners are positioned in the exact right position, extensive pretesting must take place. During these tests, the prescribed gas rates must be met in order to remain consistent over multiple test runs. Because of this, calibration is extremely important. Additionally, through the NFPA 285 test, the window burner is not activated until 5 minutes after the room burners begin. It seems as though our test will include only the window burner, so the first 5 minutes of the test may be ignored.

Test Specimen 5:

- The test specimen must be at least 17.5 feet high and 13.3 feet wide
- The edges of the test specimen must be placed as follows:
 - Below the top of the first-story slab, not less than 2 in
 - Above the top of the top slab, not less than 2 ft
 - Beyond the outside face of each side wall, not less than 1 ft
- The test specimen must completely cover the front space besides the window opening
- Window must be 30 inch high x 78 inch wide with a sill height of 30 inches above the top of the first-story test room slab
- The window opening shall be centered horizontally with respect to the test room

5.7.3* Where the test specimen contains vertical or horizontal joints or seams, joints or seams representative of standard construction practices shall be incorporated into the test specimen [1]

The exterior wall requirements for NFPA 285 are 17.5 feet high and 13.3 feet wide. These dimensions may prove to be optimal for our full scale test. Additionally, specific requirements about how to place

the material on the exterior are also important to acknowledge. Specific window placement is important as this is the main source of our burners. Finally, all joints and seams (vertical and horizontal) located within the normal construction of an exterior material shall be dealt with as the manufacturer instructs.

Temperature Measurements 6.1:

Measurements shall be taken at the following locations:

- Exterior wall surface of the test specimen
- Combustible insulation in the exterior wall panel of the test specimen
- Cavity air space within the test specimen
- Wall cavity insulation and stud cavity insulation
- Interior surface of the test specimen [1]

The measurements of temperature will be essential for us to make any conclusions for our experiments. While the temperature measurements listed above are indicative of the NFPA 285 test, which we will most likely be using, they offer insight into different areas where we should place our thermocouples. Because of the differences between panels, it is imperative that we receive specifications regarding the panels which we will be testing in order to determine the best placement of our thermocouples in our experiment.

Fire Test Procedures 8.1:

Ambient conditions during the test:

- Temperature between 50 and 90 degrees Fahrenheit
- Relative humidity between 20 and 80 percent
- Airflow across the exterior face of the test specimen shall be less than 4.4ft/second [1]

Ambient conditions must be recognized during our test in order to eliminate discrepancies. If possible, constant temperature, humidity, and airflow during each test would be optimal in order to eliminate variables.

Data Collection and Observations 9:

- Video recording shall start at least 1 minute before ignition and not end before 10 minutes after gas supply to the burners is shut off
- Data recording must occur at least every 15 seconds
- Pictures shall be taken during construction, during the test at least once every minute, and after the fire test
- Test specimen shall be dismantled and examined following the end of the test [1]

All of the above specifications can be directly used in our own experiment to create clarity and increase depth of learning following the end of the test

Conditions of Acceptance 10:

- In order to pass, the test specimen must not allow flame propagation to occur either vertically or horizontally beyond the area of the flame plume by the window burner
- Flame propagation has occurred if any of the following is measured:
 - A temperature of 1000 degrees Fahrenheit is measured by any of the thermocouples on the slab located above the second floor

- Flames greater than 10 feet above the window opening
- Flames greater than 5 feet horizontally from the centerline of the window
- Temperature within the combustible components cannot exceed a 750 degrees Fahrenheit increase
- Temperatures in the wall cavity and stud cavity insulation shall not exceed a 750 degree Fahrenheit increase.
- Temperatures measured 1 inch within the second story test room shall not exceed 500 degrees Fahrenheit
- Flames cannot occur within the second story test room
- Flames cannot occur beyond the intersection of the test specimen and the side walls [1]

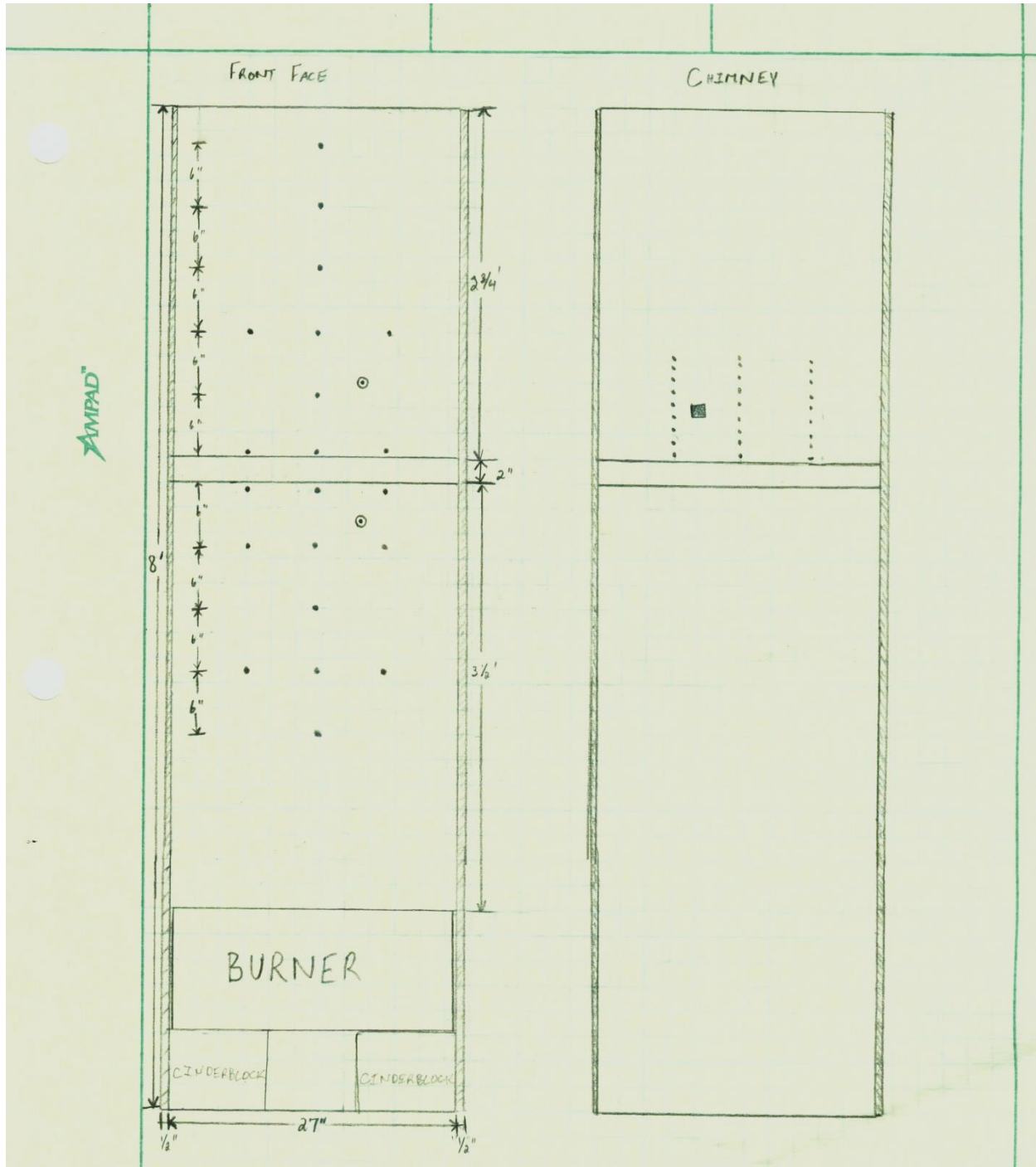
A pass or fail designation will allow us to understand if gaps do or do not lead to differences in flame propagation. By following all of the pass/fail criteria stated above, we will be able to change our gap sizes and easily understand if any of these variables result in changes in flame propagation.

Works Cited

NFPA. (2012). *NFPA 285: Standard Fire Test Method for Evaluation of Fire Propagation Characteristics of Exterior Non-Load-Bearing Wall Assemblies Containing Combustible Components*. Quincy, MA

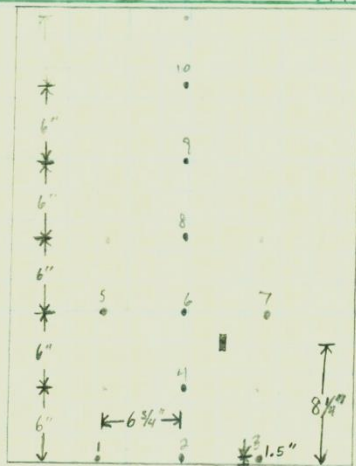
Appendix E: Assembly Details

Author: Jared Harbold

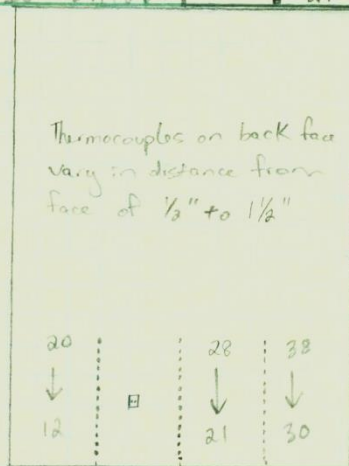


INSTRUMENTATION LAYOUT

KEY:
 • = Thermocouple
 □ = Thin Skinned Calorimeter
 ■ = BDP



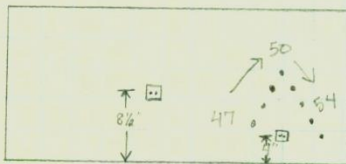
FRONT FACE - ABOVE GAP



BACK FACE - ABOVE GAP

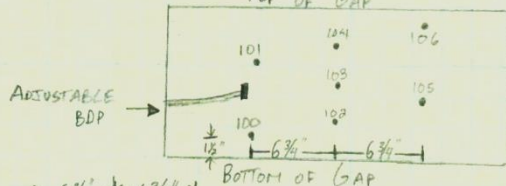
Thermocouples on back face vary in distance from face of $\frac{1}{3}$ " to $\frac{1}{2}$ "

*1" vertically between thermocouples



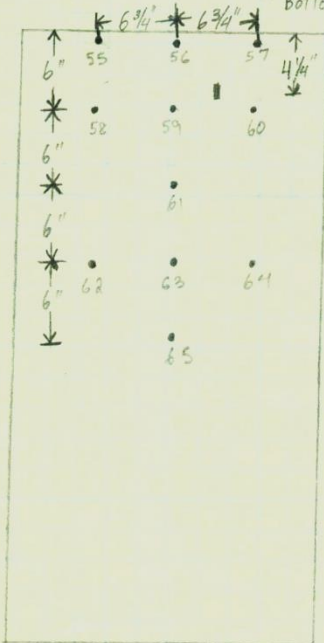
TOP OF GAP

Thermocouples in this cluster vary in height from $\frac{1}{4}$ " to $1\frac{3}{4}$ "

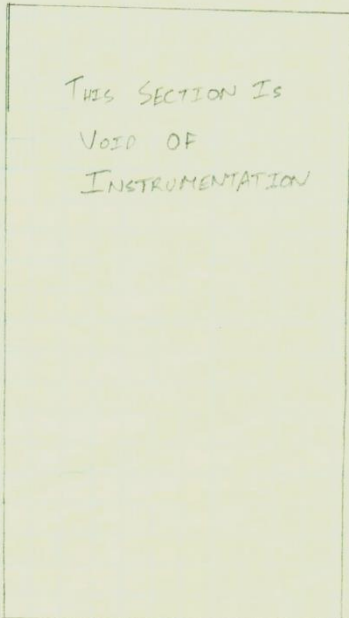


BOTTOM OF GAP

ADJUSTABLE BDP



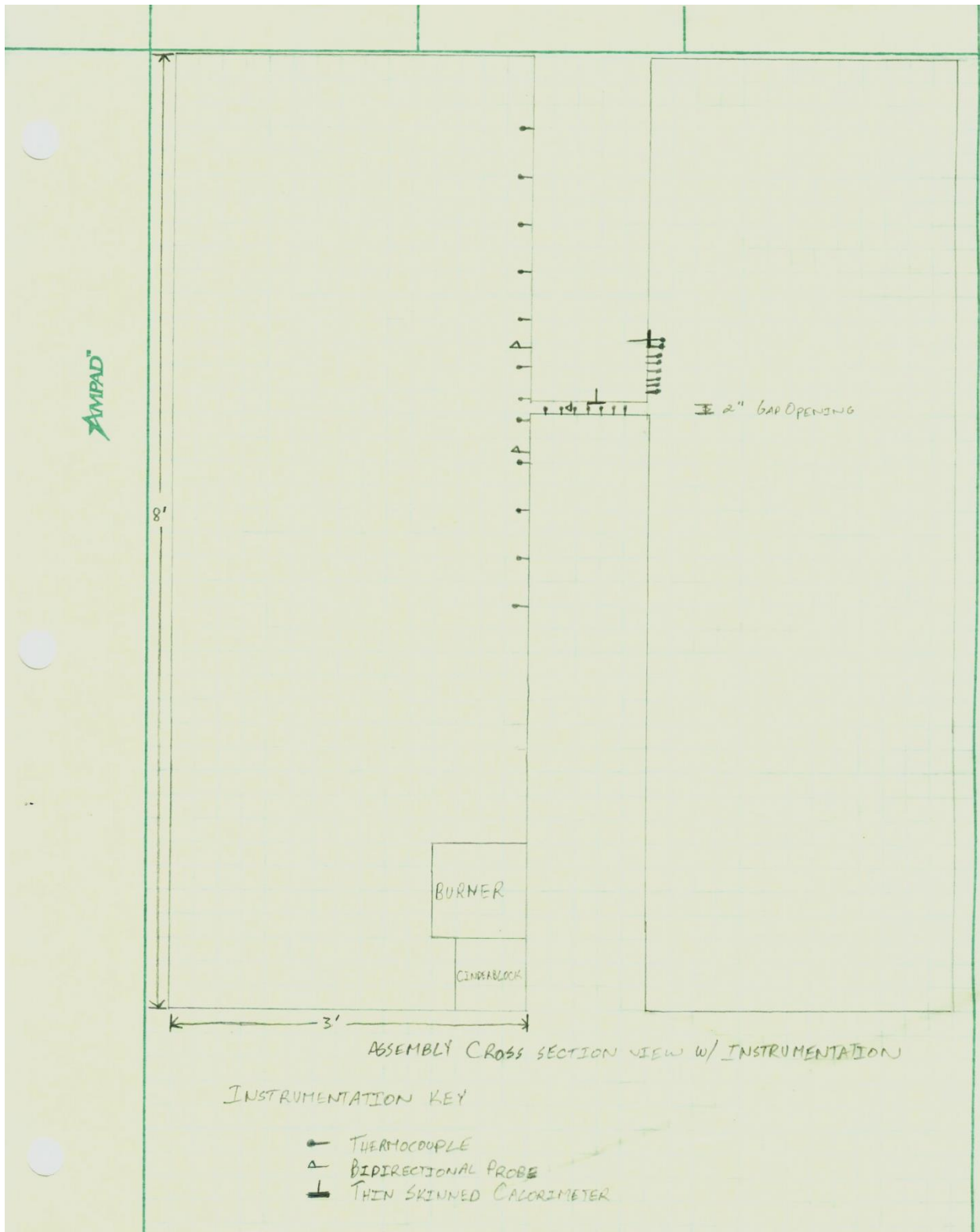
FRONT FACE - BELOW GAP



BACK FACE - BELOW GAP

THIS SECTION IS VOID OF INSTRUMENTATION

AMPAD



Appendix F: Instrumentation

Author: Camille Levy

Bidirectional probes

Bidirectional probes measure the flow velocity of a fluid using a pressure differential [1]. Figure 1 shows a front and cross sectional view of a bidirectional probe for reference. This pressure differential can then be used to calculate the subsequent flow velocity entering the probe.

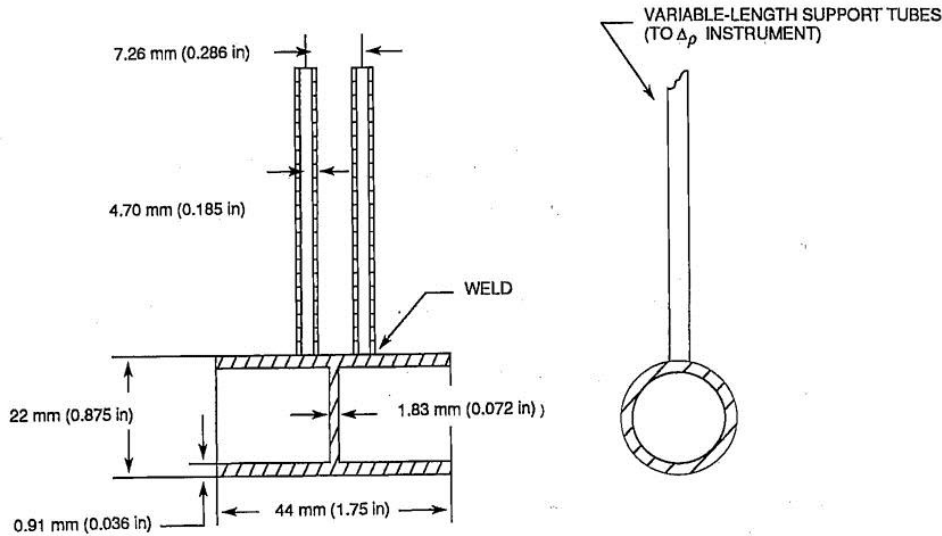


Figure 19: Bidirectional Probe [2]

When using the probes to measure air velocity, the measurements are accurate at a maximum angle of 50 degrees between the tube and the air flow [1]. This “angular insensitivity” as it’s termed in McCaffrey and Heskestad [1] is one of the major factors that makes this instrument more effective for fire applications. Compared to a pitot tube, the bidirectional probe can get much more accurate readings of flow velocity [1]. Another defining advantage the probe has on the Pitot tube and other flow measuring devices is its bi-directionality [1]. The fact that no predetermination for which way the flow will be moving is required in order to set up the instrument properly is a huge advantage. The probe can be placed in a setup without knowing exactly which direction the air will flow. This also allows the probe to take measurements even when the flow velocity reverses [1].

Calculating Velocity

Hamins’ experiment used thermocouples as this experiment did, with the thermocouples being placed 1 cm above the center of each of the bidirectional probes. The equation for gas velocity is shown below:

$$v = \frac{1}{K} \sqrt{\frac{(2\Delta p)}{\rho}}, \quad \text{where } \rho = \frac{(M)P_{\text{absolute}}}{RT}.$$

[3]

As shown in the above equation, the gas density was calculated based upon the ideal gas law for Hamins’ experiment. K is assumed as 1.08 based upon McCaffrey and Heskestad’s research. We are assuming that the gas is acting as an ideal gas for this equation to be used accurately.

Differential Pressure Transducer

The pressure differential measured by the bidirectional probe is merely physical on its own. The probe must be connected to a sensor that converts the measured physical change into an electrical signal that can be recorded in a computer. For this project, an Omega PX277-01D5V differential pressure transducer was used. This differential pressure transducer, or DPT, can be seen below.

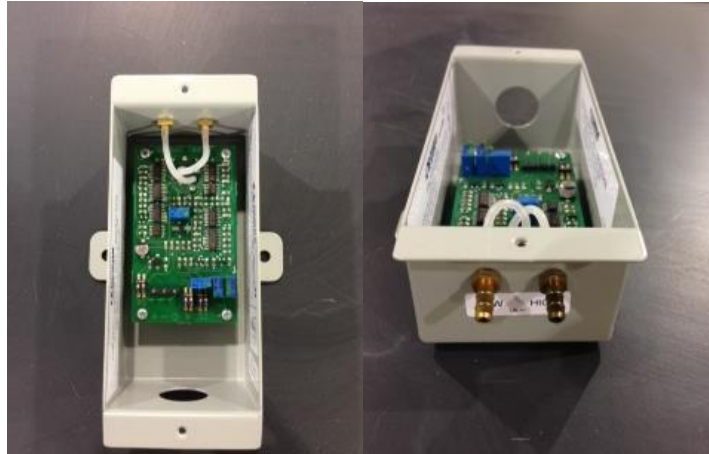


Figure 20: Differential Pressure Transducer

A direct current power supply is needed to run the DPT since it's an electrical component. A supply of 12 to 40 VDC is recommended in the Omega PX277 manual. The Fire Lab power supply used for this setup is shown below.



Figure 21: Power Supply

Thermocouples

General Information

Thermocouple sensors are used to measure temperature. Thermocouples use two conductive materials that should be very different in properties. When the thermocouple is heated up, one of the metals is used as a reference temperature to record any temperature gradients [4]. When a

temperature change occurs, a voltage is produced [5]. Unlike bidirectional probes and thin skin calorimeters, the thermocouple directly outputs the temperature data with no further calculations needed. These sensors are used for a wide range of applications because of their simplicity and durability.

There are many types of thermocouples due to the abundance of metal alloys. Different combinations of two alloys provide more accuracy and better results for various applications of the instrument [5]. Thermocouples are usually chosen based on the sensitivity needed for the specific discipline it will be used for. Platinum thermocouples are generally the most stable instruments because they use platinum instead of nickel, iron, or chrome [5]. These types of thermocouples would be most useful for our experiment because they can withstand very high temperatures without any failures [5]. While these types are fairly expensive compared to the regular thermocouples, it might be worth the cost because of their high temperature capabilities.

One important factor to consider is the exposure time that the thermocouples will endure caused by the fire. Thermometrics Corporation states that type K thermocouples can only be stable for short periods of time when exposed to high temperatures [6], however type K wires are generally chosen for use in thermocouples in fire testing.

Thin-Skin calorimeters

Thin skin calorimeters are used to measure heat fluxes on flat surfaces and are sometimes described as plate thermometers [7]. Using a metal material with known properties and measurements, the calorimeters use a one dimensional heat transfer analysis to measure data. This is also known as a lumped analysis, which is what the team will be using for the experimental calculations. Figure 2 below provides a schematic of the typical thin skin calorimeter according to the ASTM E459 standard.

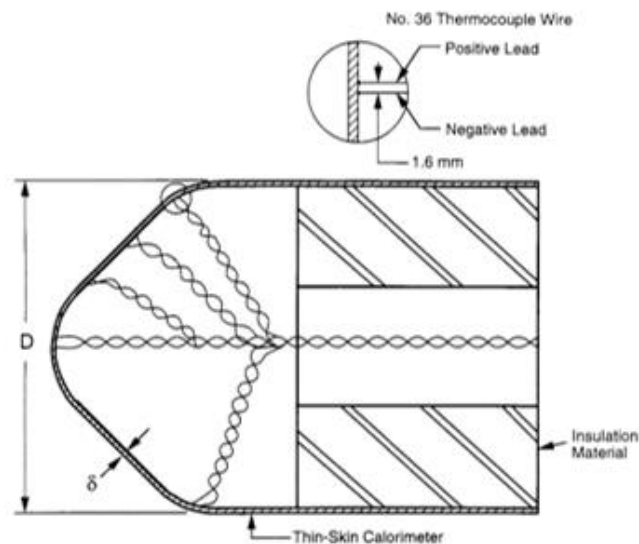


Figure 22: Thin-Skin Calorimeter Schematic [8]

It's important to understand the response time for the unheated (back) surface of the TSC compared to the heated front surface. The front surface exposed directly to the heat source is bound to heat up before the back surface does [8]. The initial response time is the time it takes for this back

unheated surface to heat up and reach the heated surface temperature [8]. The equation for response time is shown below:

$$\tau_r = 0.5 \frac{\rho C_p \delta^2}{k}$$

Figure 23: ASTM E459 Response Time Formula [8]

All necessary variables in the response time equation must be obtained based on the metal used in the thin skin calorimeter. A steel plate was used in the thin-skin calorimeter for this study. The necessary metal properties are as follows [9, 10]:

Specific heat: $c_p = 490 \frac{J}{kg K}$
 Density: $\rho = 7850 \frac{kg}{m^3}$
 Thickness: $\delta = 0.003 m$
 Thermal Conductivity: $k = 54 \frac{W}{m K}$

Response Time Calculation

$$\tau_r = 0.5 * \frac{7850 * 490 * (0.003)^2}{54} = 0.321 \text{ sec}$$

Calculating Heat Flux

The heat flux on the thin skin calorimeters can be calculated using the following equation from ASTM E459, the standard on thin skin calorimeter testing:

is approximated by a lumped parameter analysis:

$$q = \rho C_p \delta \frac{dT}{d\tau}$$

where:

- q = heat transfer rate, W/m^2 ,
- ρ = metal density, kg/m^3 ,
- δ = metal thickness, m ,
- C_p = metal specific heat, $J/kg \cdot K$, and
- $dT/d\tau$ = back surface temperature rise rate, K/s .

Figure 24: Heat Flux Formula [8]

It should be noted that the necessary properties for this calculation are based on the specific metal, not the substrate or the gas present.

Data

Acquisition System & LabVIEW

The instrument data is digitized using National Instrument's Data Acquisition System, or DAQ. This system allows instruments to be wired into physical input modules that communicate to the recording software based on the data type. For the thermocouples and thin skin calorimeters, a thermocouple input module was used since both instruments output temperature data. For the bidirectional probes/differential pressure transducers, a voltage input module was used because the

transducers output voltage data. The software used with the DAQ system is National Instrument's LabView program. This application is used for the data measurement and recording. Figure 7 shows a graphic representation of the DAQ System.

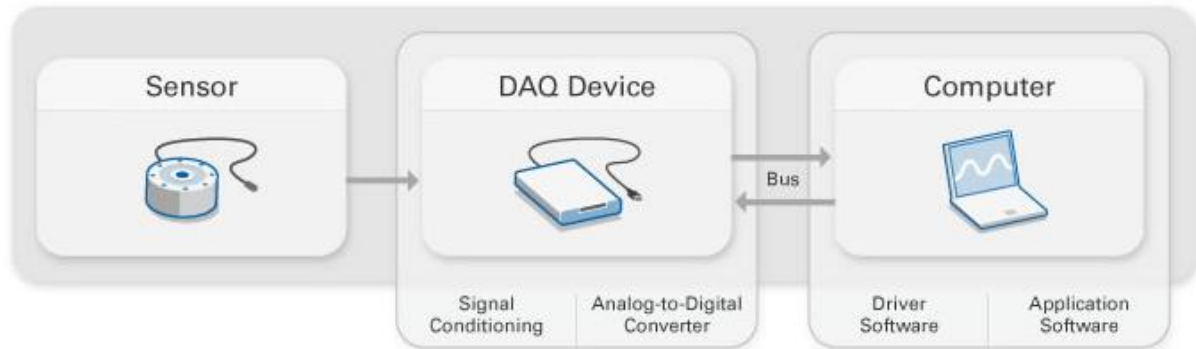


Figure 25: DAQ System Parts [11]

Checking Instrument Operation

Checking that instrumentation is working properly is of the utmost importance to the experiment. This allows the team to confirm that the devices are operating correctly, which is important when troubleshooting errors.

Thermocouples & Thin Skin Calorimeters

These two devices are fairly simple to check for proper operation. The wire is plugged into either a Voltmeter or the DAQ thermocouple input module and a temperature change is induced on the device. The team used either an electric hot air blower or a person's fingers to cause an increase in temperature. The voltmeter or DAQ software should show an increase in temperature measurement if the instrument is correctly setup.

Bidirectional Probes

Confirming the proper setup of the bidirectional probes is somewhat more complicated than the temperature measurements. The probe/DPT setup is used to measure an air flow which must be compared to a more accurate measurement of the same flow. A hot wire anemometer was used to accurately measure the air velocity for these checks. The source of the airflow is arbitrary to the check, as long as the flow is measured using both the anemometer and the probe. The team used a small electric fan on a lab bench for producing flow. A second airflow was used to confirm the probe setup; the Cone Calorimeter duct fan. The hot wire anemometer and electric fan can be seen in the figures below.



Figure 26: Hot Wire Anemometer



Figure 27: Close up of Anemometer Measuring Element



Figure 28: Electric Fan and Anemometer Setup

The probe/pressure transducer setup for this test was connected to a voltmeter. The obtained voltage differential was used to calculate the measured air velocity. This calculated velocity can be

compared to the hot wire anemometer measured velocity to determine if the probe setup is working correctly.

Works Cited

[1] McCaffrey, B. J., G. Heskestad. (1976). "A robust bidirectional low-velocity probe for flame and fire application." *Combustion and Flame* 26: 125-127.

[2] Heskestad, G. (1973) "Bidirectional flow tube for fire-induced vent flows. " Large-Scale Bedroom Fire Test". 11: 140-145.

[3] Anthony Hamins, Erik Johnsson, Michelle Donnelly, Alexander Maranghides, (2008). "Energy balance in a large compartment fire". *Fire Safety Journal*, Volume 43, Issue 3, Pages 180-188, ISSN 0379-7112, <http://dx.doi.org/10.1016/j.firesaf.2007.08.002>.
(<http://www.sciencedirect.com/science/article/pii/S0379711207000847>)

[4] "Temperature Measurements with Thermocouples: How-To Guide" *National Instruments*. National Instruments Corporation, 2014. Web. 08 Mar. 2014. <http://www.technologyreview.com/sites/default/files/legacy/temperature_measurements_with_thermocouples.pdf>.

[5] "Thermocouple Info." 2011. Web.

[6] Corporation, Thermometrics. "Type K Thermocouple." 2012. Web 2013.

[7] "Thin Skin Calorimeter - Fire Science Tools." Web 2013.
<<http://sites.google.com/site/srcombexp/home/instrumentation-diagnostics/thin-skin-calorimeter>>.

[8] American Society for Testing and Materials. Philadelphia. "Standard Test Method for Measuring Heat Transfer Rate Using a Thin-Skin Calorimeter." (2005).

[9] "Thermal Properties of Metals, Conductivity, Thermal Expansion, Specific Heat - Engineers Edge." *Engineers Edge*. N.p., n.d. Web. 12 Apr. 2014.

[10] "Thermal Conductivity of Some Common Materials and Gases." *Thermal Conductivity of Some Common Materials and Gases*. N.p., n.d. Web. 12 Apr. 2014

[11] "What Is Data Acquisition?" *National Instruments*. National Instruments Corporation, 2014. Web. 08 Mar. 2014. <<http://www.ni.com/data-acquisition/what-is/>>.

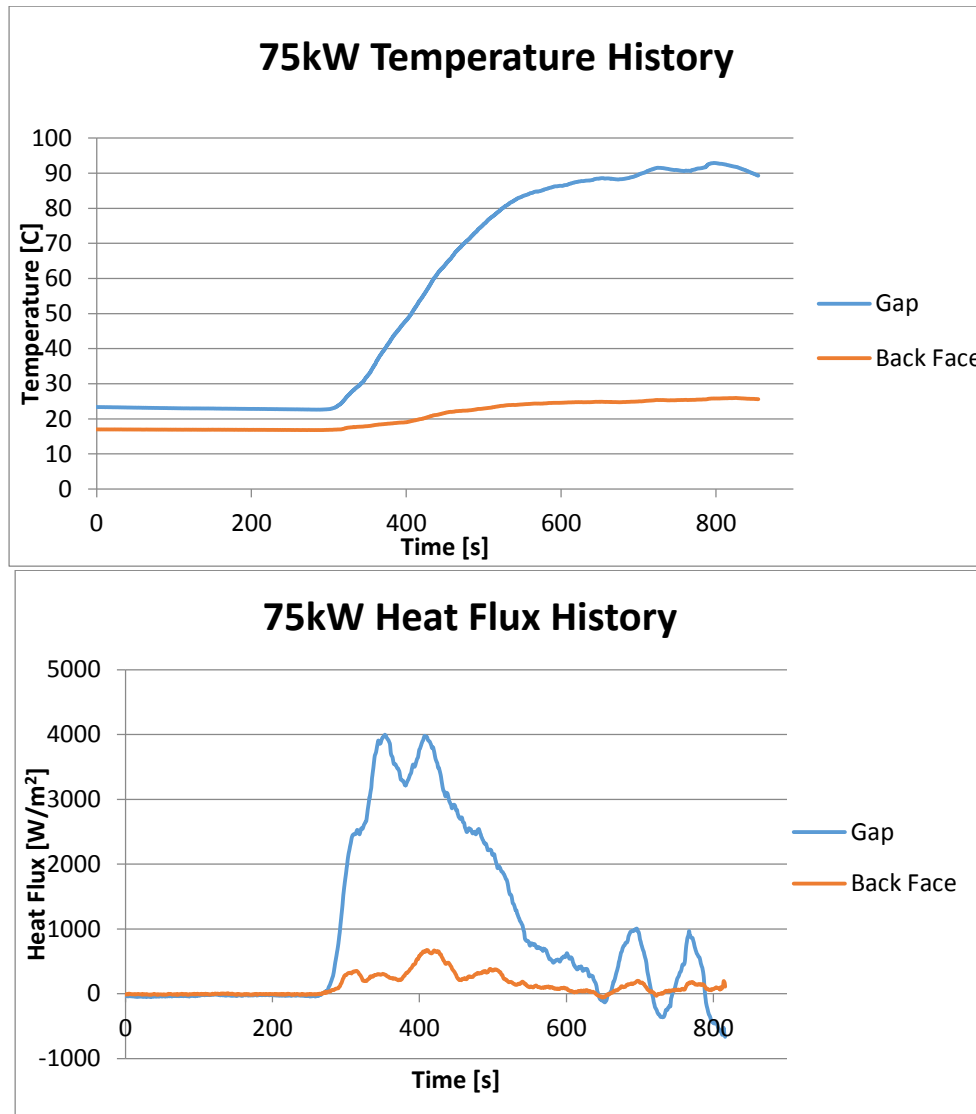
Appendix G: Raw Data (Bidirectional Probe/Thin Skin Calorimeter)

Author: Camille Levy

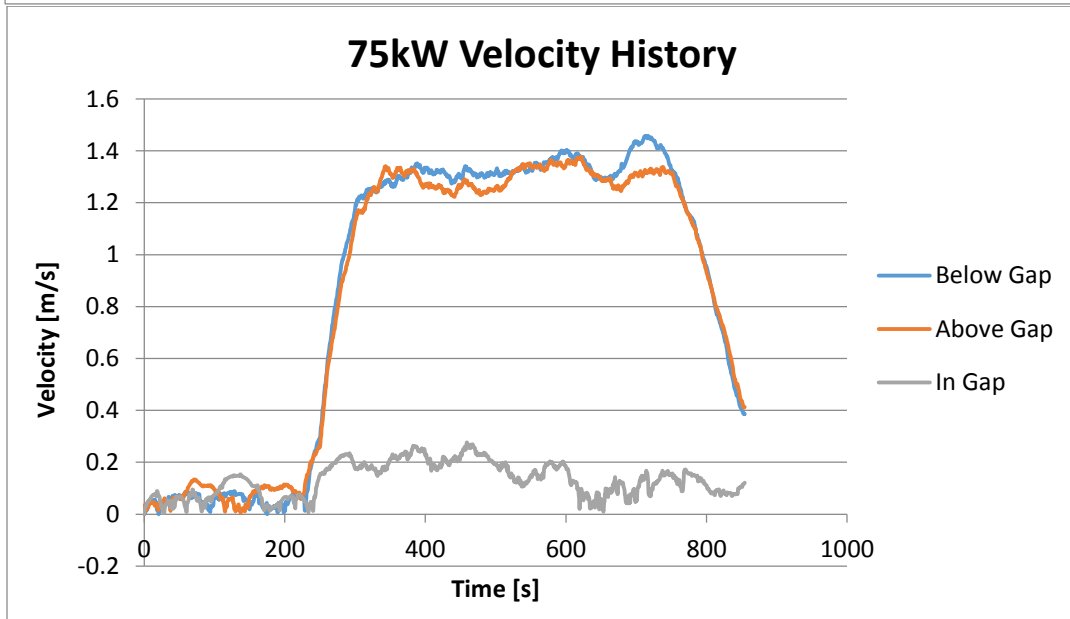
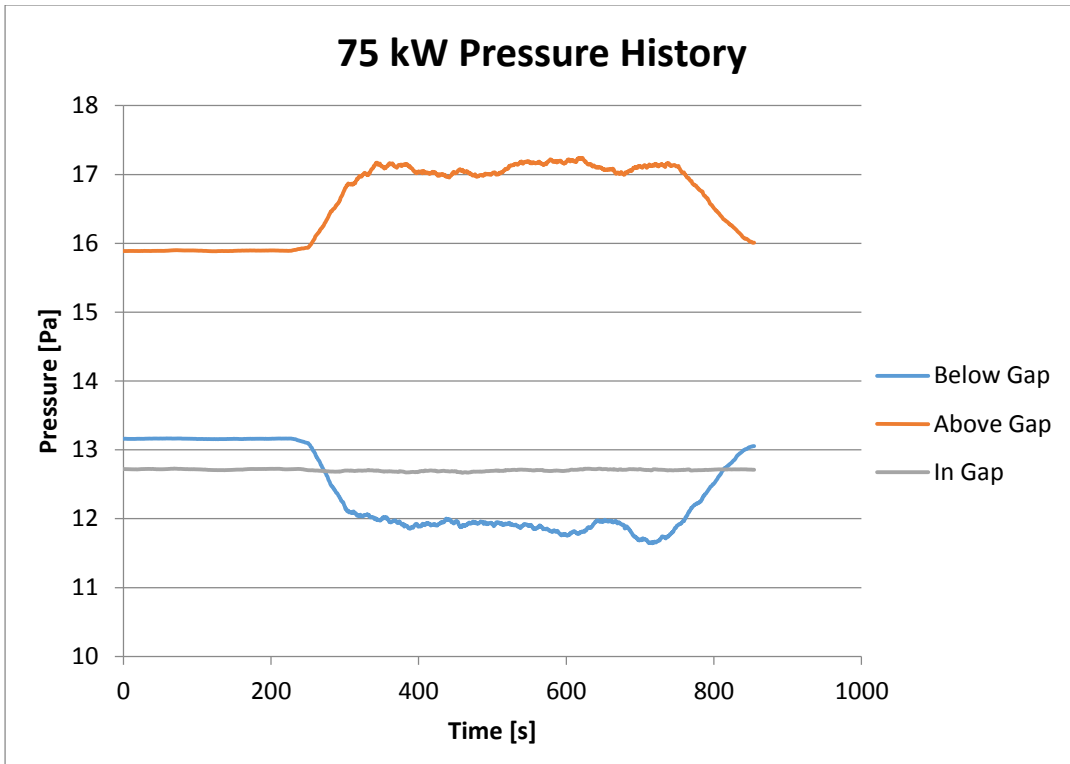
The data provided in this appendix is for one 75 kW and one 200 kW test. These were conducted on 4/04/2014. The raw temperature histories for two thin skin calorimeters are given as well as their subsequent heat flux histories. The pressure histories from the three bidirectional probes are given as well as their respective velocity histories. The plot legends specify curves with their instrument's location in the assembly.

75 kW Fire

Thin Skin Calorimeter Data

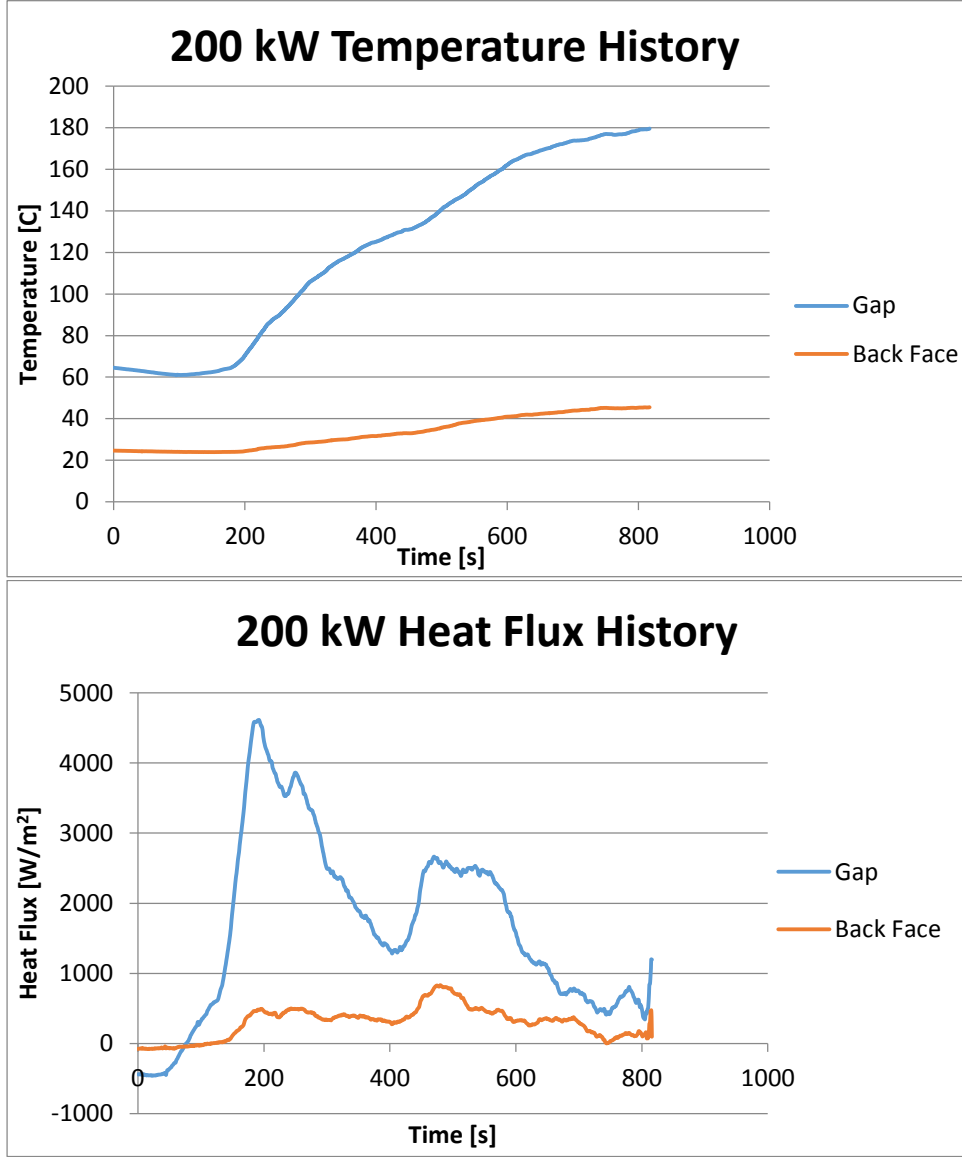


Bidirectional Probe Data



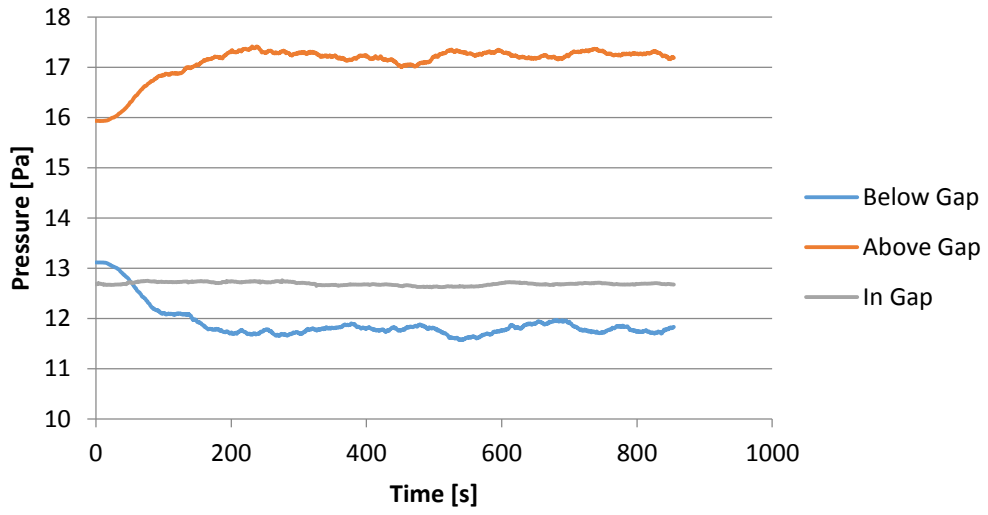
200 kW Fire

Thin Skin Calorimeter Data

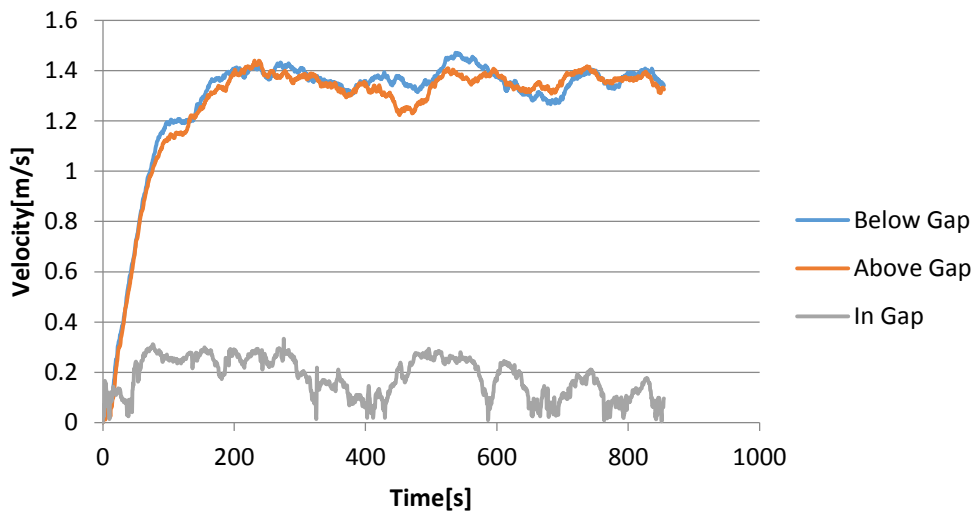


Bidirectional Probe Data

200 kW Pressure History



200 kW Velocity History

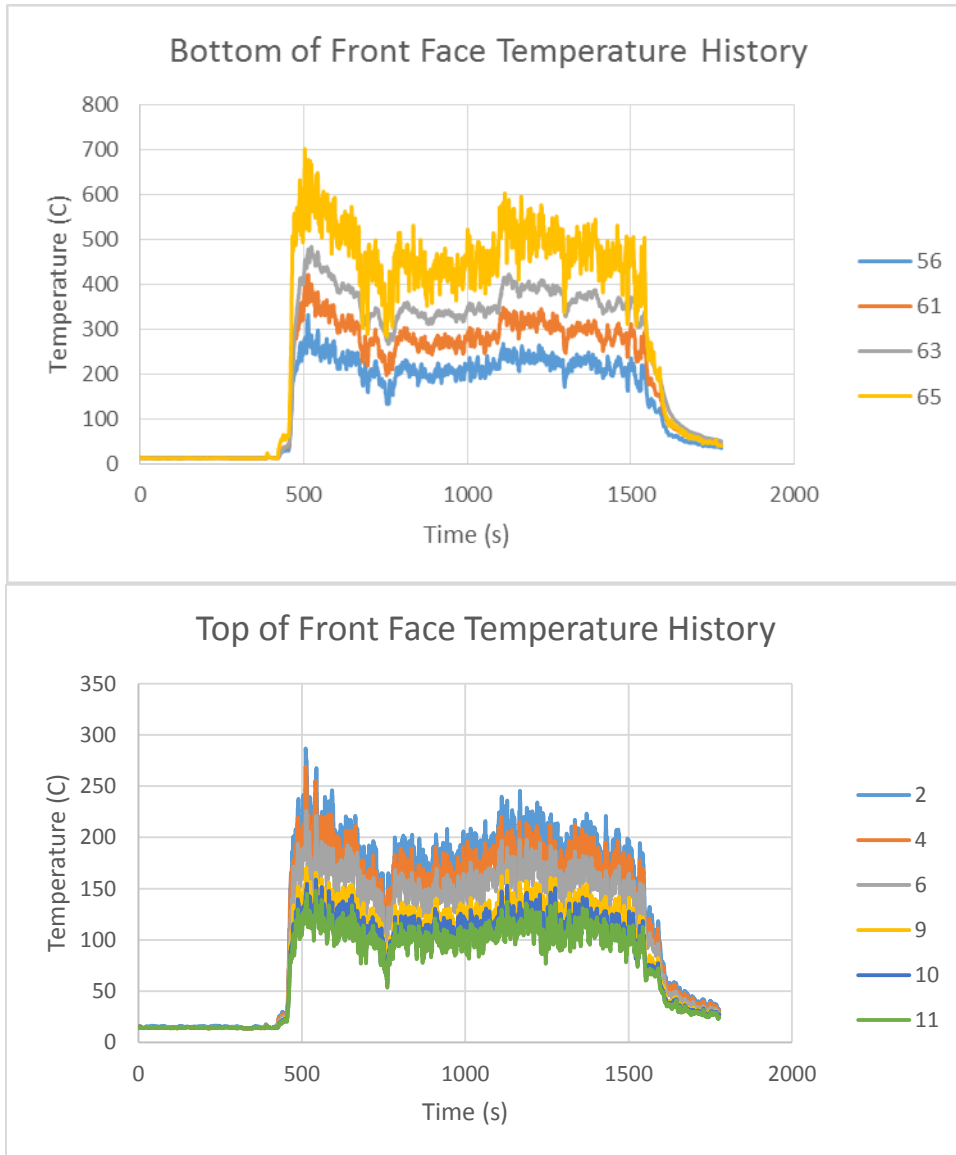


Appendix H: Time Averaging of Front Face Temperature Results

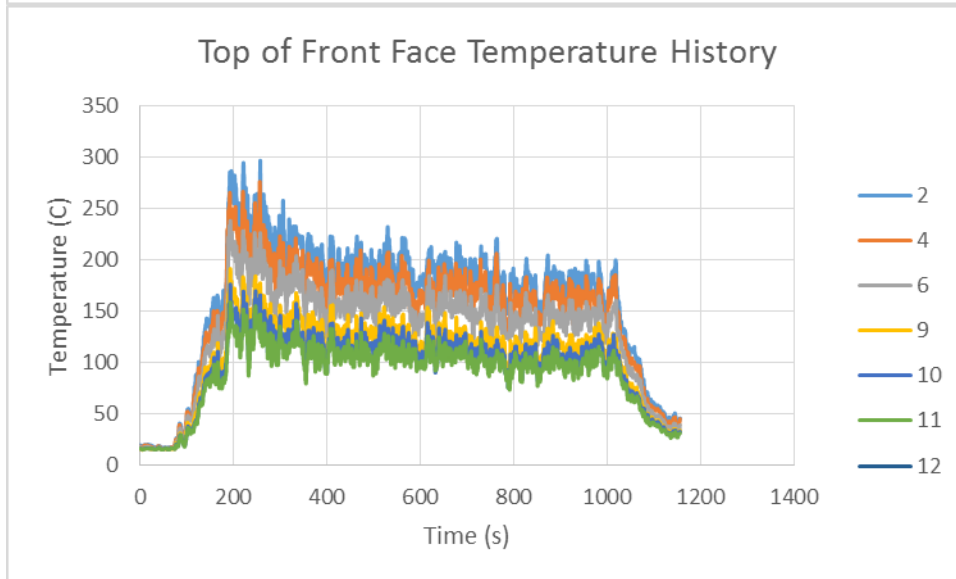
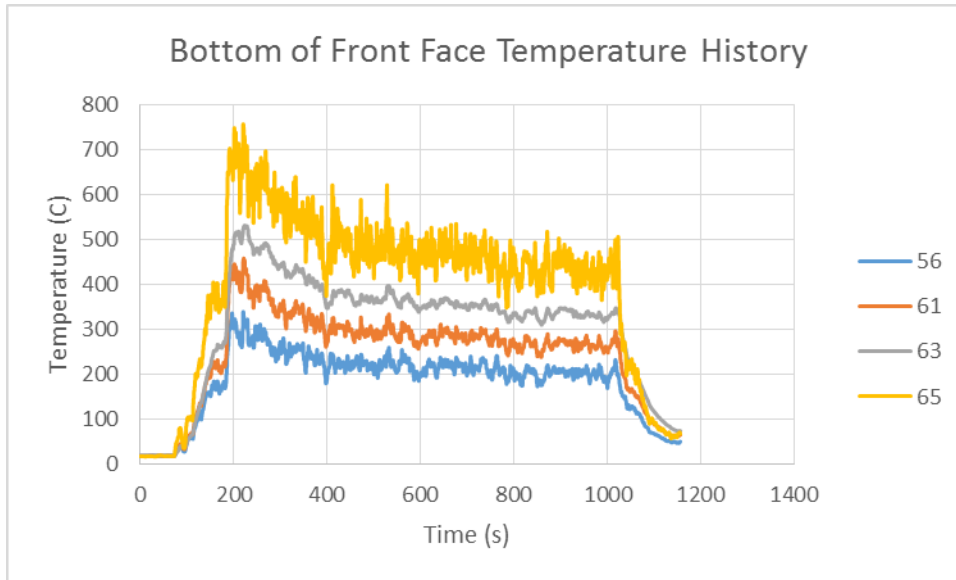
Author: Brendan Kerrigan

To determine the average temperatures the temperature histories were plotted and then averaged over the periods that appear to be approximately steady state. In each graph the numbers in the legend correspond to the thermocouple numbers as described in Appendix E. The temperature history graphs for the front face are as follows:

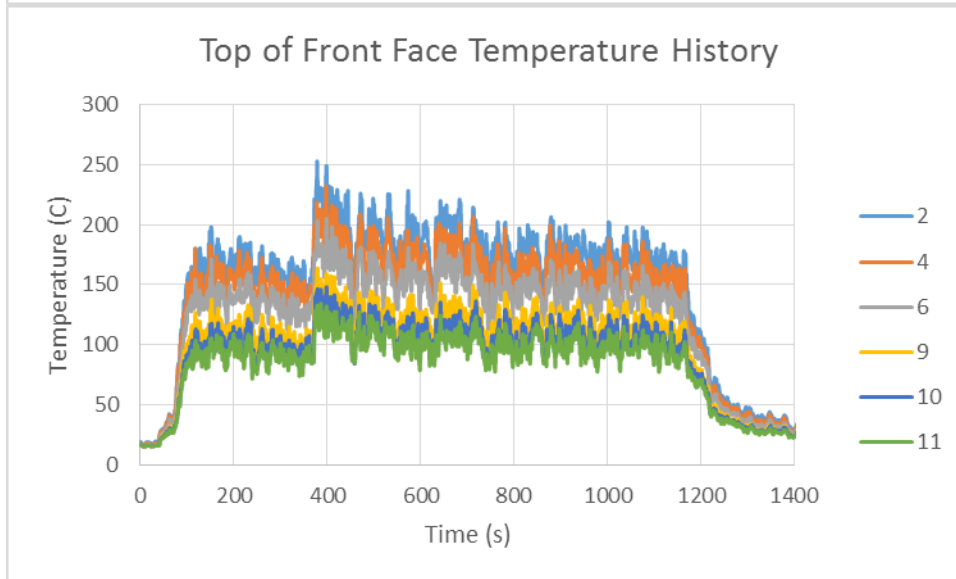
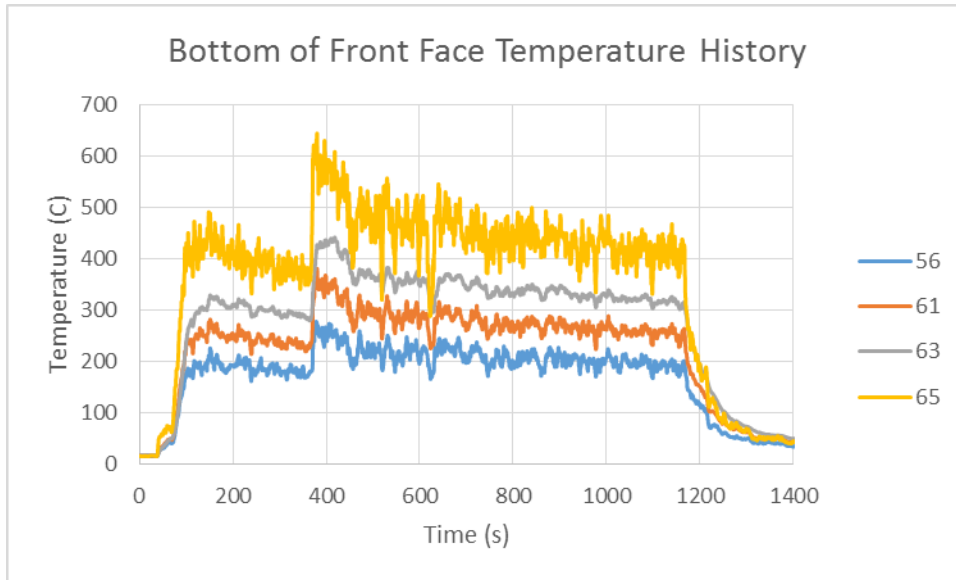
75 kW Test 1



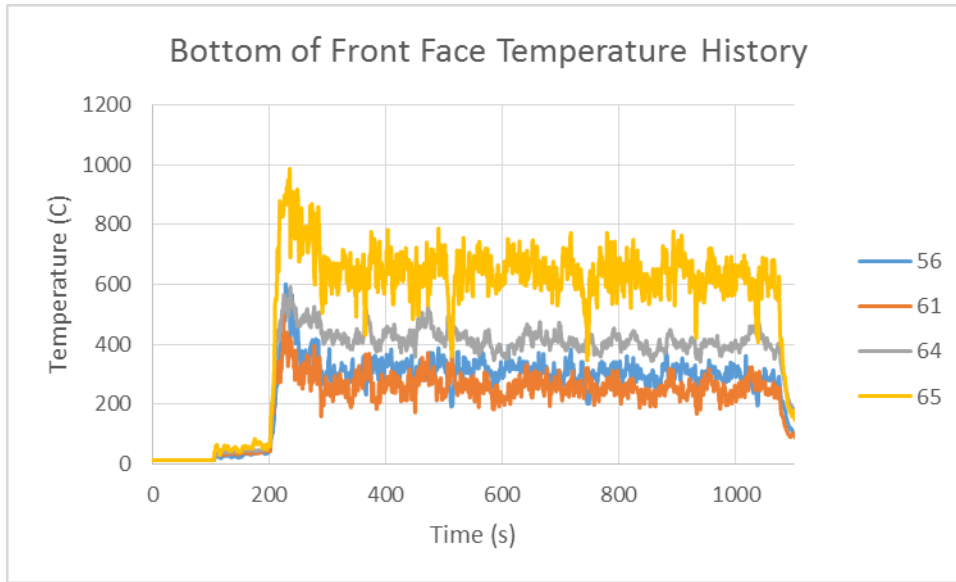
75 kW Test 2



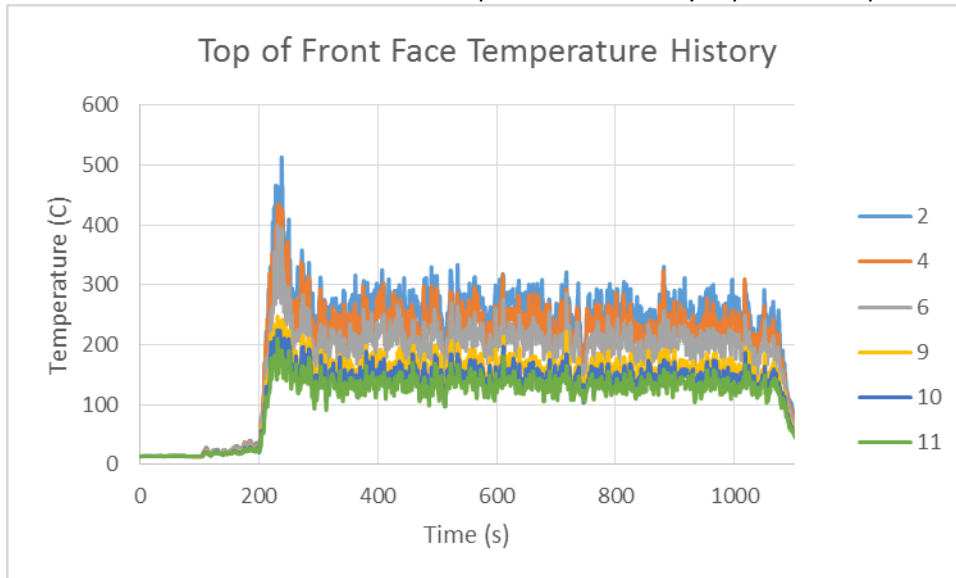
75 kW Test 3



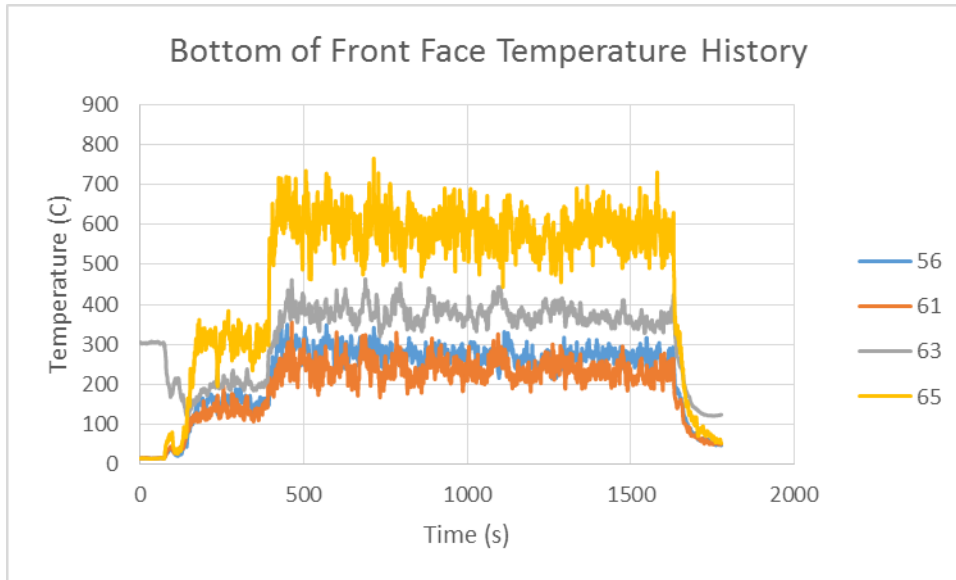
150 kW Test 1



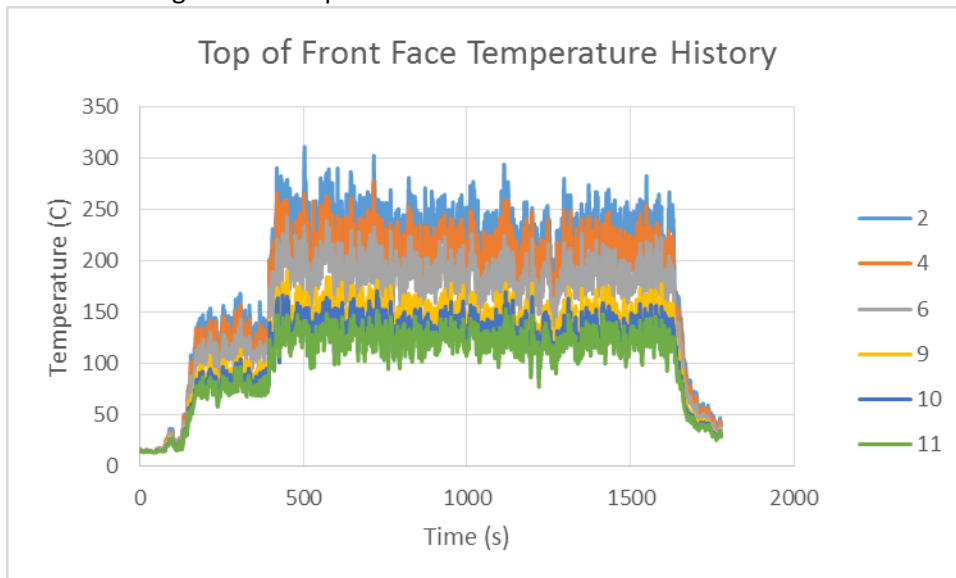
During this run we encountered issues with some of our instrumentation. Namely thermocouple 63 was broken for this test and thermocouple 61 consistently reported temperatures that were too low.



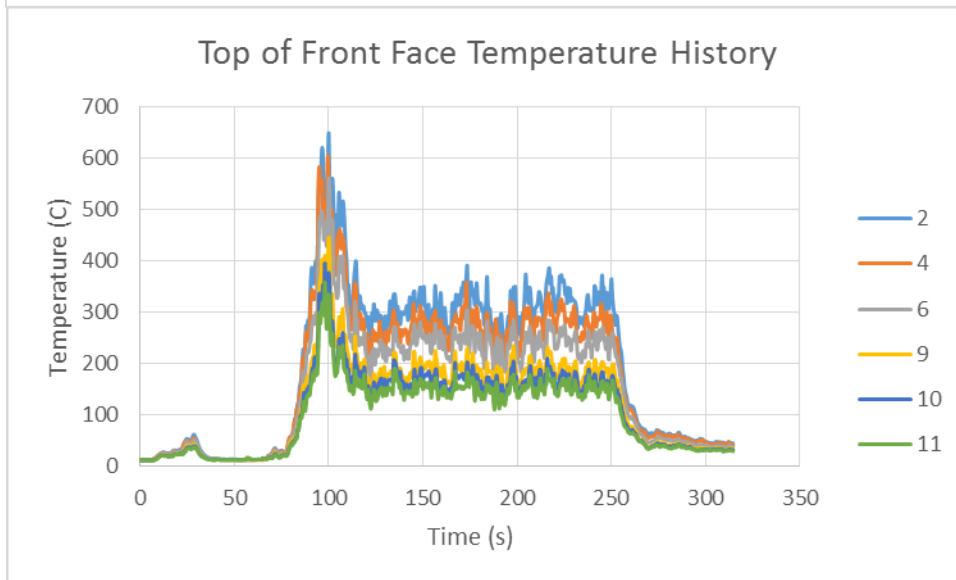
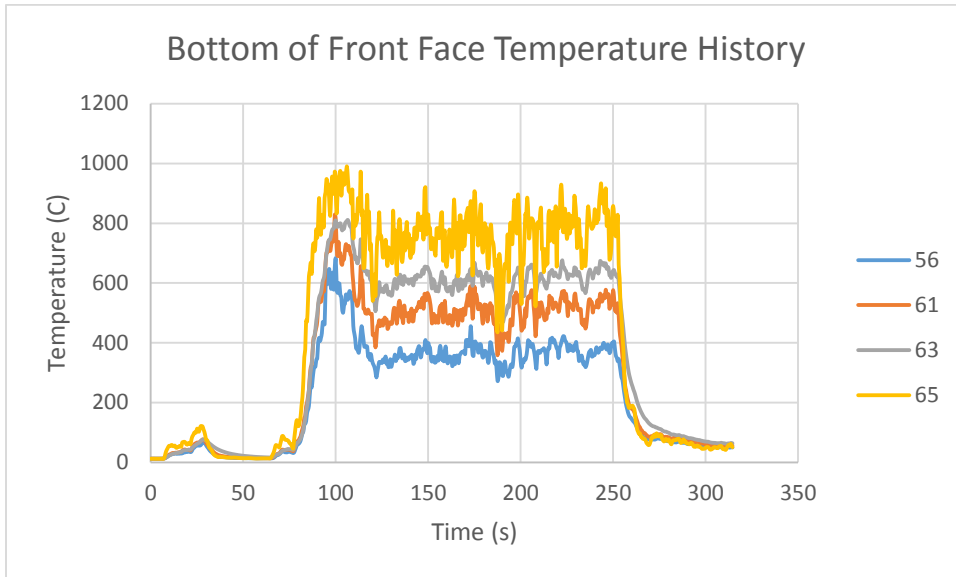
150 kW Test 2



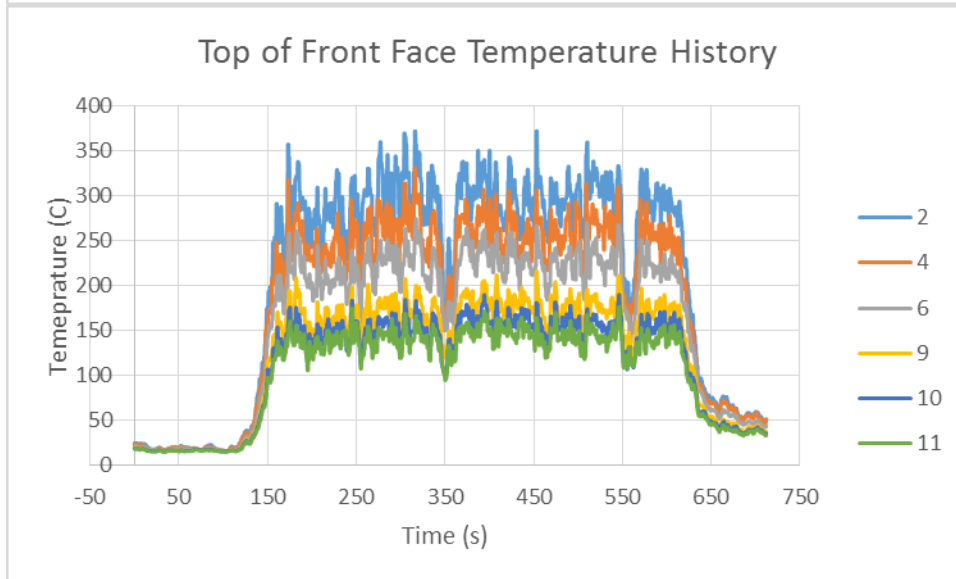
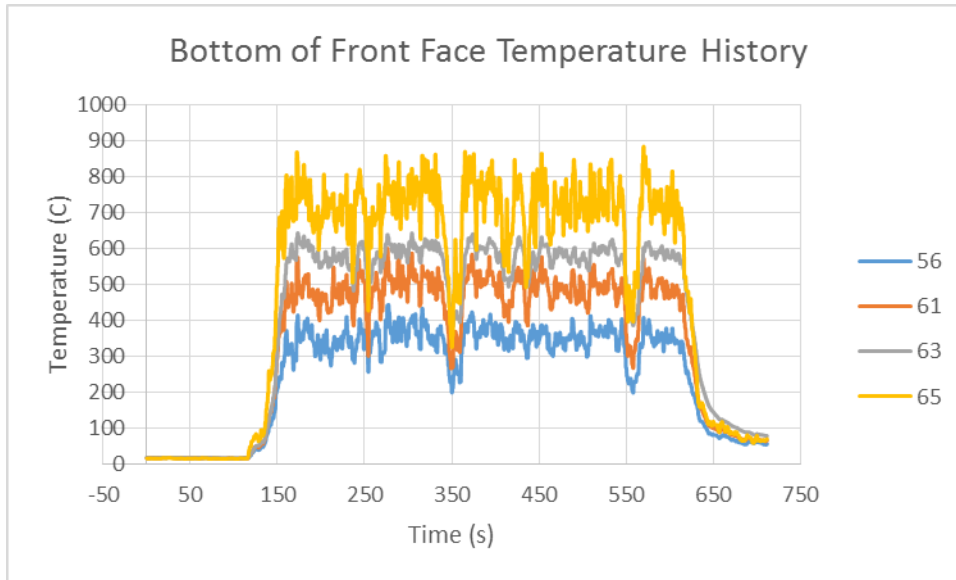
The same issues the 150 kW Test 1 run persisted in this run. These are the only two runs effected by the malfunctioning thermocouples.



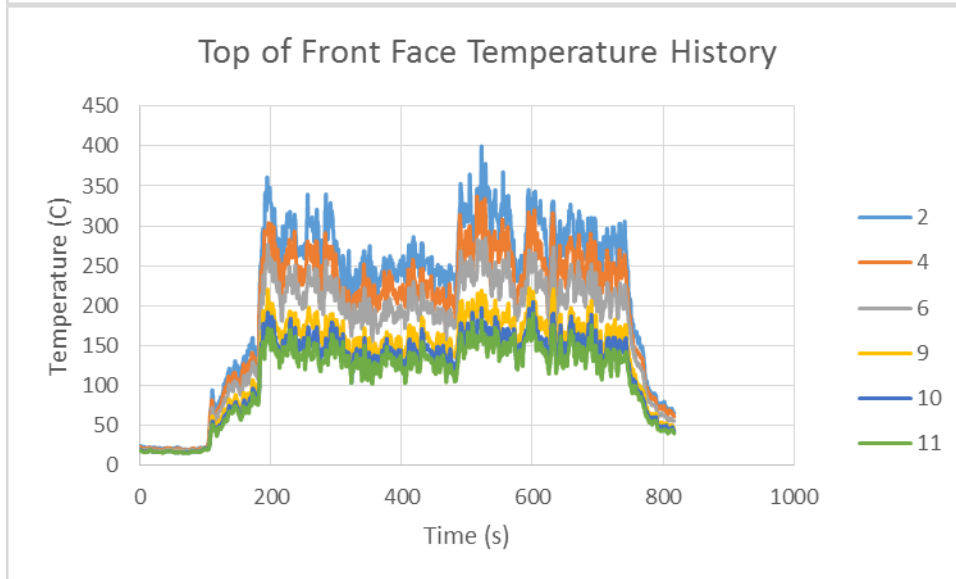
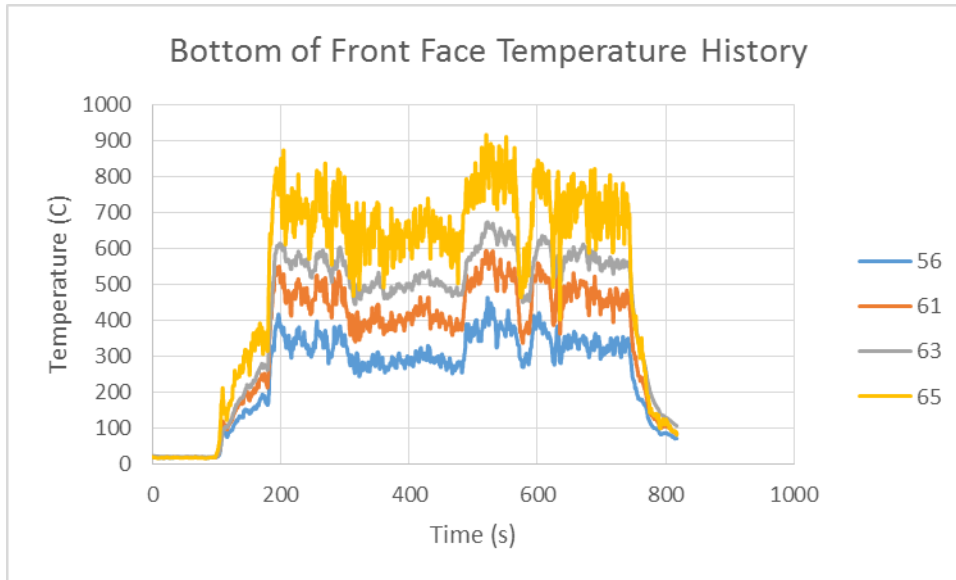
150 kW Test 3



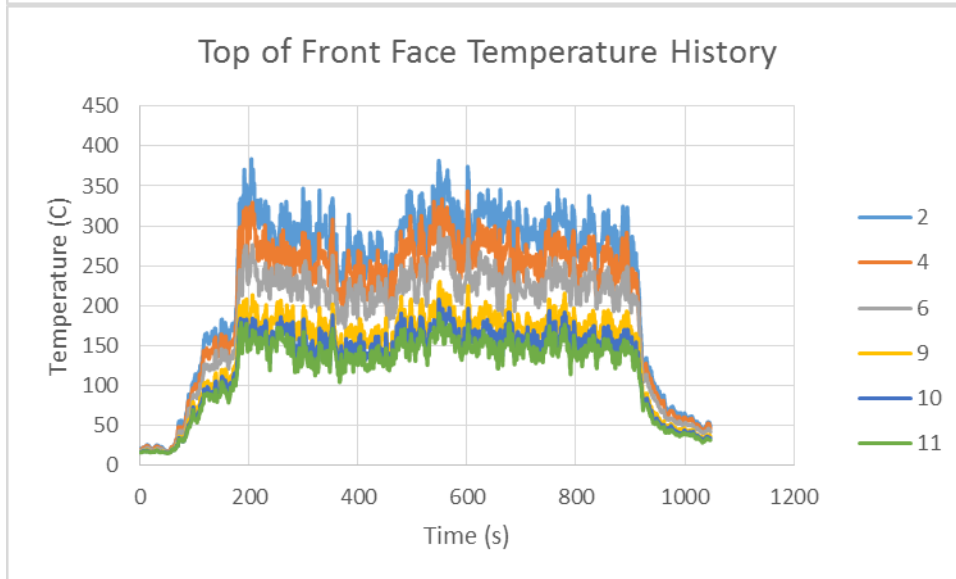
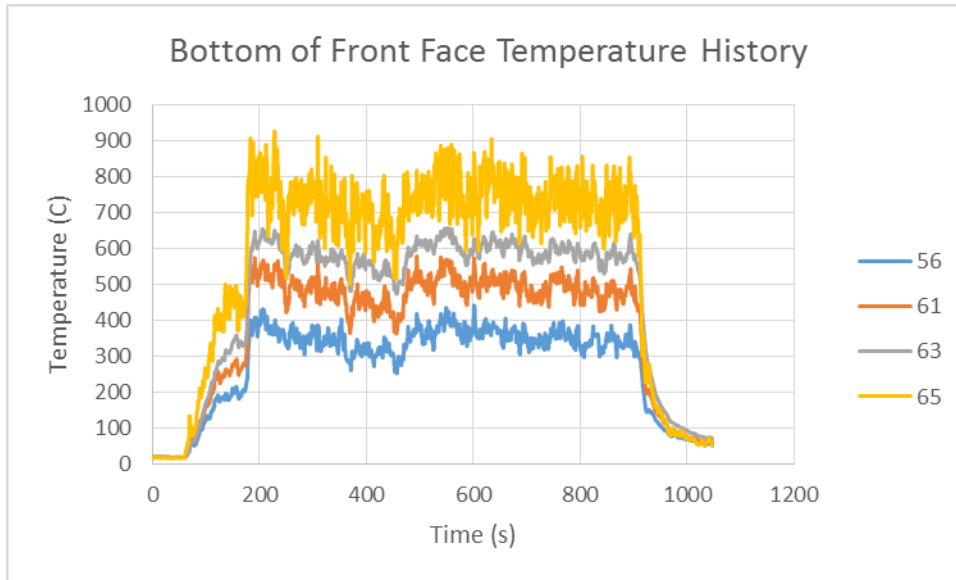
150 kW Test 4



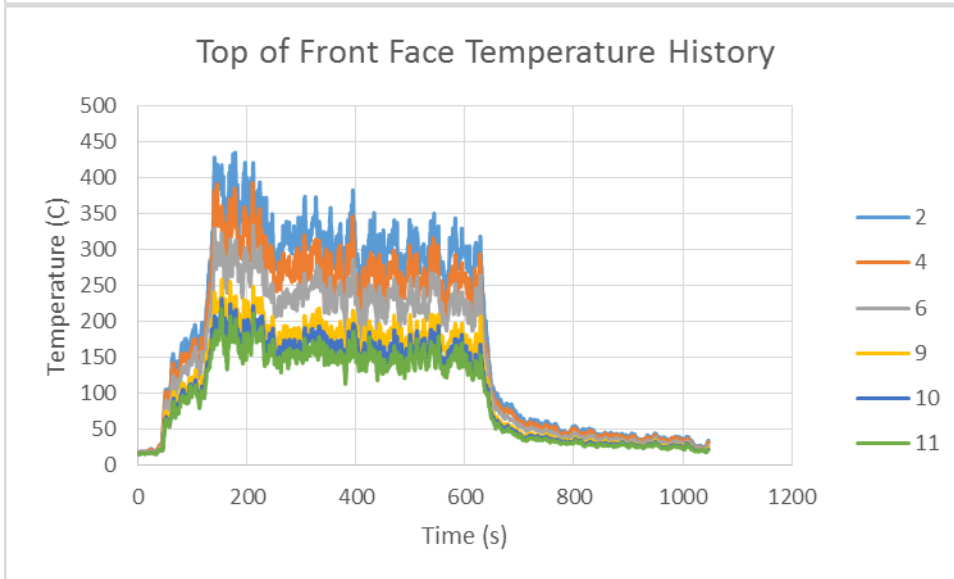
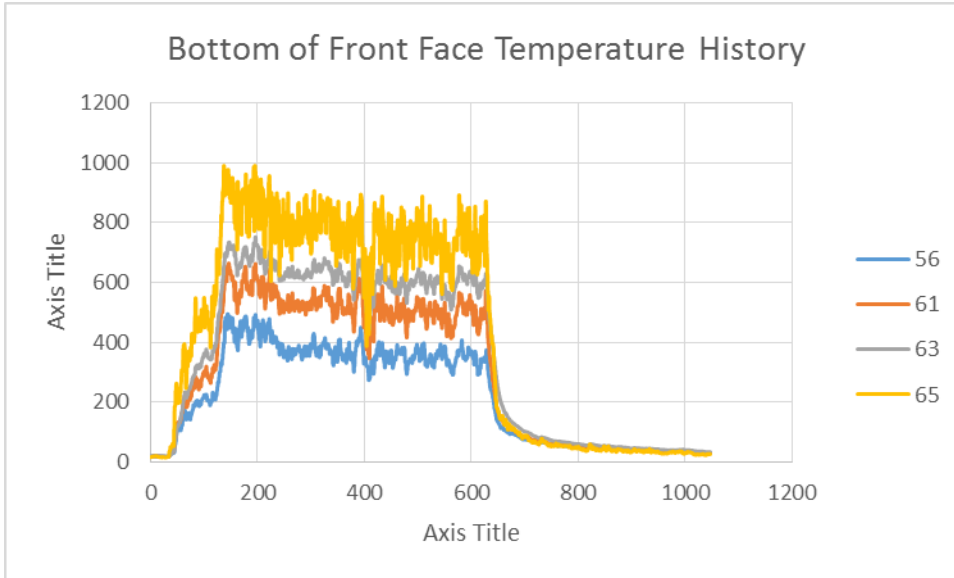
200 kW Test 1



200 kW Test 2



200 kW Test 3

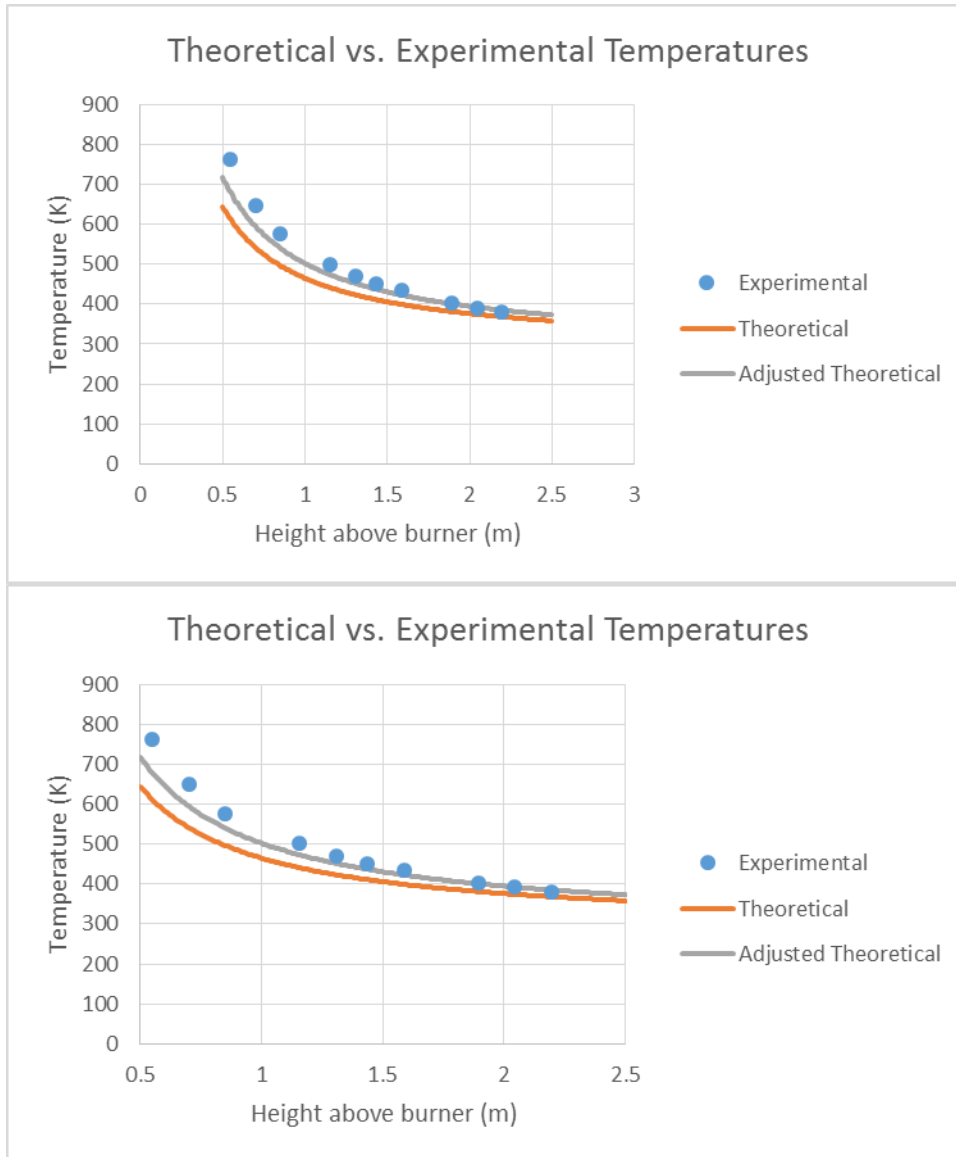


Appendix I: Yuan & Cox Theory Applied to Front Face

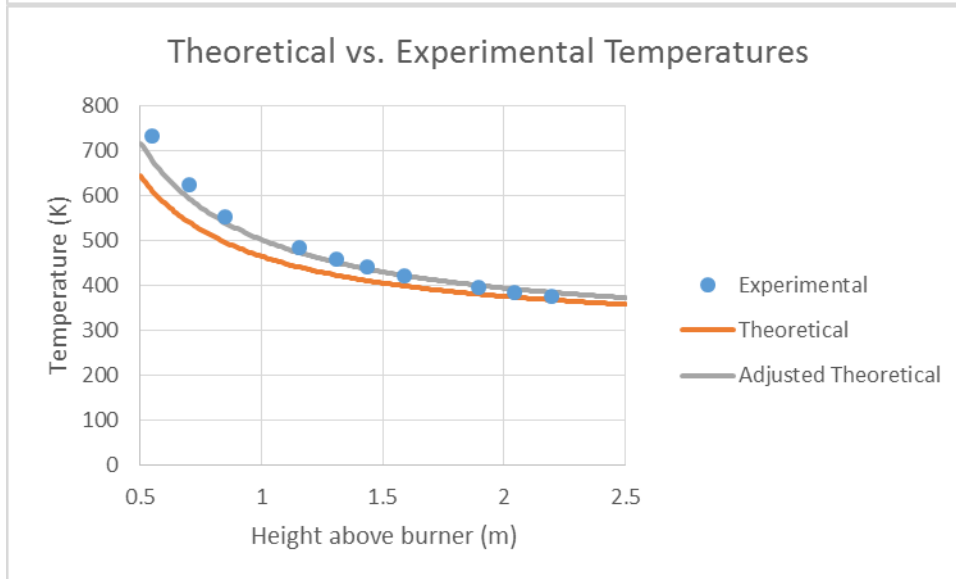
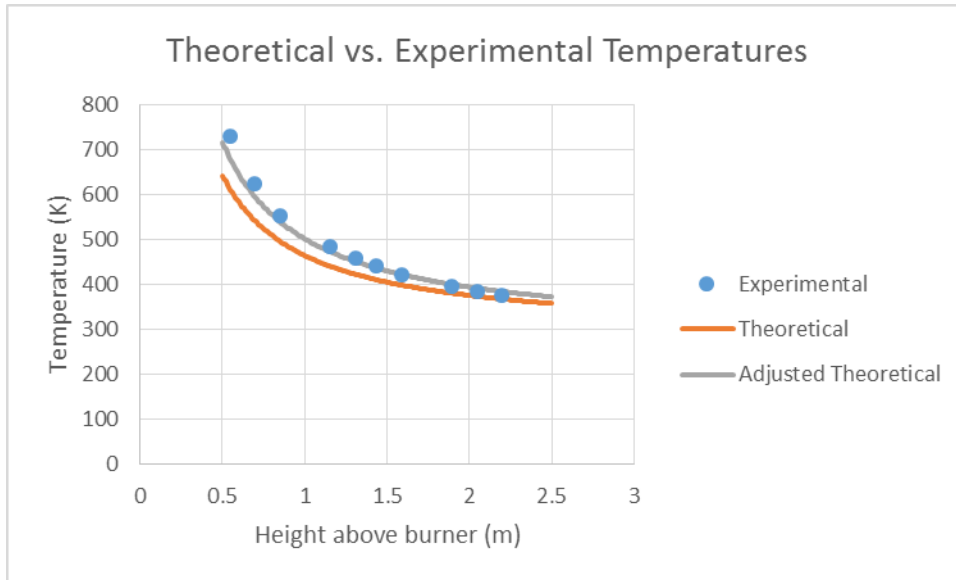
Author: Brendan Kerrigan

This is a compilation of each test where we applied the Yuan & Cox theory, as well as our adjusted constant, to the temperature data gathered. These graphs show that the Yuan & Cox theory as well as our adjusted coefficient provide us with a reasonable method for approximating the temperature at a point on our front face.

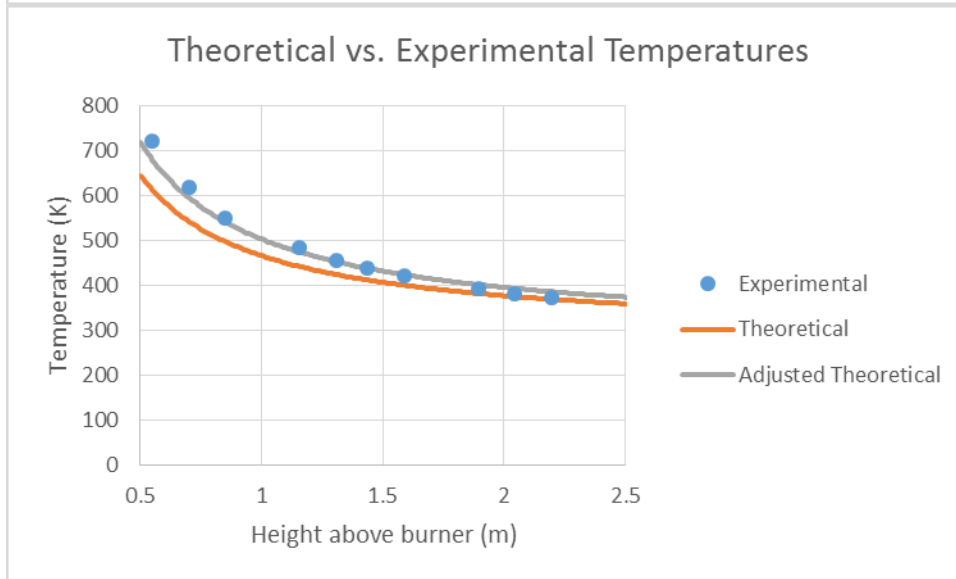
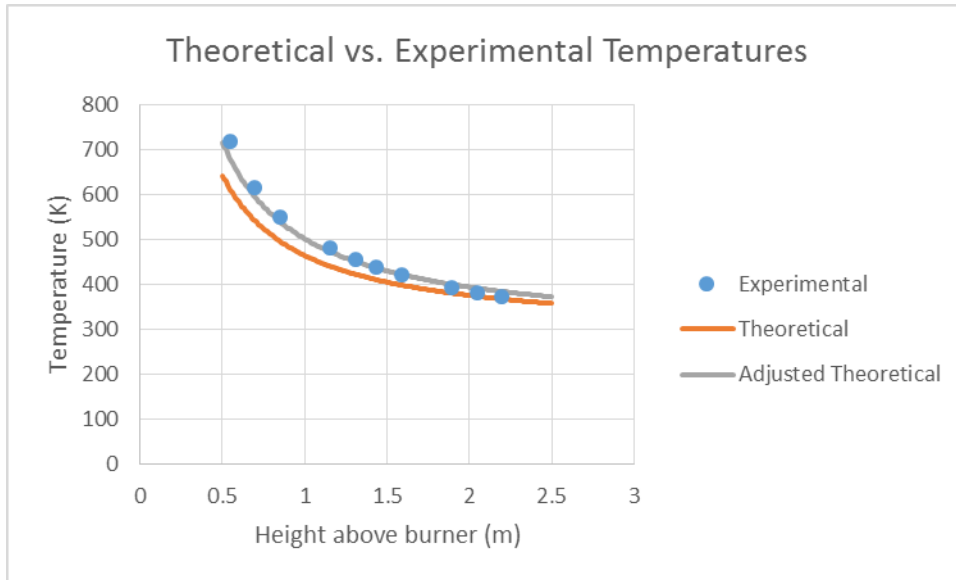
75 kW Test 1



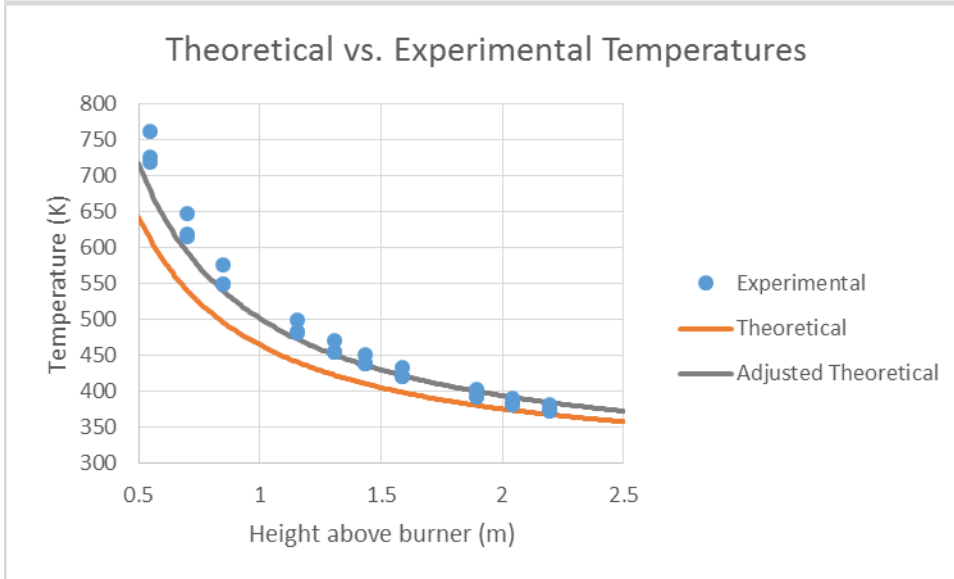
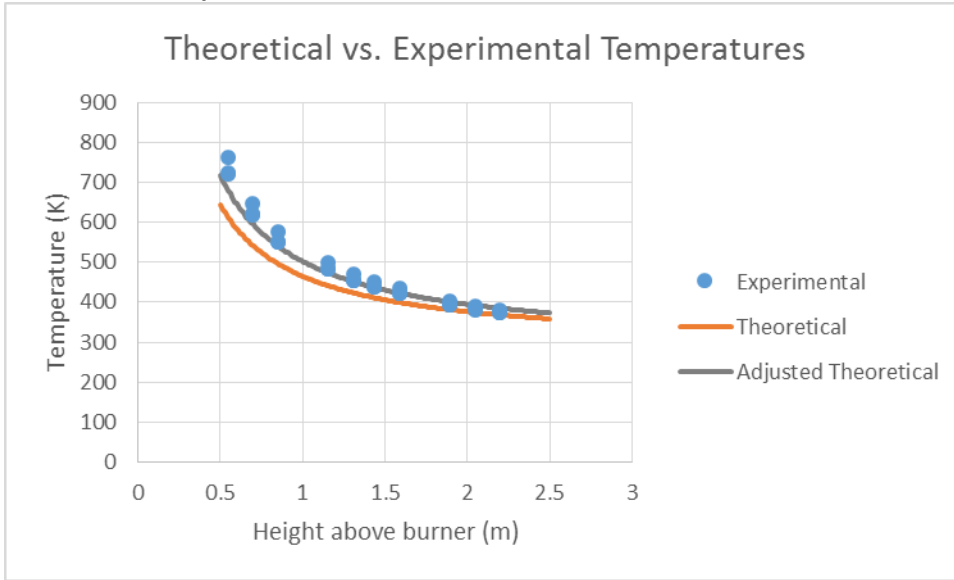
75 kW Test 2



75 kW Test 3

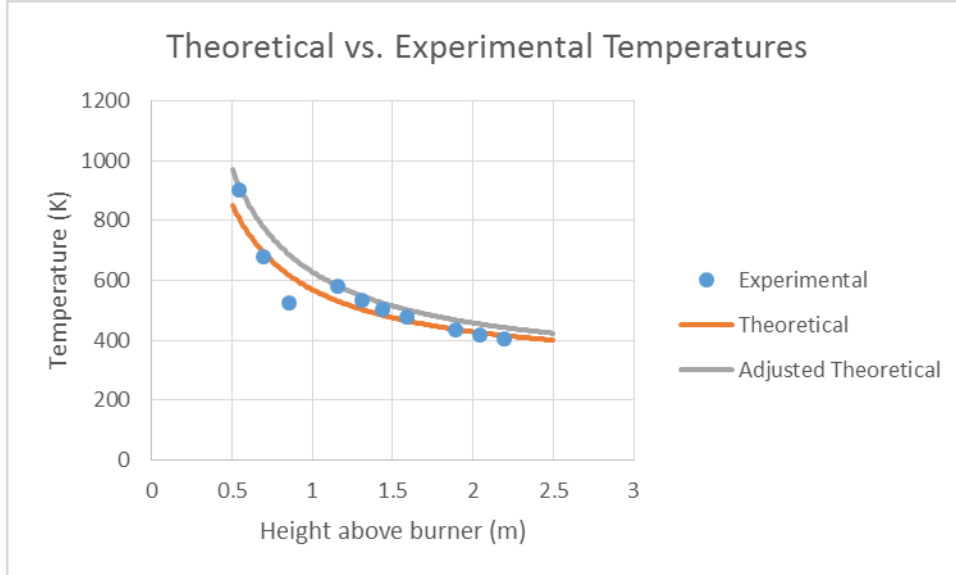


75 kW Test Compilation

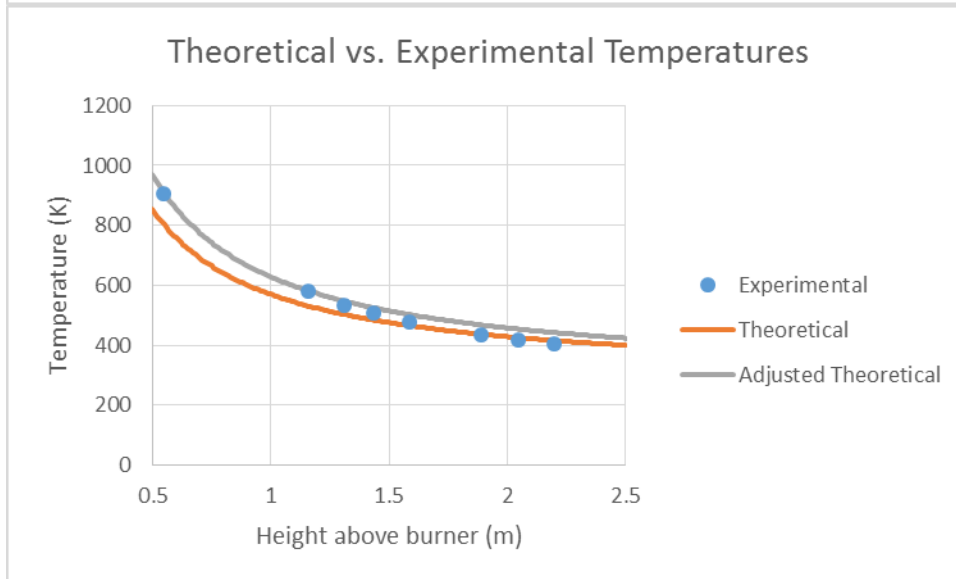
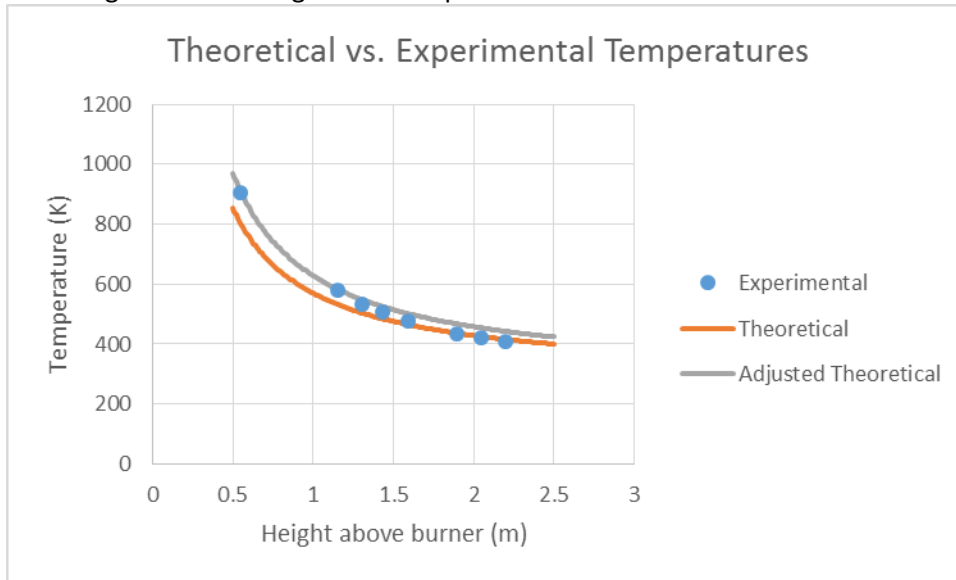


150 kW Test 1

Including malfunctioning thermocouples:

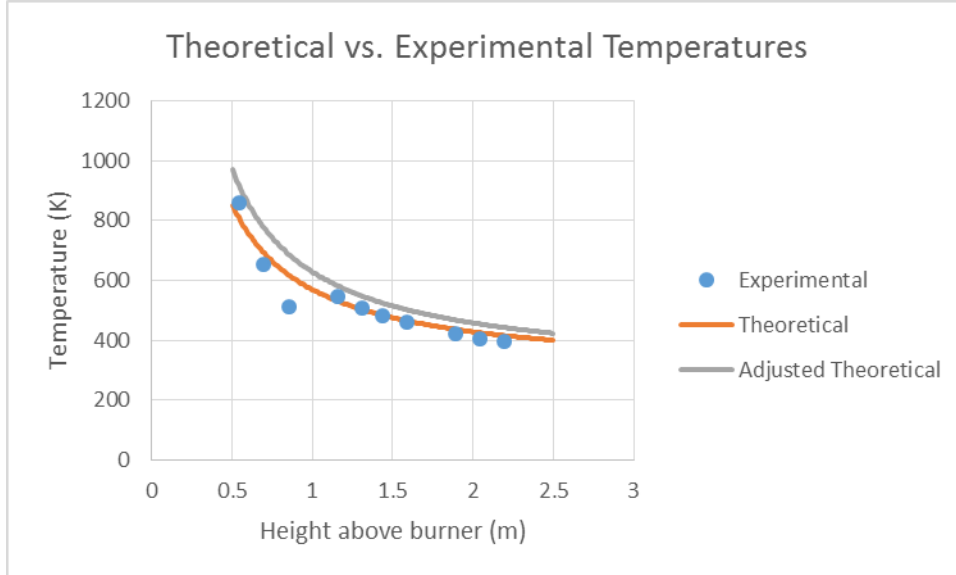


Excluding malfunctioning thermocouples:

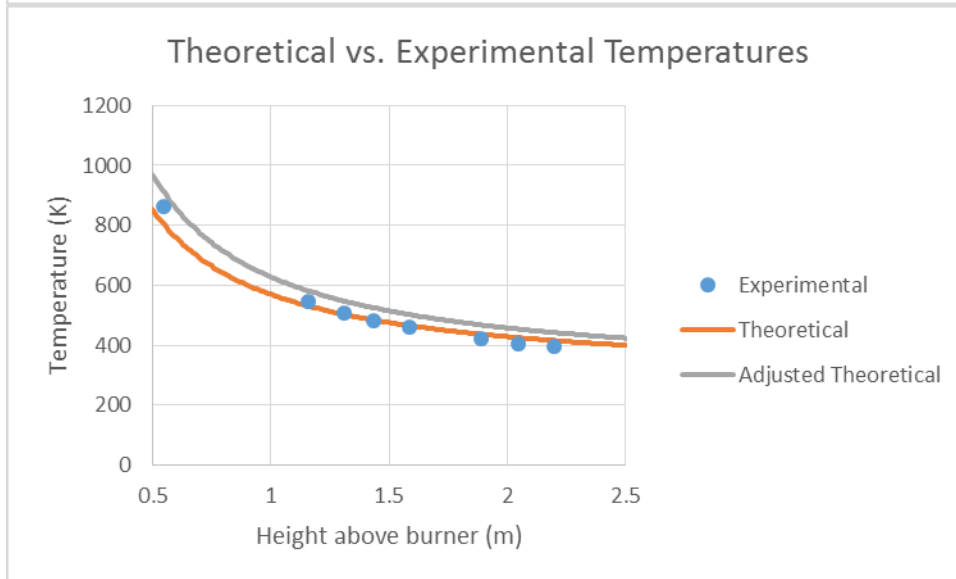
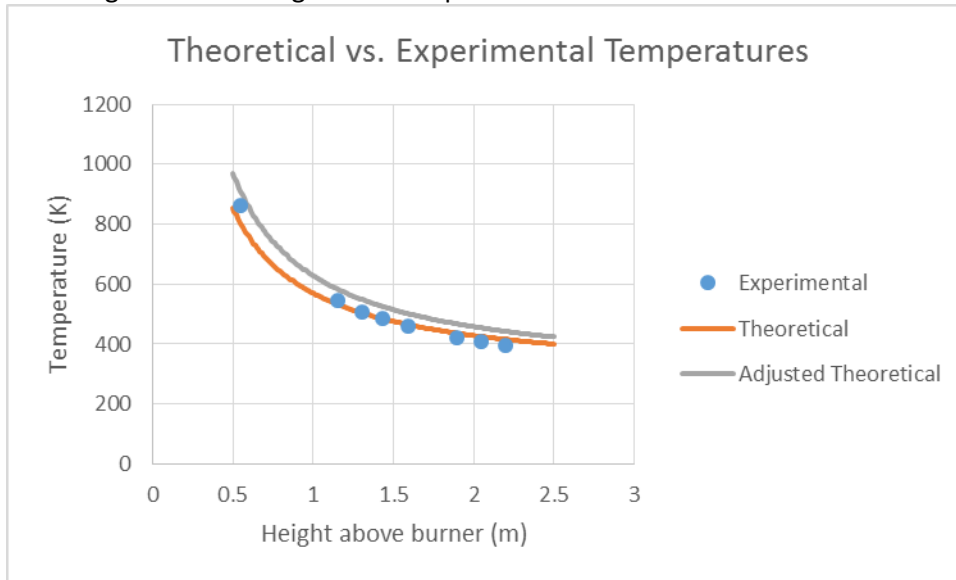


150 kW Test 2

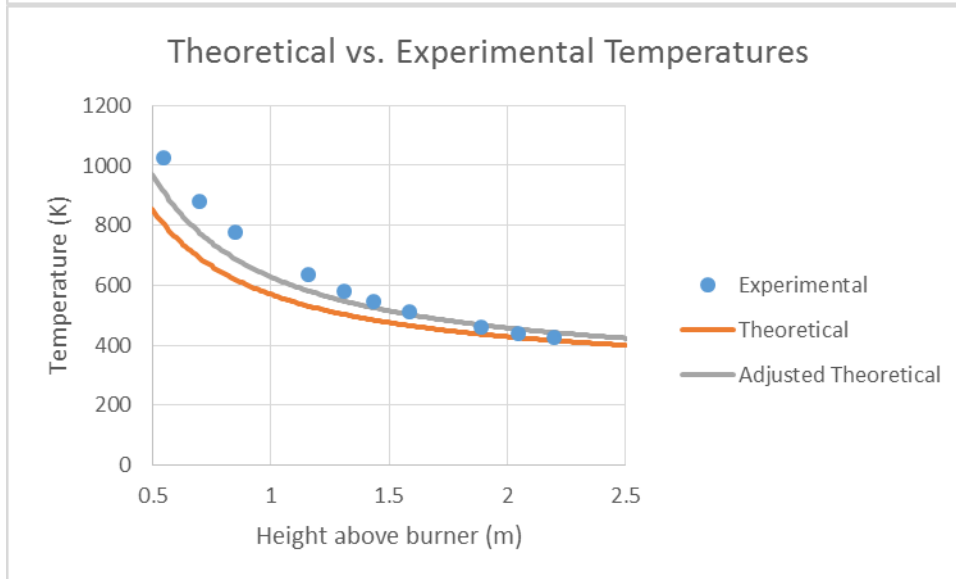
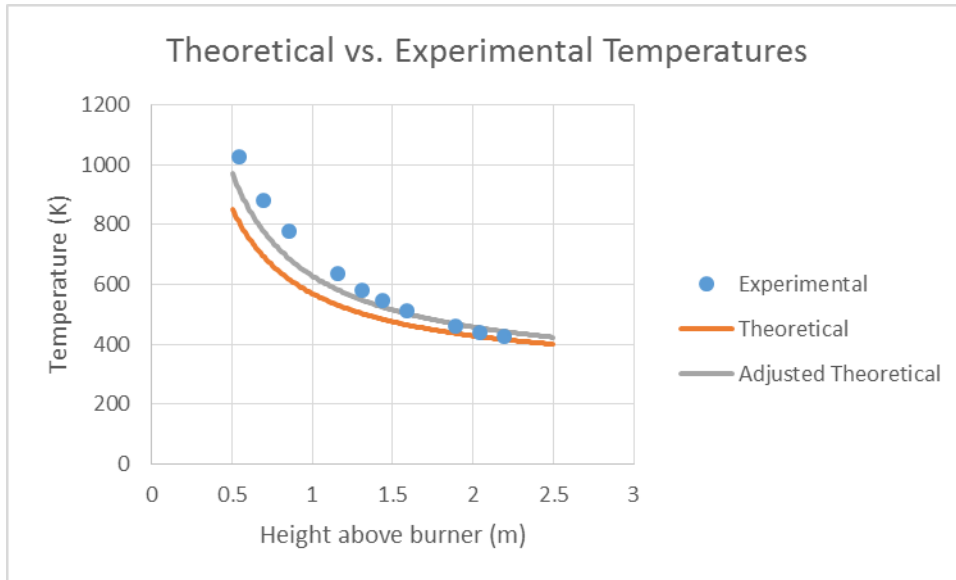
Including malfunctioning thermocouples:



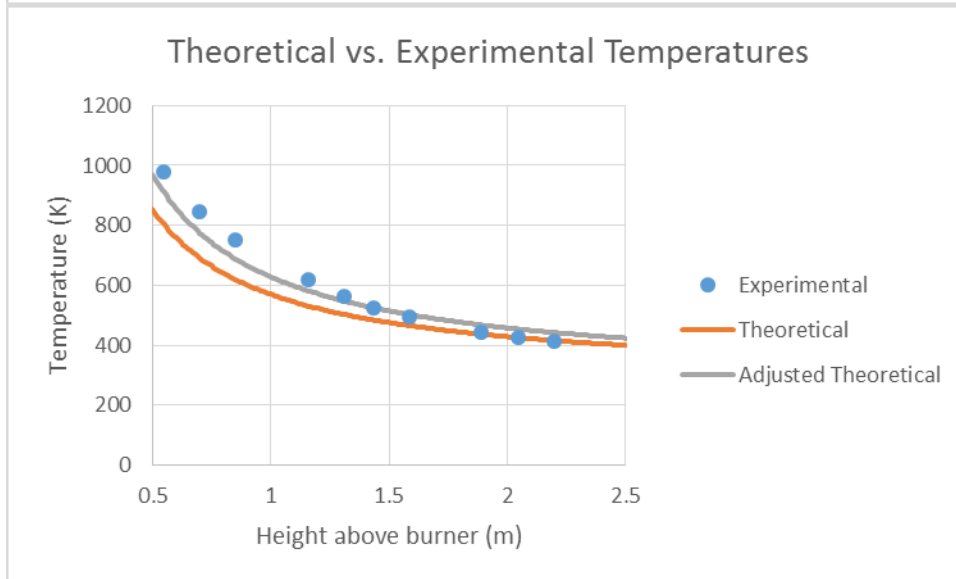
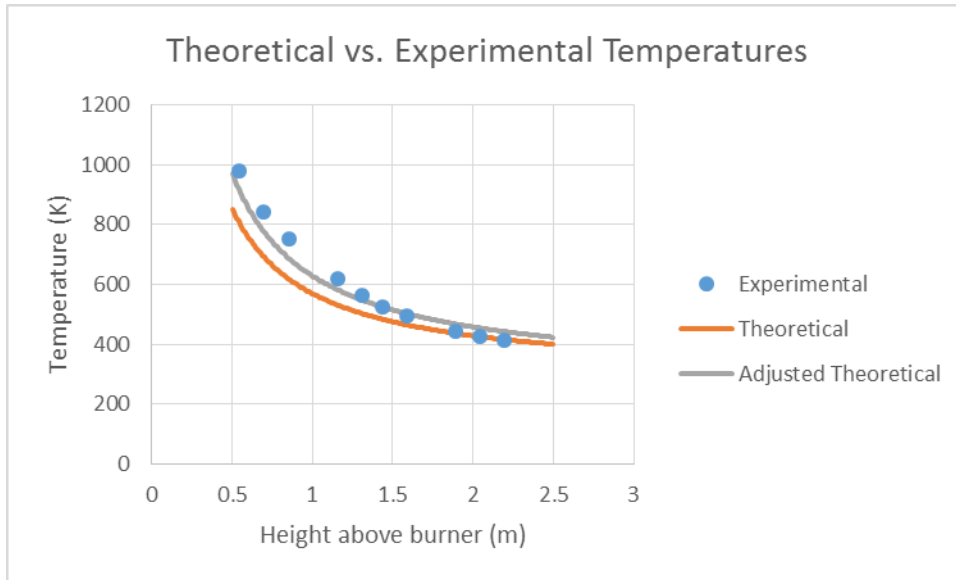
Excluding malfunctioning thermocouples:



150 kW Test 3

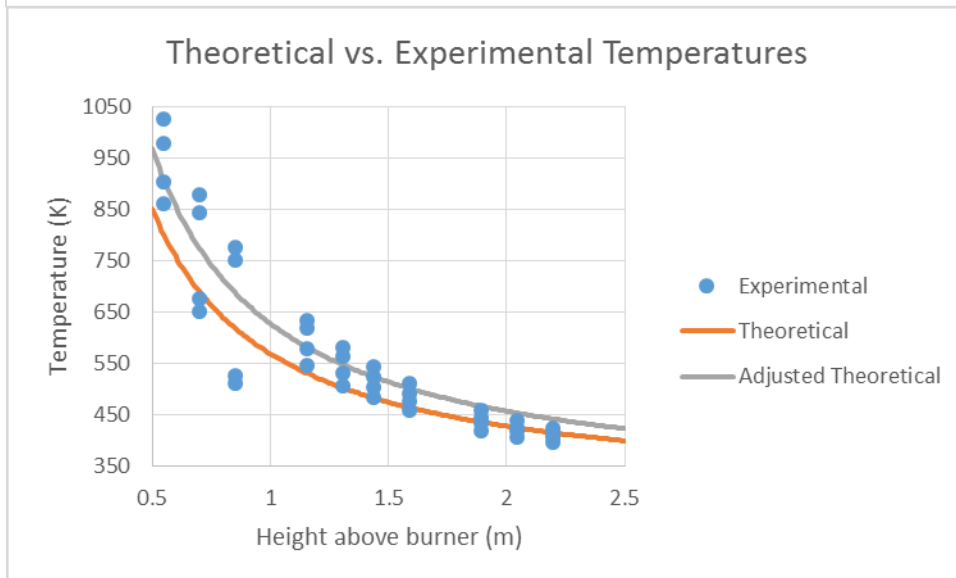
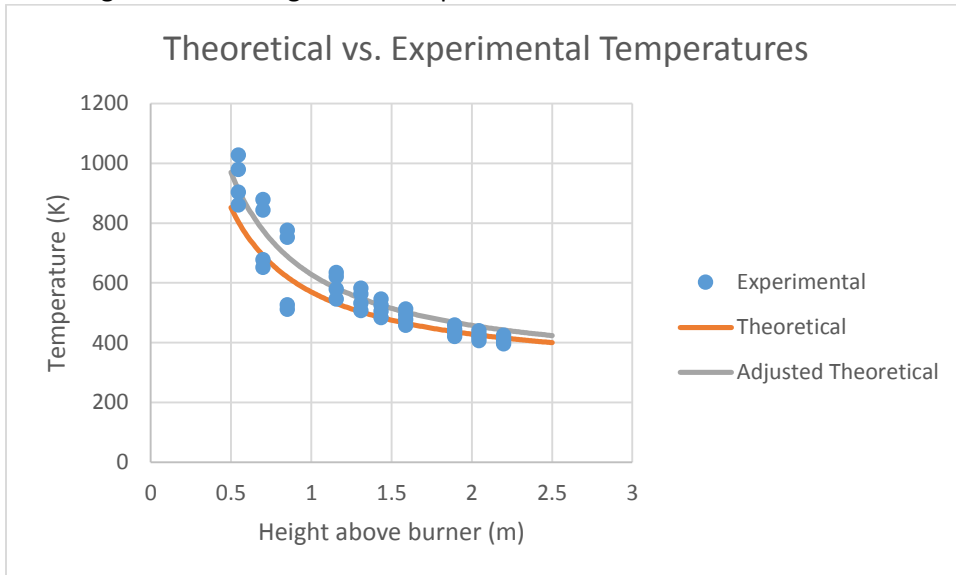


150 kW Test 4

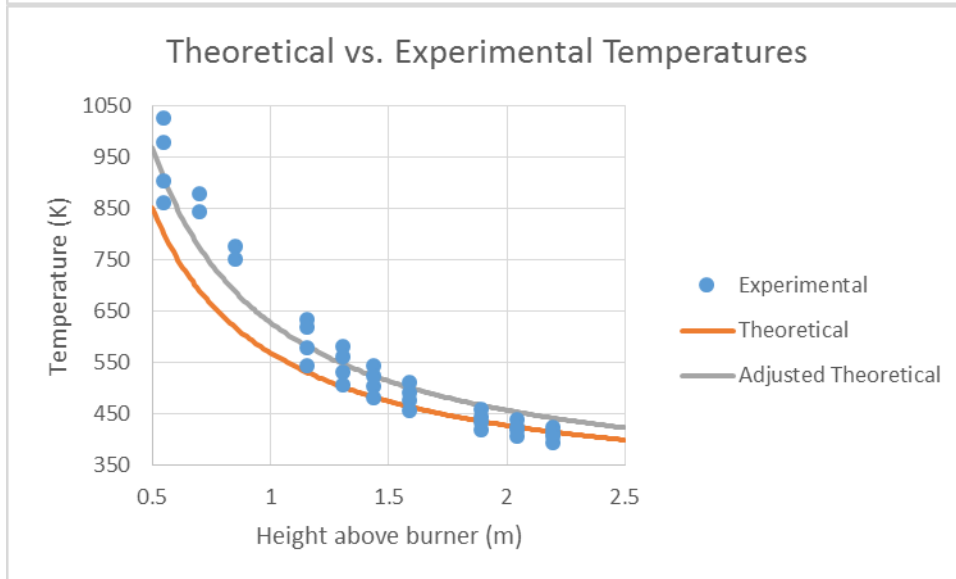
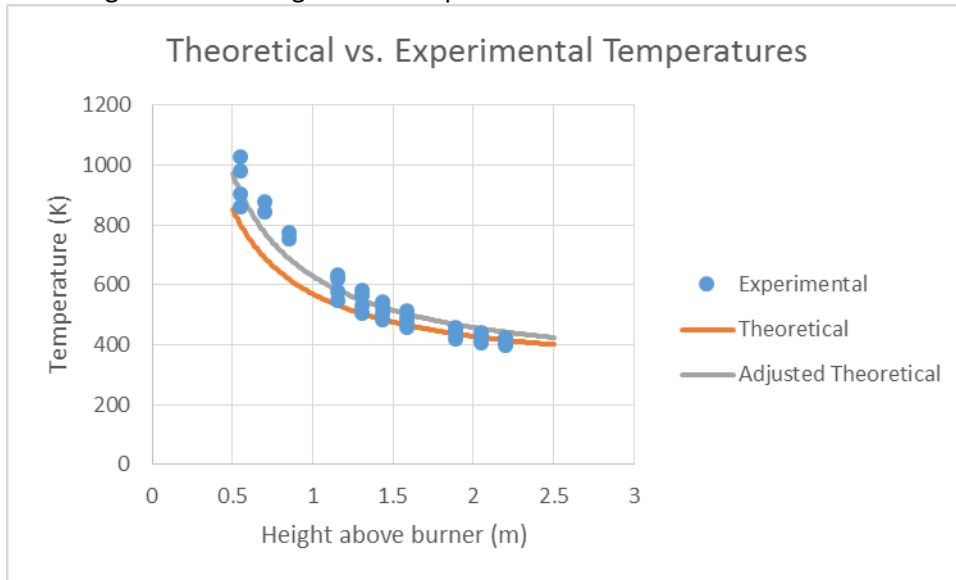


150 kW Compilation

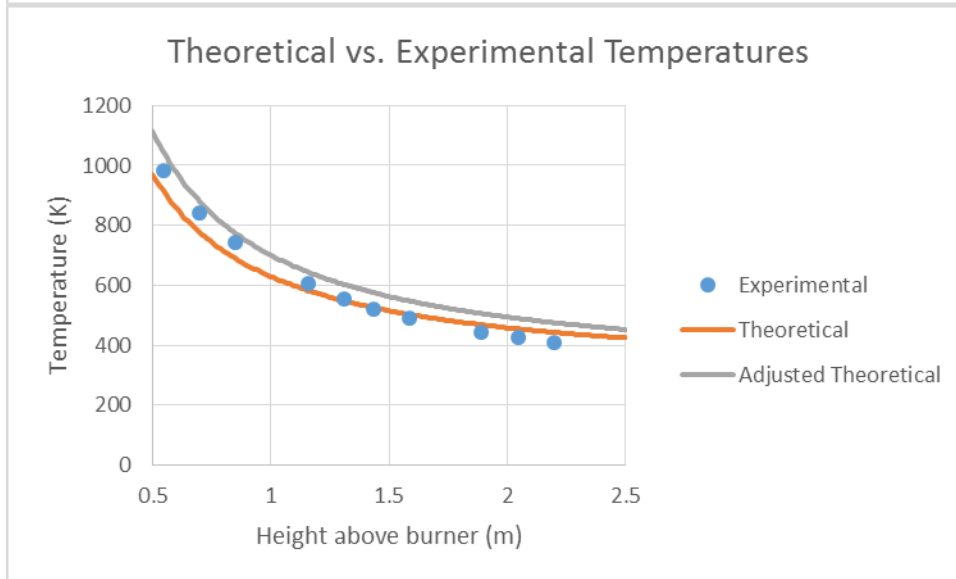
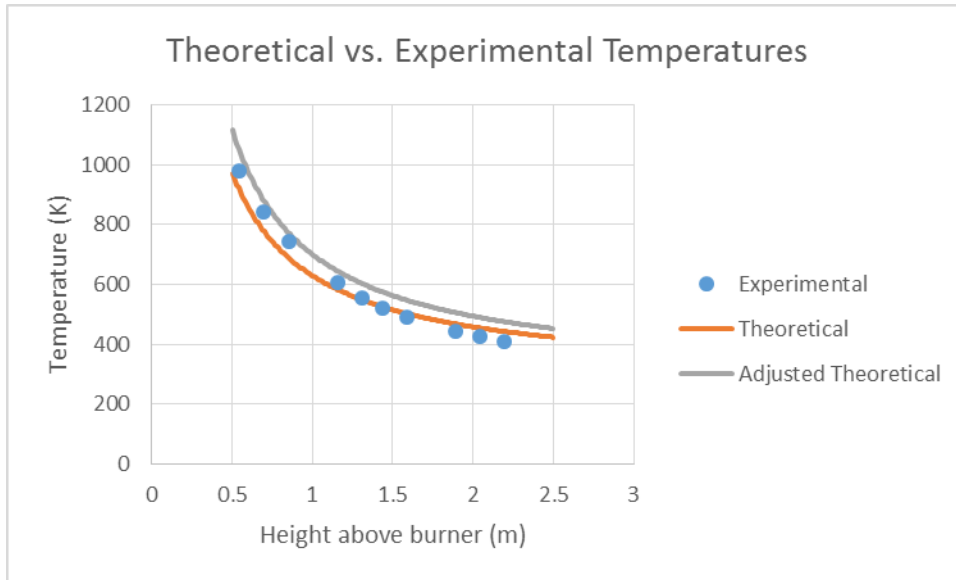
Including malfunctioning thermocouples:



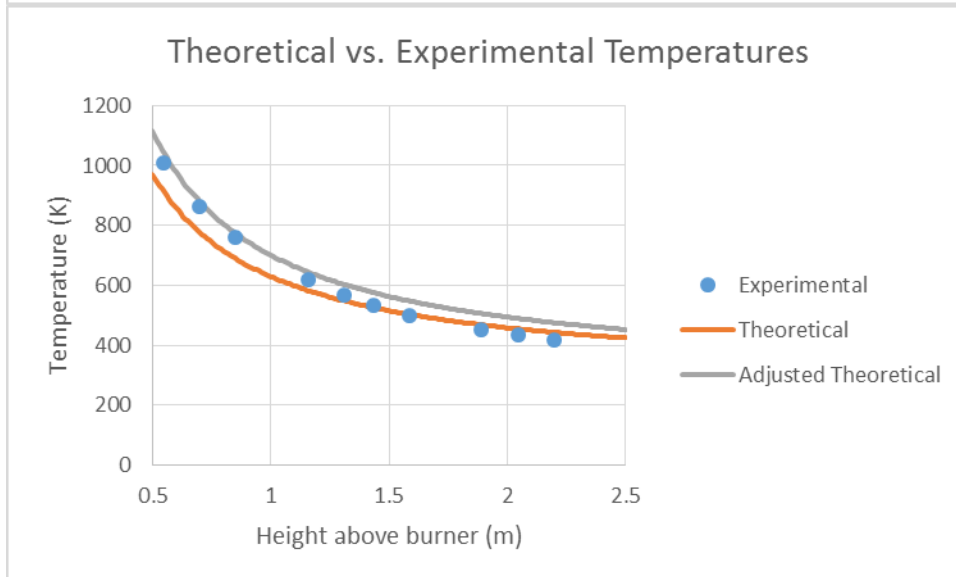
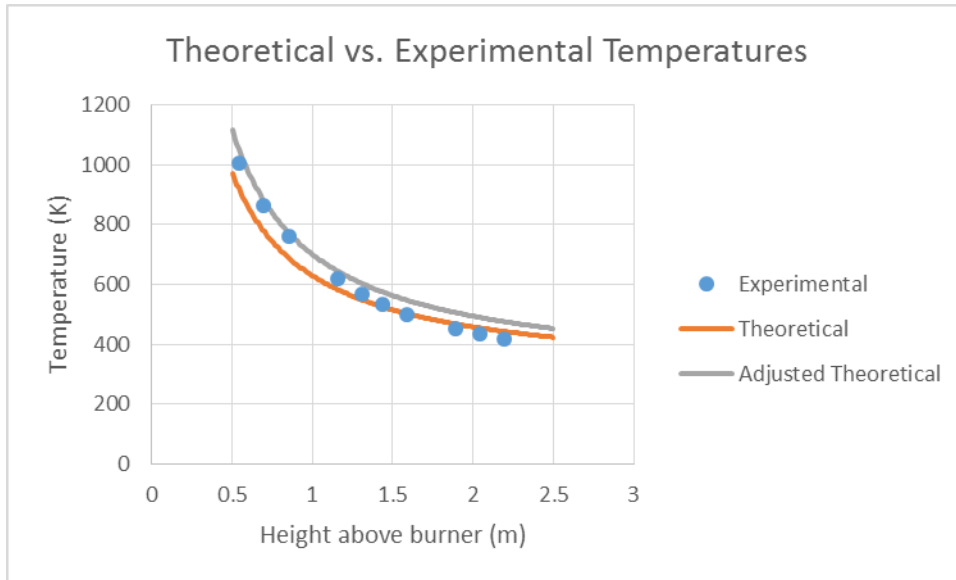
Excluding malfunctioning thermocouples:



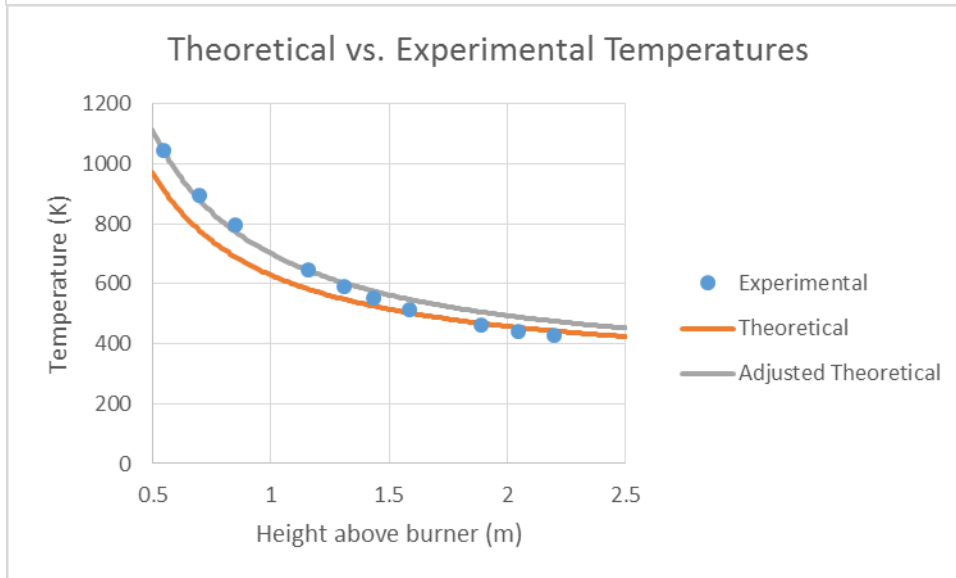
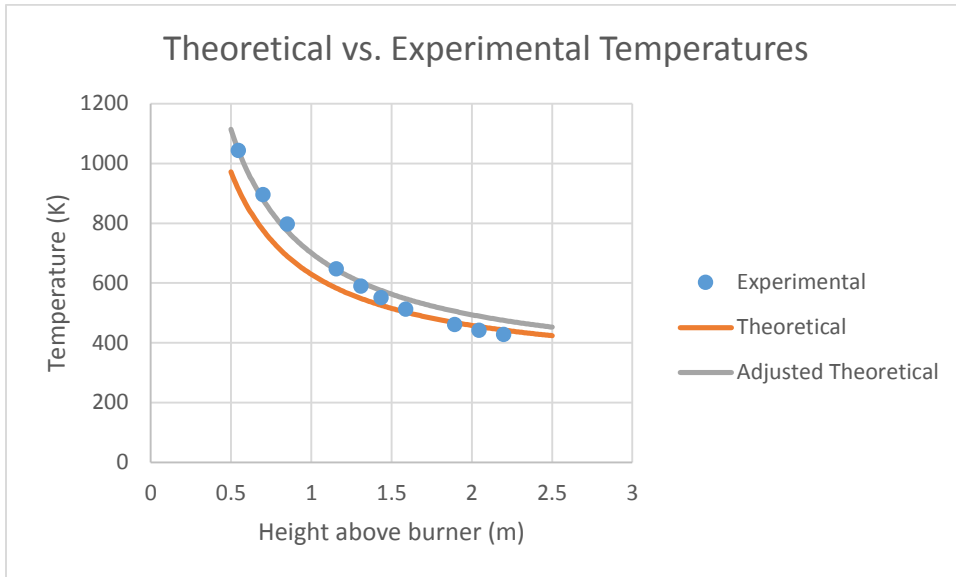
200 kW Test 1



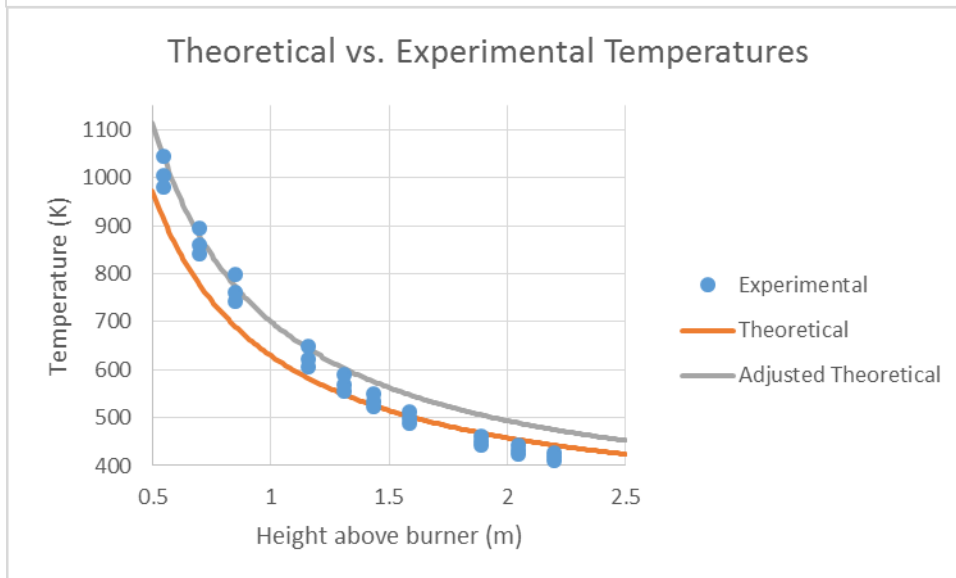
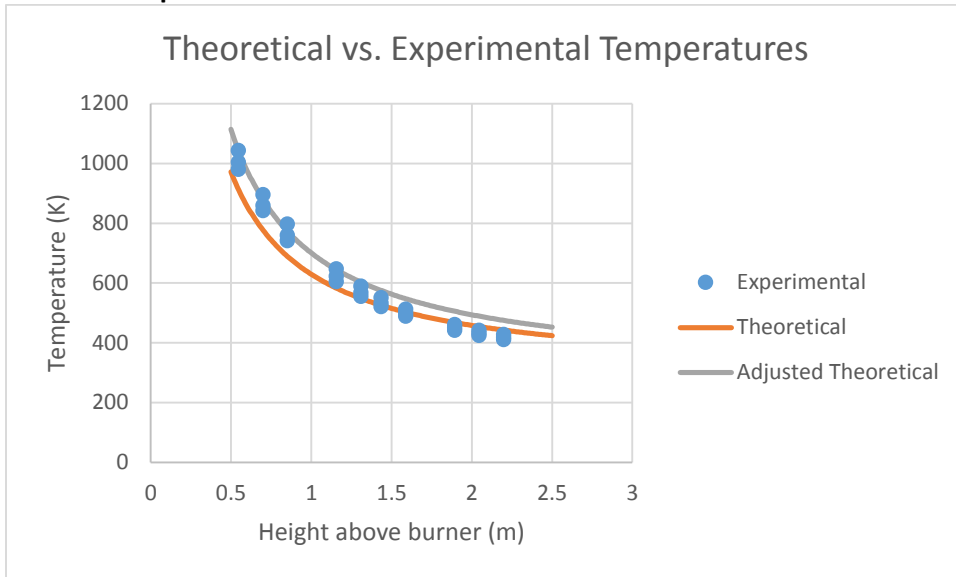
200 kW Test 2



200 kW Test 3



200 kW Compilation



Appendix J: Velocity Profile Formulation

Author: Sarah Meehan

75 kW velocity profile formulation (x height in gap)

$$x = 0, v = 0 \quad (c = 0)$$

$$x_1 = 0.0254 \text{ m}, v = 0.27 \text{ m/s}$$

$$x_2 = 0.0508 \text{ m}, v = 0 \text{ m/s}$$

$$v = ax^2 + bx + c$$

$$v_{\max} = 0.27 \text{ m/s} = a(x_1)^2 + bx_1$$

$$(1*) \quad 0.27 \text{ m/s} = a(0.0254)^2 + b(0.0254)$$

$$\frac{dv}{dx} = 2ax + b$$

$$@ \quad x = x_1 = 0.0254 \text{ m}$$

$$\frac{dv}{dx} = 0$$

$$0 = 2ax_1 + b$$

$$0 = 2a(0.0254) + b$$

$$(2*) \quad b = -0.0508a$$

plug into (1*)

$$(1*) \quad 0.27 \text{ m/s} = 0.00064516a + (-0.0508a)(0.0254)$$

$$0.27 \text{ m/s} = 0.00064516a - 0.00129032a$$

$$0.27 \text{ m/s} = -0.00064516a$$

$$a = -418.50$$

$$b = 21.26$$

$$\boxed{V_{75\text{kW}}(x) = -418.50x^2 + 21.26x}$$

$$\int_0^{0.0508} v(x) dx = 0.009144$$

o integrate & divide for average velocity...

(1)

SKM
(75)

$$\frac{0.009144}{\text{total length}} \Rightarrow \frac{0.009144}{0.0508} = 0.18 \text{ m/s}$$

$$\underline{V_{75} = 0.18 \text{ m/s}}$$

average

(2)

150kW velocity profile formulation (x height in gap)

SKM
(150)

$x = 0m \rightarrow v = 0 (c=0)$

$x_1 = 0.0254m \rightarrow v = 0.25 m/s$

$x_2 = 0.0508m \rightarrow v = 0$

$v = ax^2 + bx + c$

$v_{max} = 0.25 m/s = ax_1^2 + bx_1$

#1 $0.25 m/s = a(0.0254)^2 + b(0.0254)$

$\frac{dv}{dx} = 2ax + b$

@ $x = x_1 = 0.0254m$

$\frac{dv}{dx} = 0$

$0 = 2ax_1 + b$

$0 = 2a(0.0254) + b$

#2 $b = -0.0508 a$

plug into #1

$0.25 m/s = 0.00064516a + (-0.0508a)(0.0254)$

$0.25 m/s = -0.00064516a$

$a = -387.50$

$b = 19.69$

$V(x)_{150kW} = -387.50x^2 + 19.69x$

integrate...

$\int_0^{0.0508} v(x) dx = 0.0084731$

divide for average velocity...

①

SKM
(150)

$$\frac{\int v(x) dx}{\text{length}} = V_{\text{avg}}$$

$$\frac{0.0084731}{0.0508} = 0.1668 \text{ m/s}$$

$$\underline{V_{\text{avg}} = 0.17 \text{ m/s}}$$

1504W

②

200kW velocity profile formulation (x height in gap)

SKM
(200)

$$x=0 \quad v=0 \quad (c=0)$$

$$x_1 = 0.0254 \text{ m} \quad v = 0.18 \text{ m/s}$$

$$\underline{x_2 = 0.0508 \text{ m} \quad v = 0}$$

$$V = ax^2 + bx + c$$

$$V_{\max} = 0.18 \text{ m/s} = ax_1^2 + bx_1$$

$$\textcircled{\#1} \quad 0.18 \text{ m/s} = a(0.0254)^2 + b(0.0254)$$

$$\frac{dV}{dx} = 2ax + b$$

$$\textcircled{\text{a}} \quad x = x_1 = 0.0254 \text{ m}$$

$$\frac{dV}{dx} = 0$$

$$0 = 2ax_1 + b$$

$$0 = 2a(0.0254) + b$$

$$\textcircled{\#2} \quad b = -0.0508a$$

plug into $\textcircled{\#1}$

$$0.18 \text{ m/s} = 0.00064514a + (-0.0508a)(0.0254)$$

$$0.18 \text{ m/s} = -0.00064516a$$

$$a = -279.00$$

$$b = 14.17$$

$$\boxed{V(x)_{200\text{kW}} = -279x^2 + 14.17x}$$

integrate ...

$$\int_0^{0.0508} v(x) dx = 0.00609186$$

①

divide for average velocity

SKM
(200)

$$\frac{\int v(x) dx}{\text{length}} = V_{\text{avg}}$$

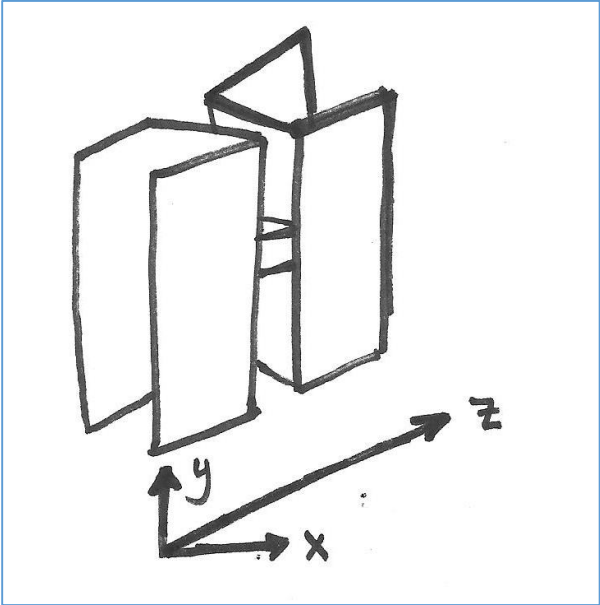
$$\frac{0.00409186}{0.0508} = 0.1199 \text{ m/s}$$

$$\underline{V_{\text{avg}} = 0.12 \text{ m/s}}$$

2002W

2

The figure below represents the overall coordinate system for our assembly. In the above velocity calculations we used the variable x to represent the y direction.



Appendix K: Yuan & Cox Theory Applied to Thermal Plume up the Back Face

Author: Brendan Kerrigan

Summary of calculated heat release rates per unit length (kW/m), and heat release rate per unit length converted to heat release rate (kW):

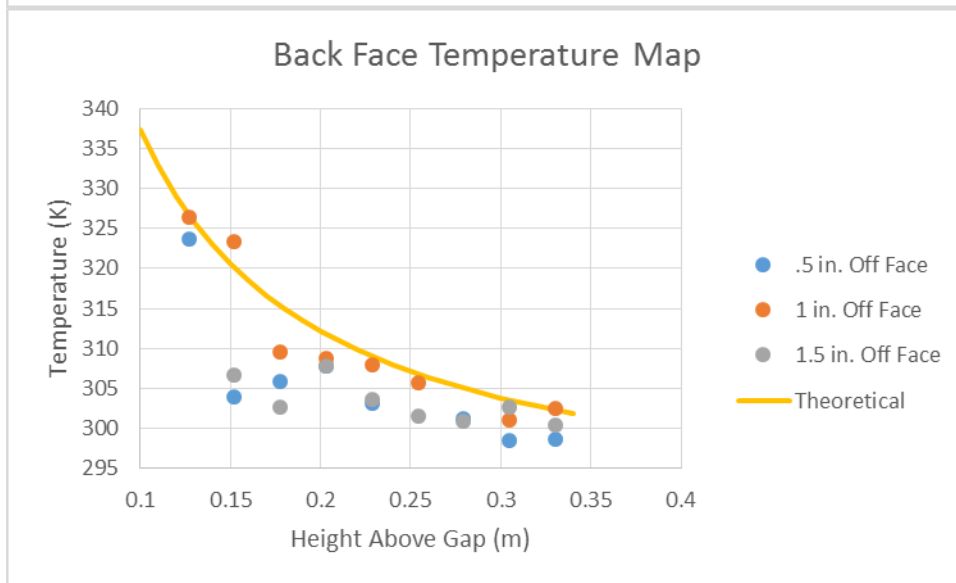
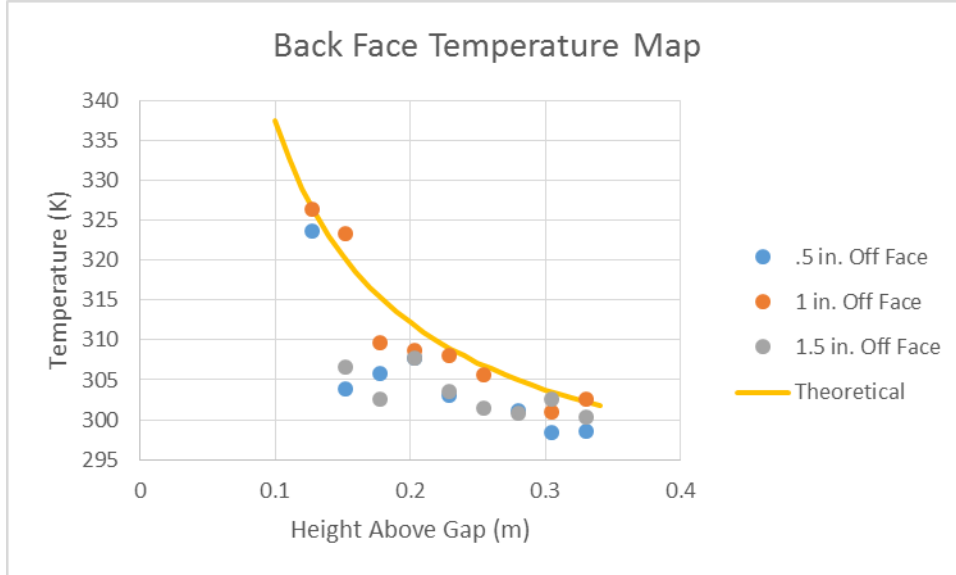
Summary of calculated heat release rates per unit length (Ql)					
	kW/m		kW/m		kW/m
75 kW:	0.729	150 kW:	0.580	200 kW:	1.293
	0.501		0.696		1.063
	0.412		0.471		0.978
	0.579				
Average:	0.555		0.582		1.111

Summary of calculated heat release rates					
	kW		kW		kW
75 kW:	0.500	150 kW:	0.398	200 kW:	0.887
	0.344		0.477		0.729
	0.283		0.323		0.671
	0.397				
Average:	0.381		0.399		0.762

These calculations indicate that we expect a relatively small amount of energy to come through our gap.

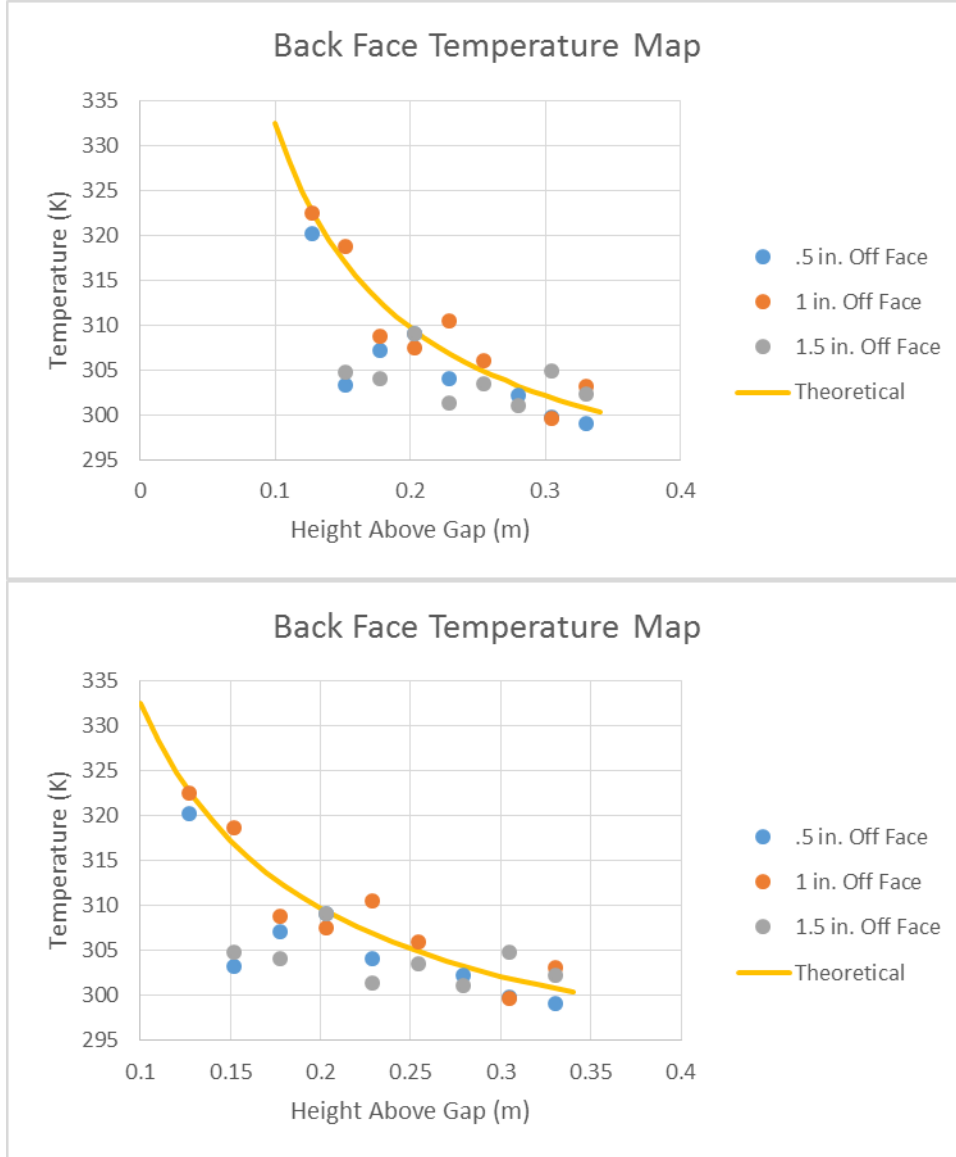
75 kW Test 1

Calculated heat release rate per unit length: .585 kW/m



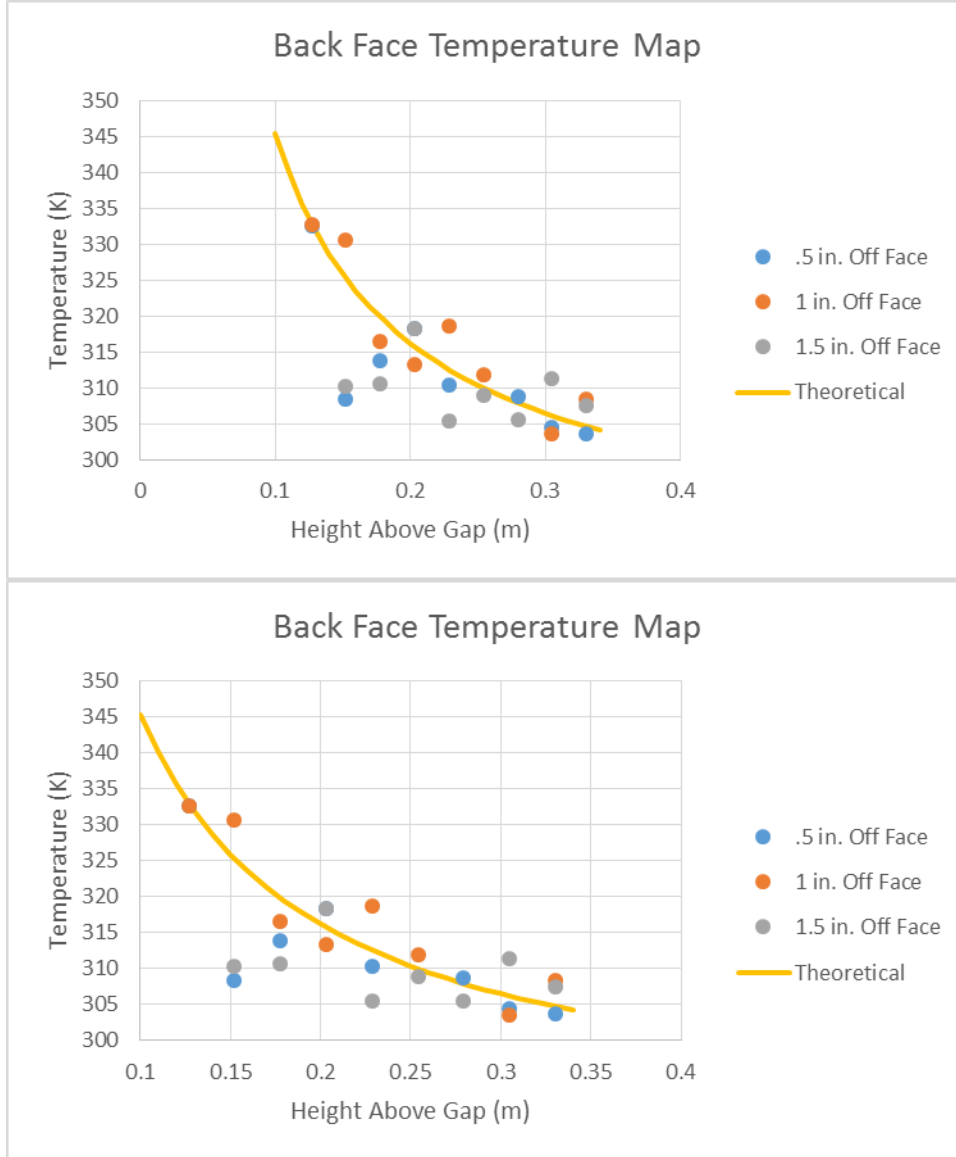
75 kW Test 2

Calculated heat release rate per unit length: .501 kW/m



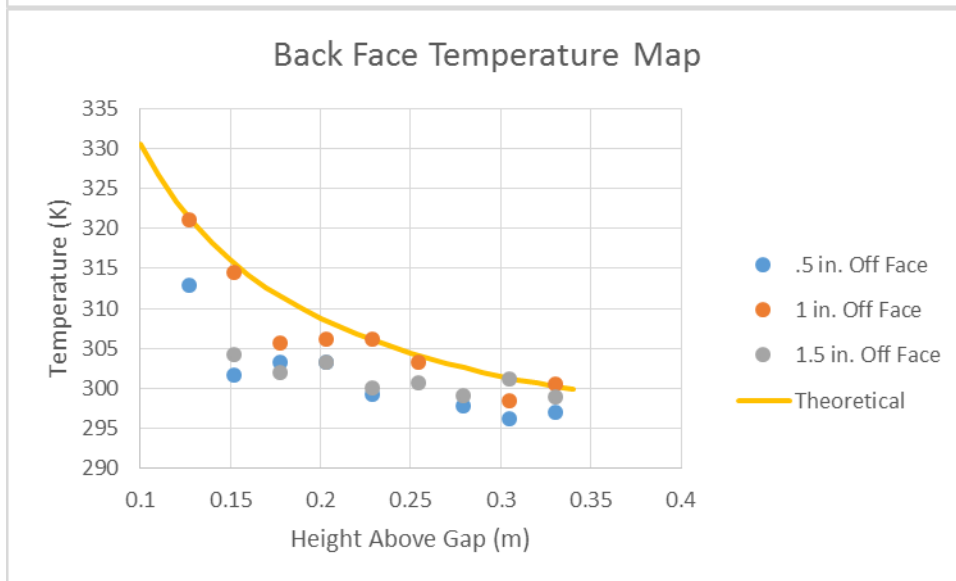
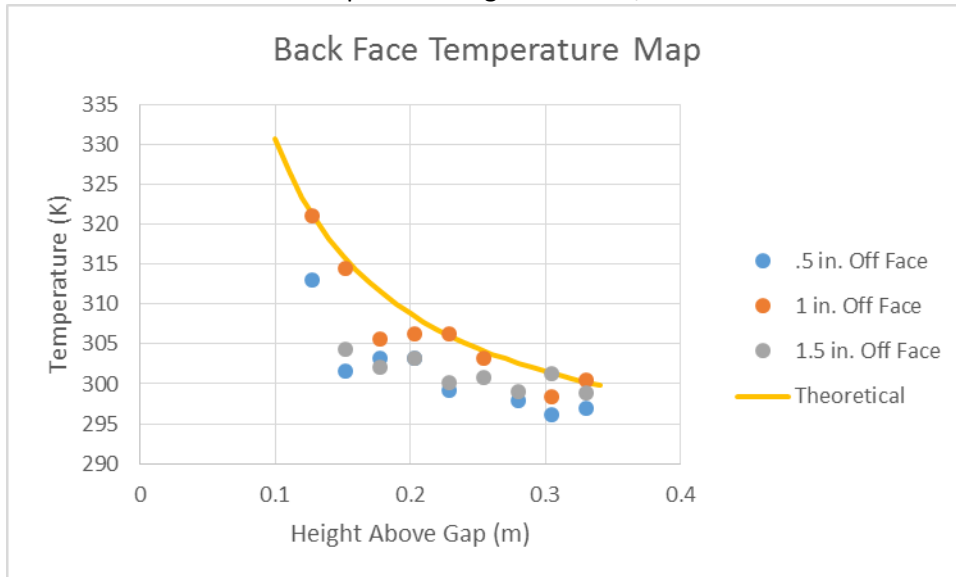
75 kW Test 3

Calculated heat release rate per unit length: .729 kW/m



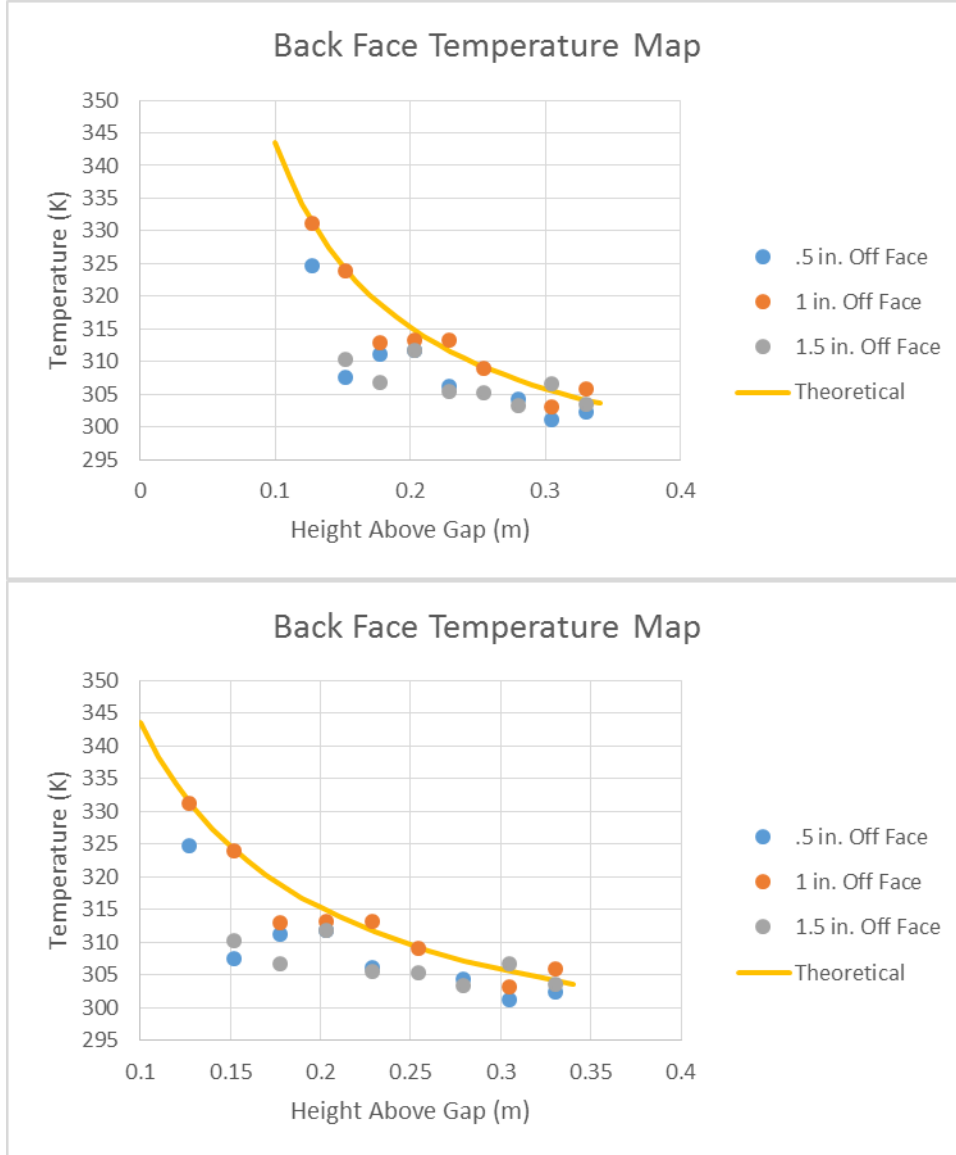
150 kW Test 1

Calculated heat release rate per unit length: .471 kW/m



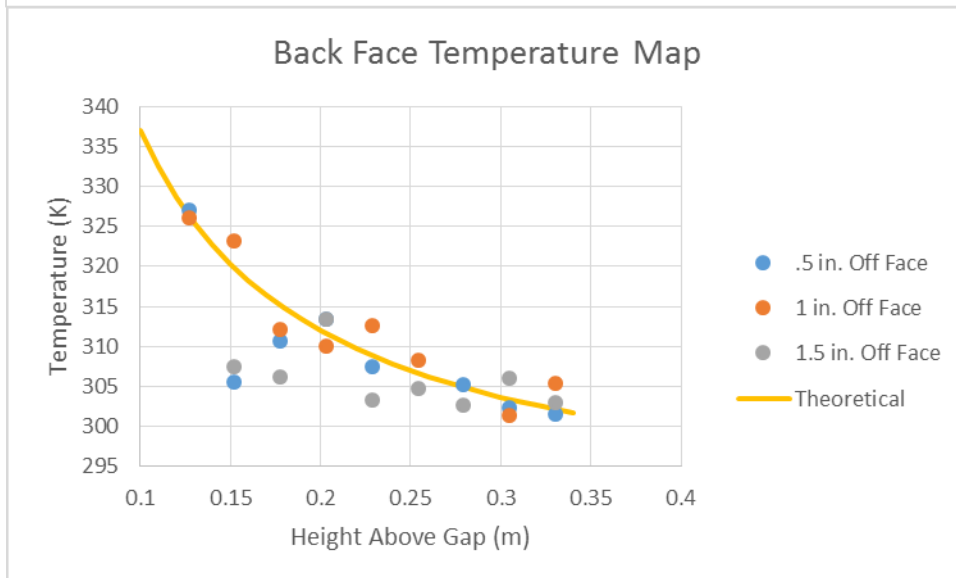
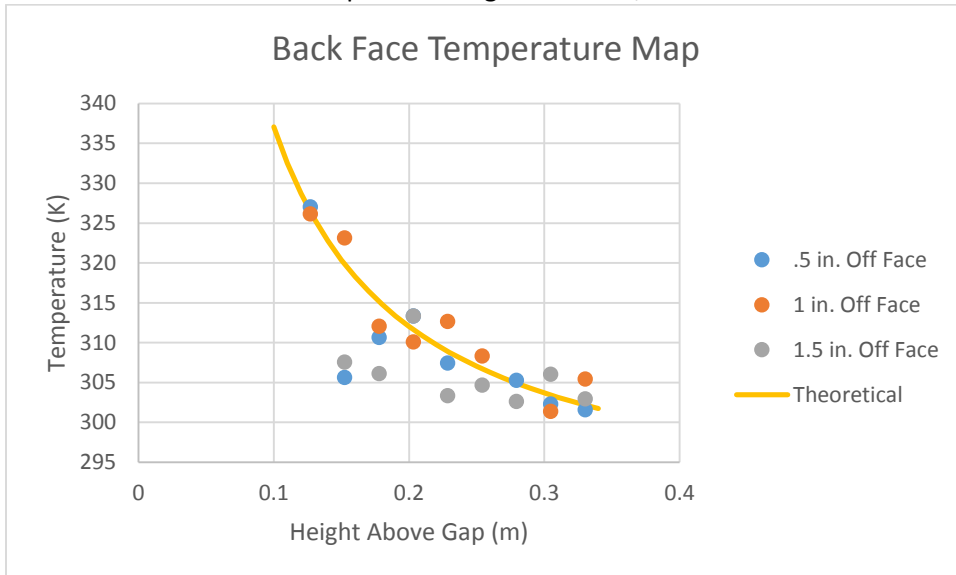
150 kW Test 2

Calculated heat release rate per unit length: .696 kW/m



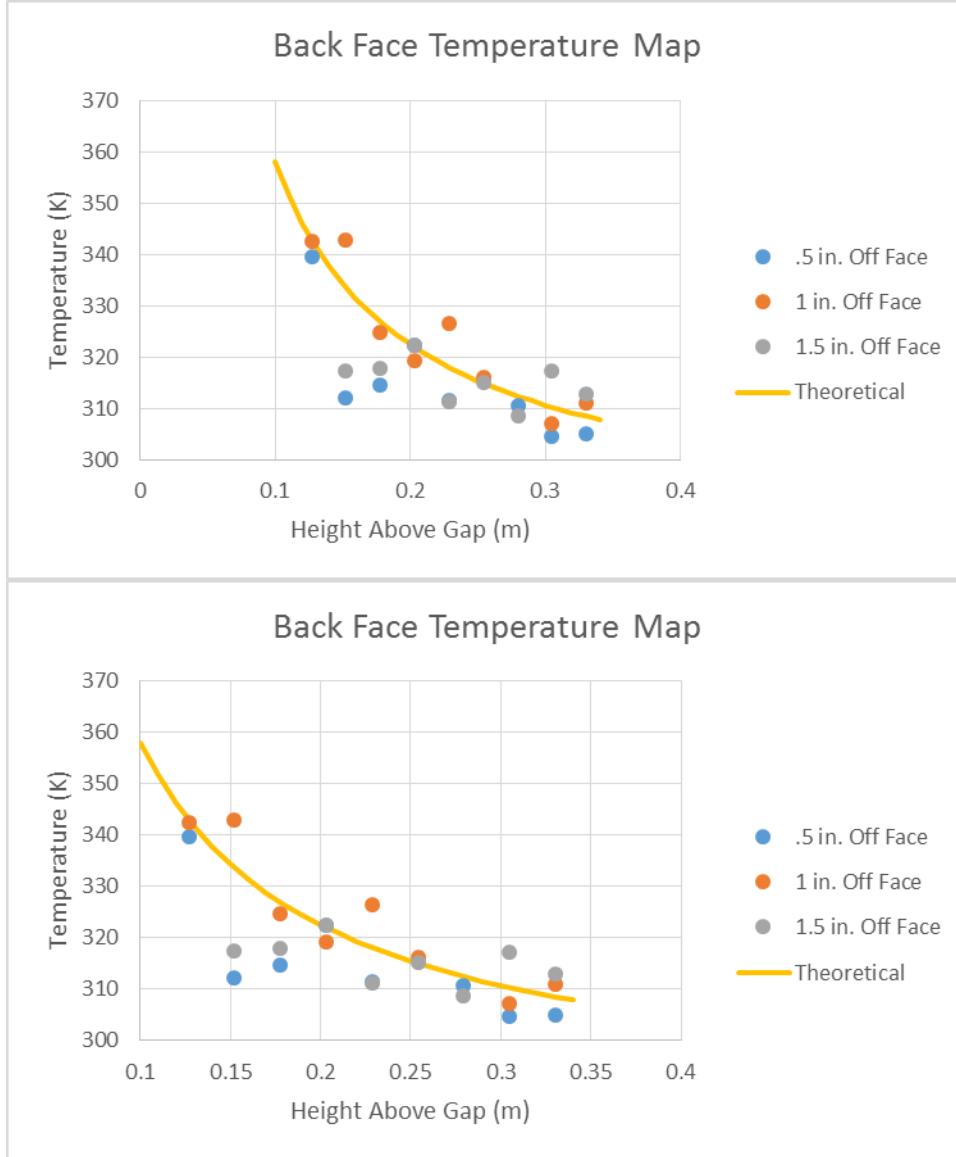
150 kW Test 3

Calculated heat release rate per unit length: .580 kW/m



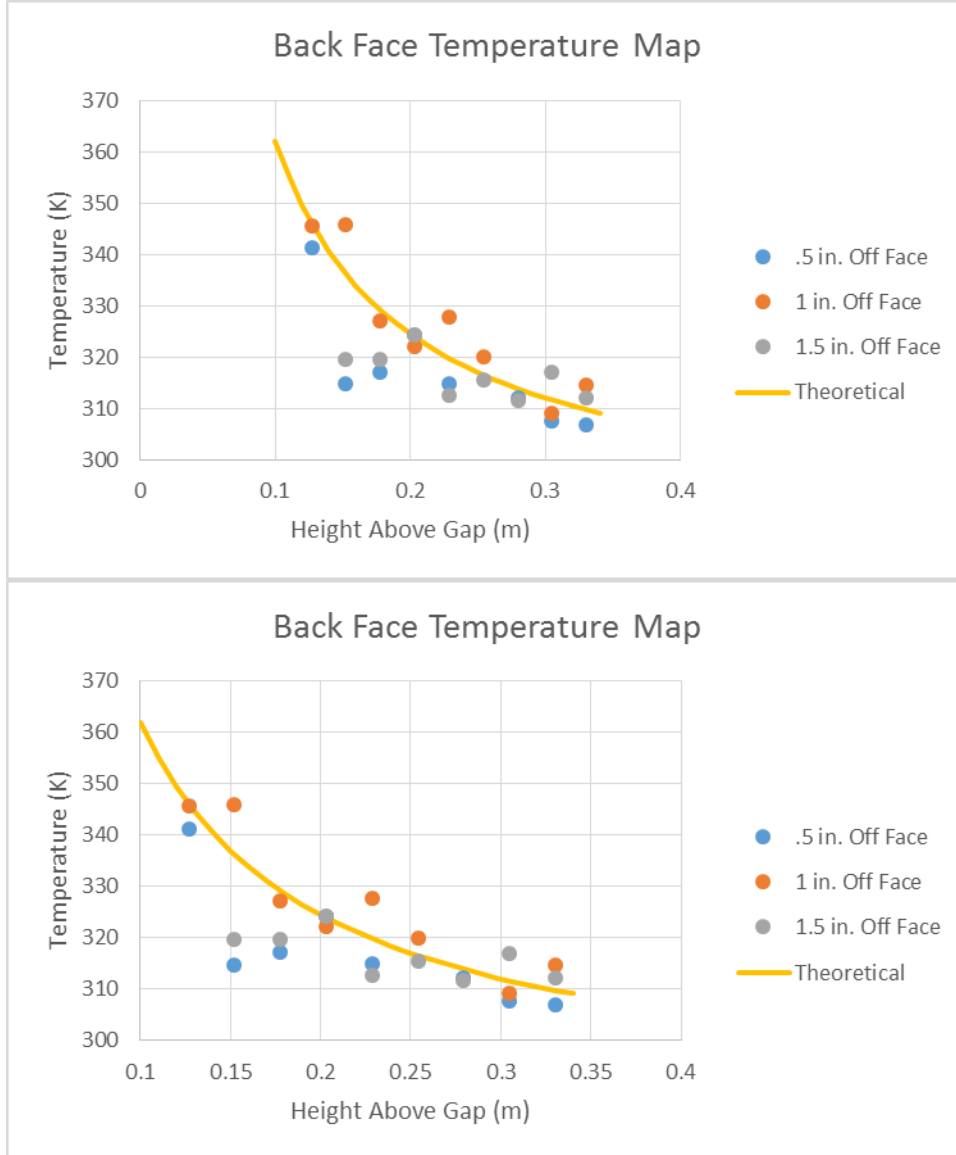
200 kW Test 1

Calculated heat release rate per unit length: .978 kW/m



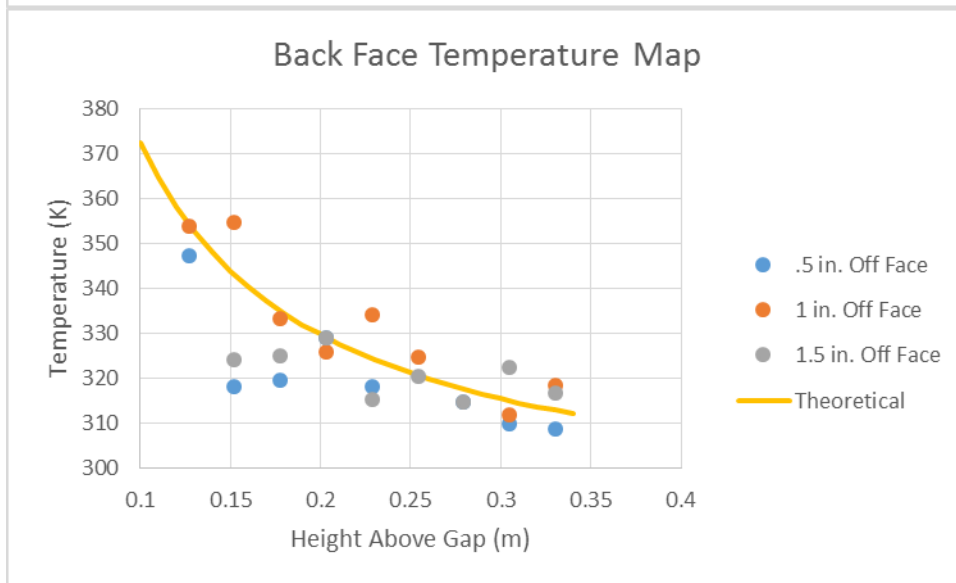
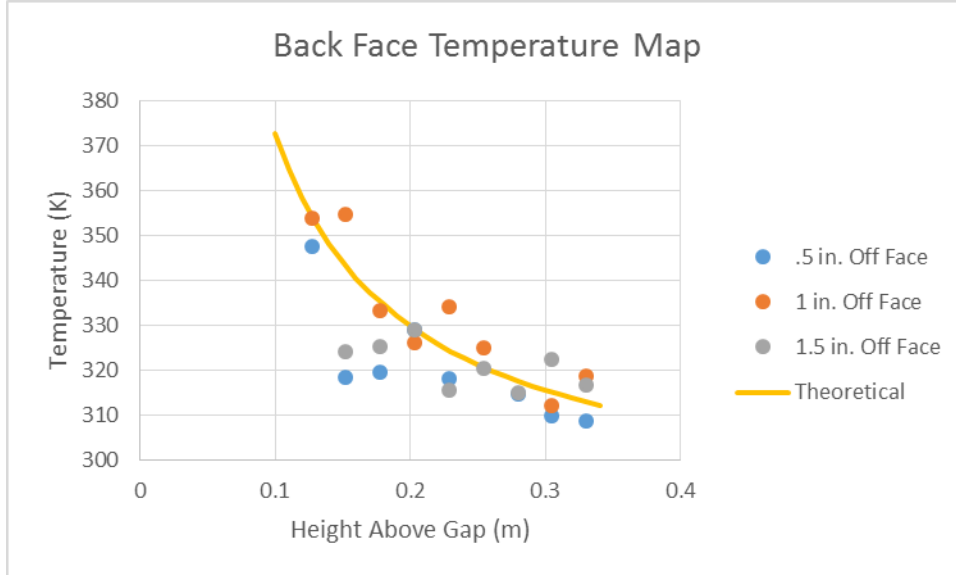
200 kW Test 2

Calculated heat release rate per unit length: 1.06 kW/m



200 kW Test 3

Calculated heat release rate per unit length: .129 kW/m



Appendix L: TEMPERATURE DISTRIBUTIONS – 75KW (X)

Author: Sarah Meehan

Table 1 shows the x-position, the assigned thermocouple number, the channel number, and the average temperature for each thermocouple used for the x-direction temperature distributions.

Table 5: 75kW x-positions, thermocouple numbers, channel numbers, and average temperatures

X-Position (m)	Thermocouple #	Channel #	Average Temperature K
0.33655	103	TC Mod2_ai2	402.0734618
0.1651	100	TC Mod2_ai3	398.823106
0.33655	102	TC Mod2_ai5	432.2099792
0.508	105	TC Mod2_ai6	431.316261
0.508	106	TC Mod2_ai7	335.3775555
0.1651	101	TC Mod5_ai2	386.8472558
0.33655	104	TC Mod5_ai8	287.6065939

For Figure 1 all of thermocouples on the bottom gap are taken into consideration, however in Figure 2 thermocouples number 106 and 104 were taken out due to the fact that they were outliers, thermocouple 104 is determined to be broken as the temperature did not change throughout the experiments.

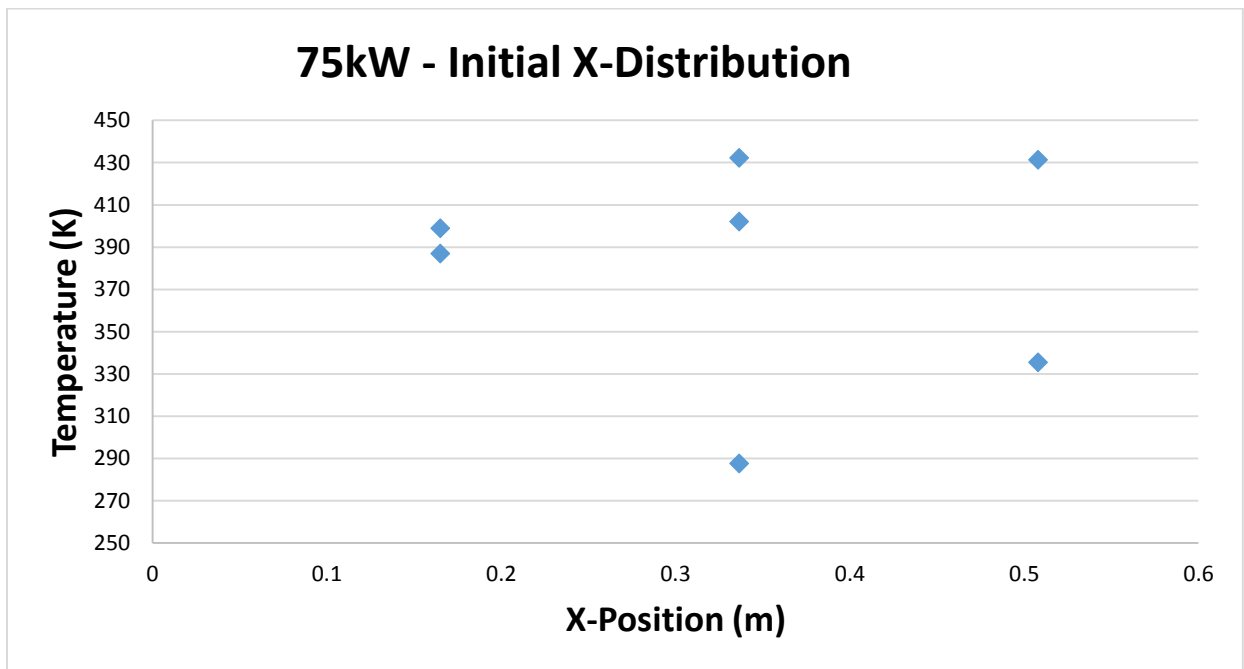


Figure 29: 75kW Initial X-Distribution

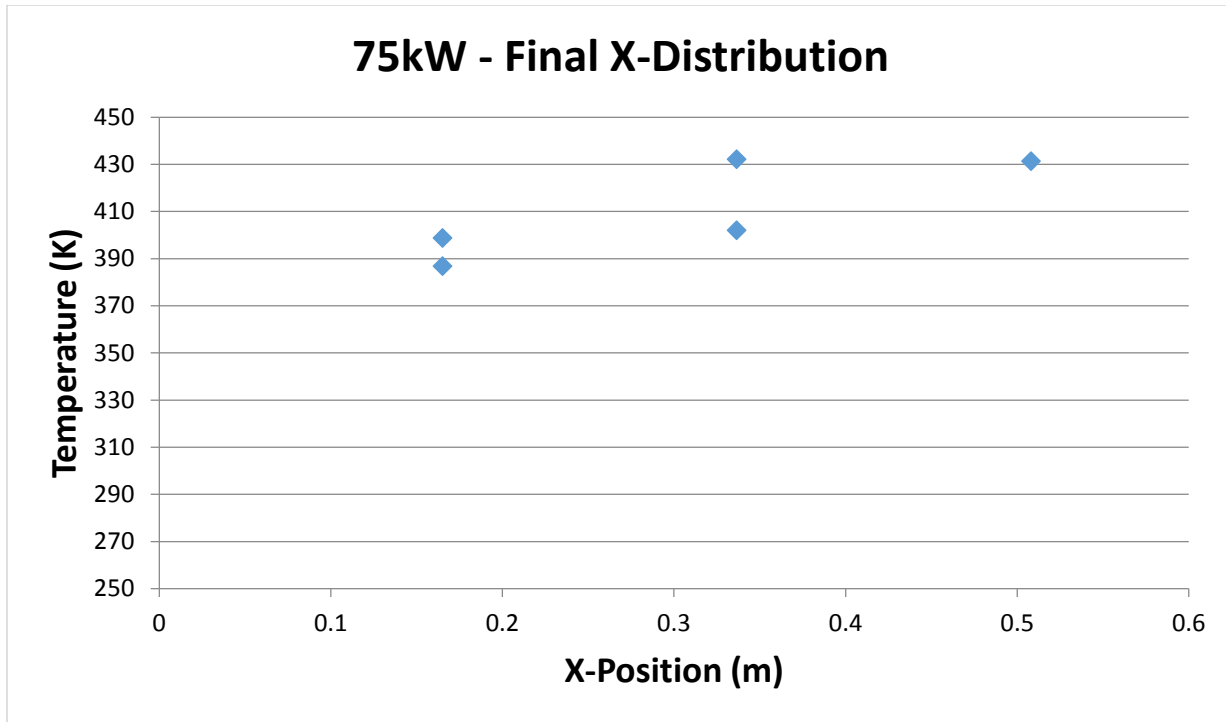


Figure 30: 75kW Final X-Distribution

TEMPERATURE DISTRIBUTIONS – 150KW (X)

Table 2 shows the x-position, the assigned thermocouple number, the channel number, and the average temperature for each thermocouple used for the x-direction temperature distributions.

Table 6: 150kW x-positions, thermocouple numbers, channel numbers, and average temperatures

X-Position (m)	Thermocouple #	Channel #	Average Temperature K
0.33655	103	TC Mod2_ai2	398.0204884
0.1651	100	TC Mod2_ai3	405.0132204
0.33655	102	TC Mod2_ai5	440.2129881
0.508	105	TC Mod2_ai6	437.7338598
0.508	106	TC Mod2_ai7	327.470871
0.1651	101	TC Mod5_ai2	391.413437
0.33655	104	TC Mod5_ai8	326.6450752

For Figure 3 all of thermocouples on the bottom gap are taken into consideration, however in Figure 4 thermocouples number 106 and 104 were taken out due to the fact that they were outliers, thermocouple 104 is determined to be broken as the temperature did not change much throughout the experiments.

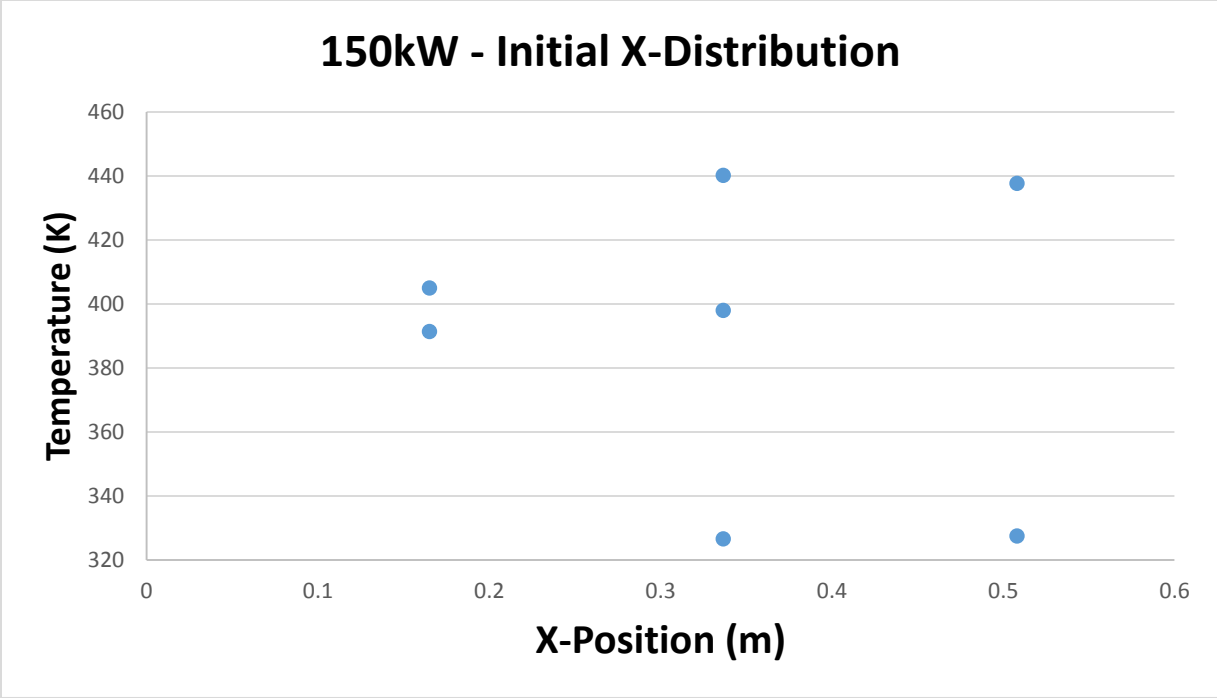


Figure 31: 150kW Initial X-Distribution

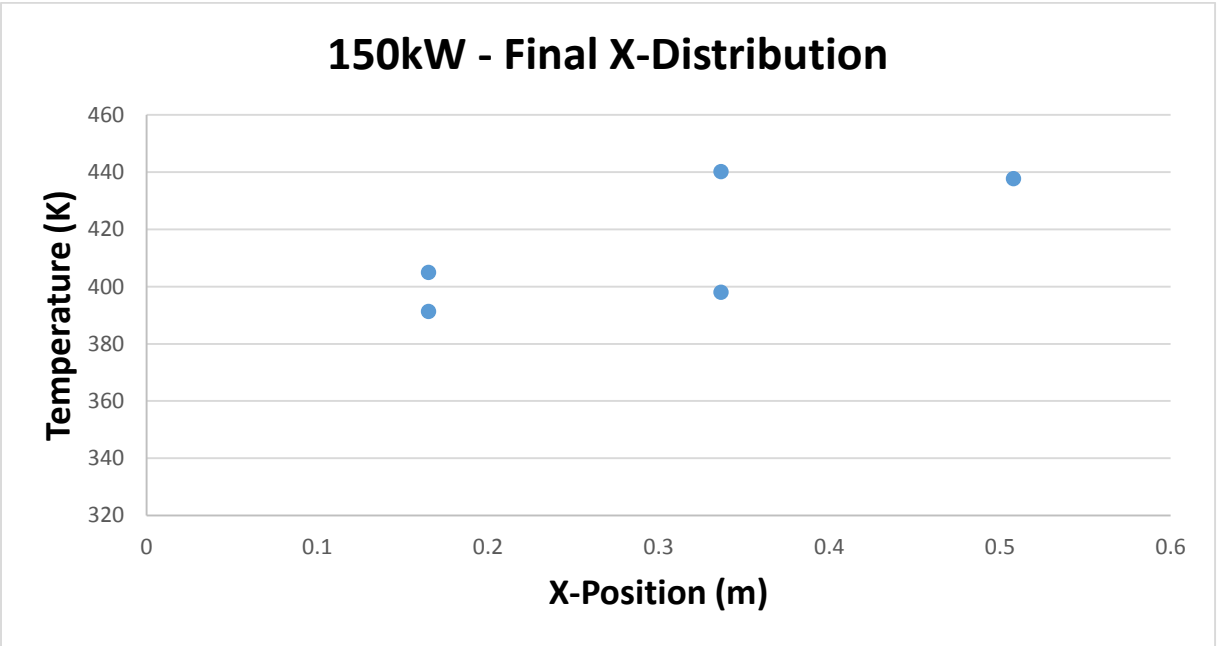


Figure 32: 150kW Final X-Distribution

TEMPERATURE DISTRIBUTIONS – 200kW (X)

Table 3 shows the x-position, the assigned thermocouple number, the channel number, and the average temperature for each thermocouple used for the x-direction temperature distributions.

Table 7: 200kW x-positions, thermocouple numbers, channel numbers, and average temperatures

X-Position (m)	Thermocouple #	Channel #	Average Temperature K
0.33655	103	TC Mod2_ai2	456.6535772
0.1651	100	TC Mod2_ai3	443.7376289
0.33655	102	TC Mod2_ai5	495.5455516
0.508	105	TC Mod2_ai6	491.9954426
0.508	106	TC Mod2_ai7	363.4455258
0.1651	101	TC Mod5_ai2	424.2909715
0.33655	104	TC Mod5_ai8	287.9701061

For Figure 5 all of thermocouples on the bottom gap are taken into consideration, however in Figure 6 thermocouples number 106 and 104 were taken out due to the fact that they were outliers, thermocouple 104 is determined to be broken as the temperature did not change much throughout the experiments.

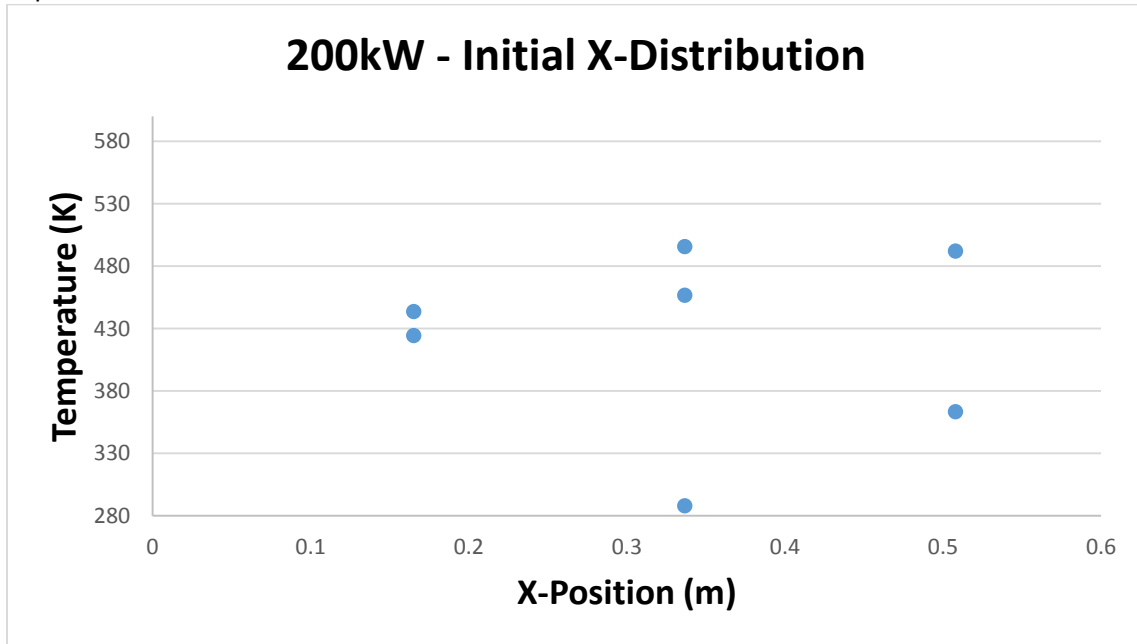


Figure 33: 200kW Initial X-Distribution

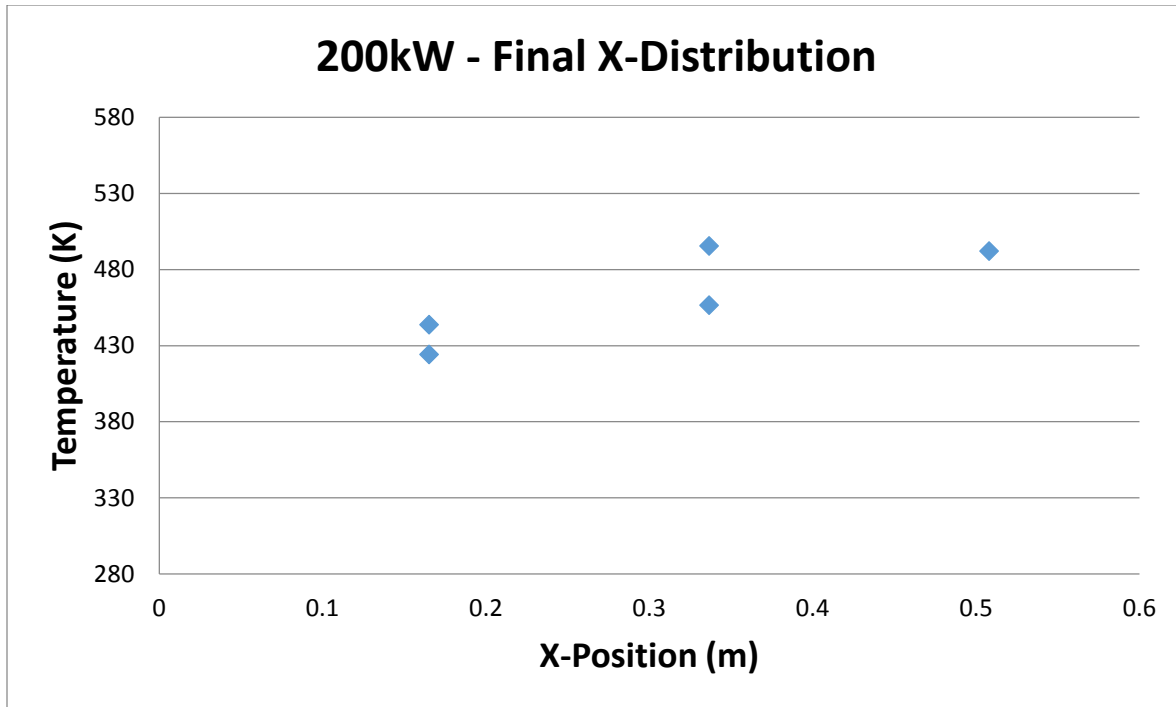


Figure 34: 200kW Final X-Distribution

TEMPERATURE DISTRIBUTIONS – 75KW (Y)

Table 4 shows the x-position, the assigned thermocouple number, the channel number, and the average temperature for each thermocouple used for the x-direction temperature distributions. Figure 7 shows the final distribution of temperature in the y-direction.

Table 8: 75kW y-positions, thermocouple numbers, channel numbers, and average temperatures

Y-Position (m)	Thermocouple #	Channel #	Average Temperature K
0.03175	52	TC Mod6ai8	413.1784
0.0381	51	TC Mod6ai9	407.5635
0.04445	50	TC Mod6ai10	386.3482
0.01905	54	TC Mod6ai11	422.0829
0.0254	53	TC Mod6ai12	417.1786
0.00635	48	TC Mod6ai13	388.6681
0.0127	49	TC Mod6ai14	386.9115

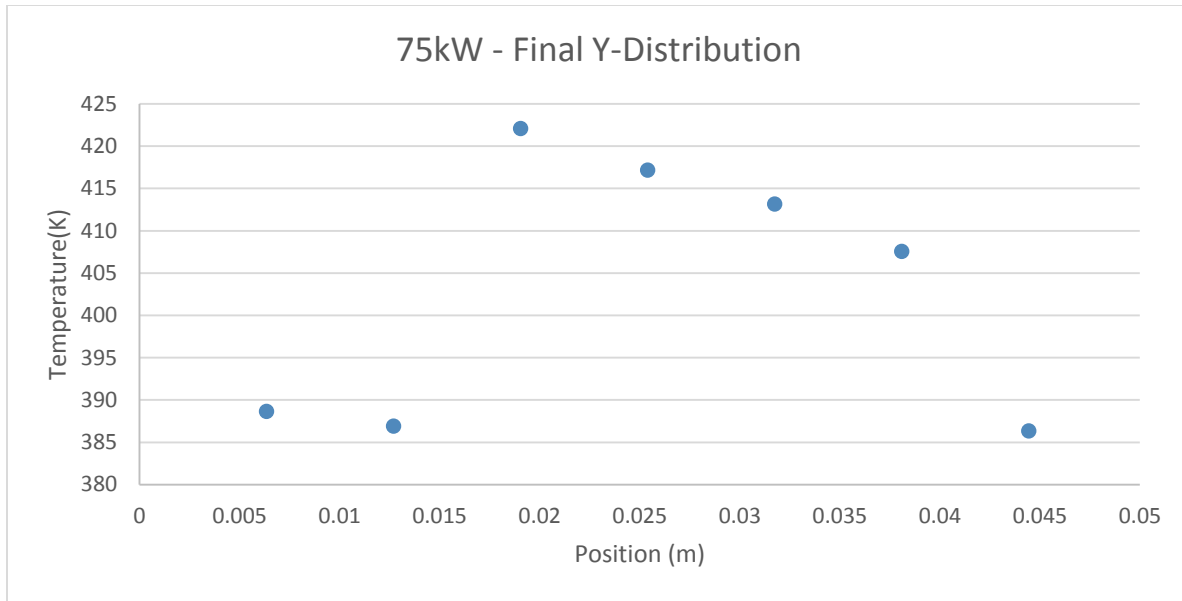


Figure 35: Final Y-Distribution for 75kW

TEMPERATURE DISTRIBUTIONS – 150KW (Y)

Table 5 shows the x-position, the assigned thermocouple number, the channel number, and the average temperature for each thermocouple used for the x-direction temperature distributions. Figure 8 shows the final distribution of temperature in the y-direction.

Table 9: 150kW y-positions, thermocouple numbers, channel numbers, and average temperatures

Y-Position (m)	Thermocouple #	Channel #	Average Temperature K
0.03175	52	TC Mod6ai8	430.413
0.0381	51	TC Mod6ai9	424.0945
0.04445	50	TC Mod6ai10	397.7527
0.01905	54	TC Mod6ai11	441.3156
0.0254	53	TC Mod6ai12	435.6184
0.00635	48	TC Mod6ai13	397.1129
0.0127	49	TC Mod6ai14	395.5658

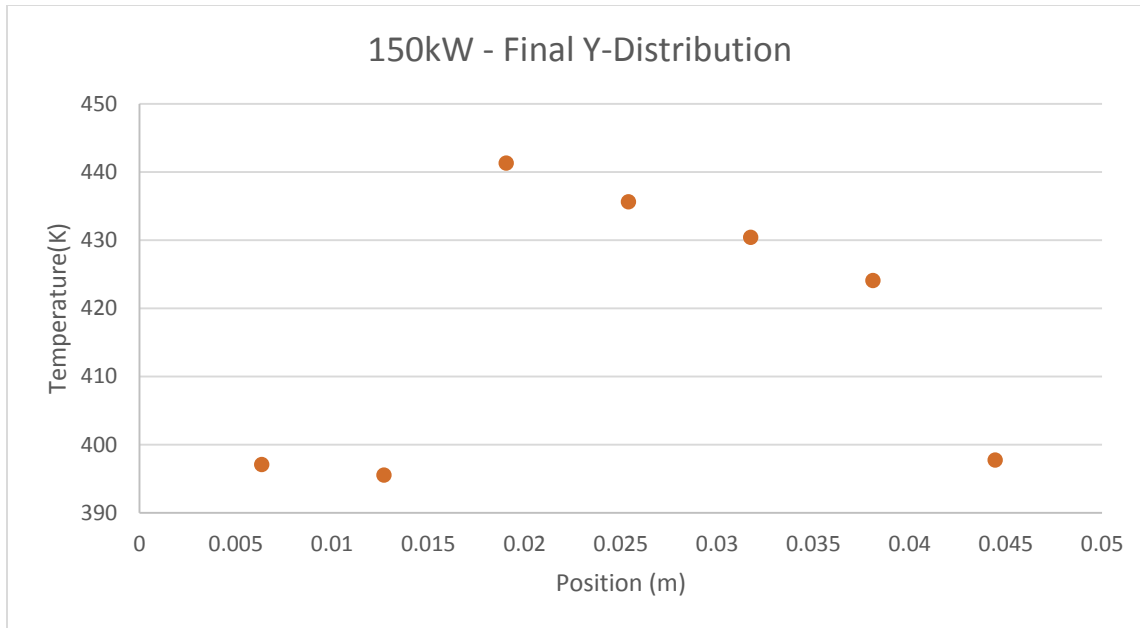


Figure 36: Final Y-Distribution for 150kW

TEMPERATURE DISTRIBUTIONS – 200KW (Y)

Table 6 shows the x-position, the assigned thermocouple number, the channel number, and the average temperature for each thermocouple used for the x-direction temperature distributions. Figure 9 shows the final distribution of temperature in the y-direction.

Table 10: 200kW y-positions, thermocouple numbers, channel numbers, and average temperatures

Y-Position (m)	Thermocouple #	Channel #	Average Temperature K
0.03175	52	TC Mod6ai8	462.5797
0.0381	51	TC Mod6ai9	455.8506
0.04445	50	TC Mod6ai10	424.9183
0.01905	54	TC Mod6ai11	475.901
0.0254	53	TC Mod6ai12	468.2672
0.00635	48	TC Mod6ai13	436.7292
0.0127	49	TC Mod6ai14	432.5687

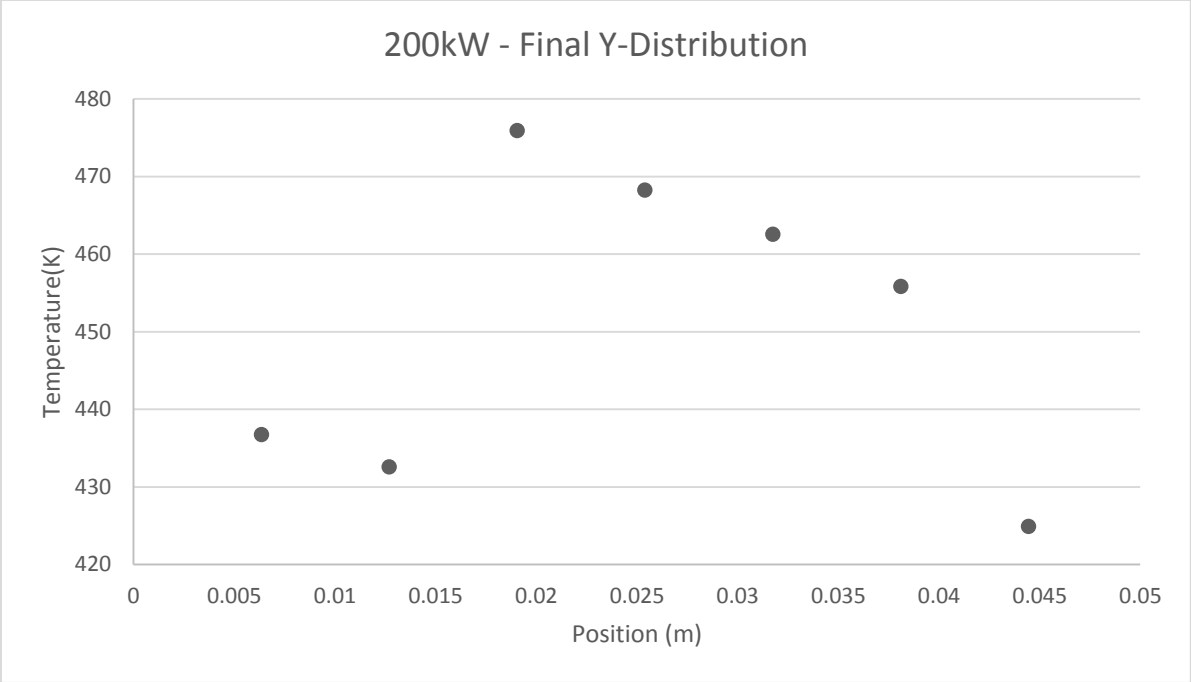


Figure 37: Final Y-Distribution for 200kW

Appendix M: Enthalpy Calculations

Author: Sarah Meehan

To determine enthalpy flow in the gap the total enthalpy can be calculated with the equation below.

$$\text{total enthalpy} = \int_{T_{\text{ambient}}}^{T_{\text{average}}} c_p dT \int_0^A \rho v dA \quad [1]$$

Where c_p is the specific heat capacity (kJ/kgK) and ρ is the density (kg/m³), both values were taken at average temperatures for each fire size. dT represents the difference between the average temperatures and ambient. Area is the cross sectional area of the gap (width x height). The velocity component of this calculation, v , was determined through velocity readings and correction factors shown below:

$$v = v_{\text{max}} * c_y * c_x$$

$$c_y = v_{x\text{avg}} / v_{\text{max}}$$

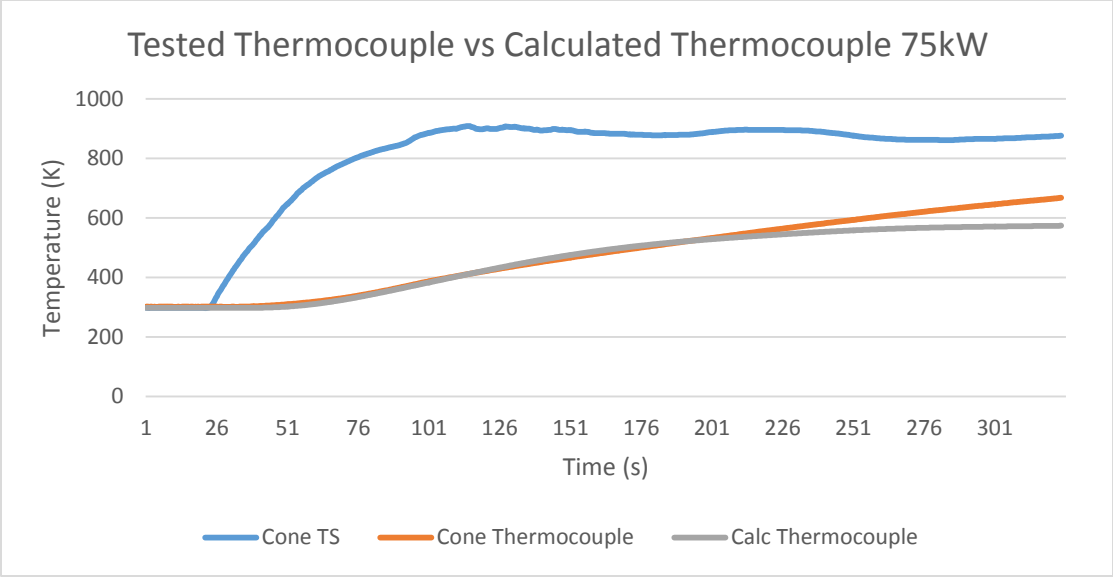
$$c_x = v_{y\text{avg}} / v_{\text{max}}$$

Based on velocity and temperature profiles the x-direction velocity is determined to be constant, which in turn makes the correction factor for that component equal to zero.

Vmax (m/s)	Vavg (m/s)	Cy	Cx	Velocity (m/s)	Cp average (kJ/kgK)	ρ average (kg/m ³)	dT (K)	Area (m ²)	total enthalpy (kJ/s)
0.27	0.18	1	0.7	0.18	1.01	0.876	118	0.03	0.583598
0.25	0.17	1	0.7	0.17	1.01	0.854	132	0.03	0.602311
0.18	0.12	1	0.7	0.12	1.02	0.779	166	0.03	0.490586

Next, based on the temperature loss in the gap a loss in enthalpy was calculated by applying the percentage temperature loss in the gap. Q_{loss} , calculated with the thin-skin calorimeter data, was determined for each fire size based on steady-state conditions in the gap. This Q_{loss} term can be compared to our change in enthalpy flow. In the table below it is confirmed that we have similar values for Q_{loss} and change in enthalpy.

Fire Size	% Temperature Change In Gap	Total Enthalpy Through Gap	Q_{loss}	Change In Enthalpy Flow
75kW	7.7%	0.6 kW	0.2 kW	0.1 kW
150kW	11.1%	0.6 kW	0.2 kW	0.1 kW
200kW	14.4%	0.5 kW	0.3 kW	0.1 kW



[1] Martin, M. (1986). Elements Of Thermodynamics. Prentice-Hall, Eaglewood Cliffs, NJ. 66-68

Appendix N: Verification of Bidirectional Probe

Author: Camille Levy

Verification of the bidirectional probe (BDP) and differential pressure transducer setup was necessary to ensure the validity of the velocity data. A hot wire anemometer (HWA) was used to measure the known velocities due to its fine spatial resolution [1]. The bidirectional probe and HWA were set in the same air flows and the recorded data was compared to confirm validity.

Experimental Set-up

The bidirectional probe was used with the Omega PX277-0.1D5V differential pressure transducer [2]. The output setting for the transducer was set to 0-5 Volts. The known velocity source was measured with an Omega HHF2005HW hot wire anemometer, shown in figure 1 [3]. This instrument outputs velocity so no extra calculations were necessary. The HWA measurement range is 0.2-20 m/s with a resolution of 0.1 m/s [3]. An electric desktop fan was used as the velocity source. The velocities were calculated from probe/pressure transducer setup as explained in Appendix O.



Figure 38: Hot Wire Anemometer

The probe and anemometer were secured together to allow velocity measurements to

be taken simultaneously. This can be seen in figure 2. The test setup was initially bench top in the main Fire Lab; however this caused some variation in the velocity measurements. The setup was then moved into a still air room within the lab in order to eliminate external sources of error. These included people walking by the experiment and other uncontrollable sources of air flow in the main lab. The final version of the setup was in the still air room. Five tests were run for this verification.

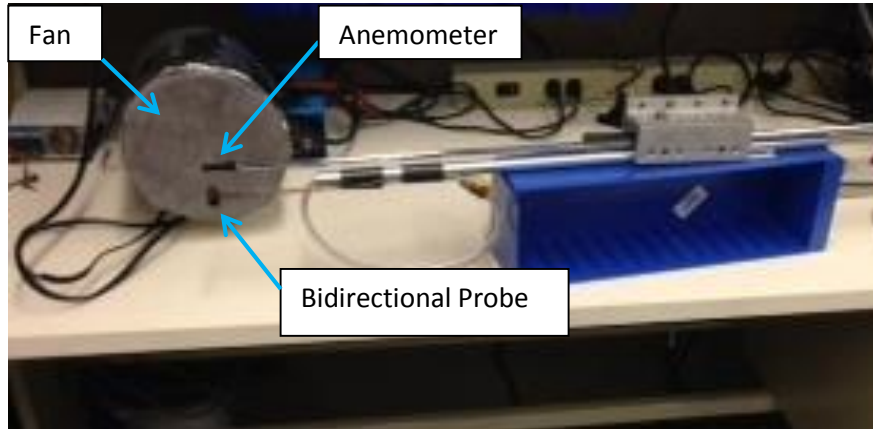


Figure 2: Bidirectional Probe & Anemometer Setup

Results & Analysis

The air velocities used for verification ranged from 0.15-1.4 m/s. Table 1 presents the data from the five tests. Figure 3 provides a graph of this data with a comparison to the $y=x$ line.

Table 11: Velocity Data

Velocity [m/s]		
Anemometer	BDP	Uncertainty
0.15	0.2308407	0.080840681
0.35	0.3162874	0.033712571
0.5	0.6261115	0.126111486
0.75	0.7399764	0.010023581
1.4	1.3600466	0.039953418

The bidirectional probe measurements were very close to the anemometer velocities, with the highest uncertainty being 0.126 m/s. The probe data was determined to be quite

accurate based on the fact that the HWA spatial resolution is 0.1 m/s and the highest uncertainty is close to this resolution.

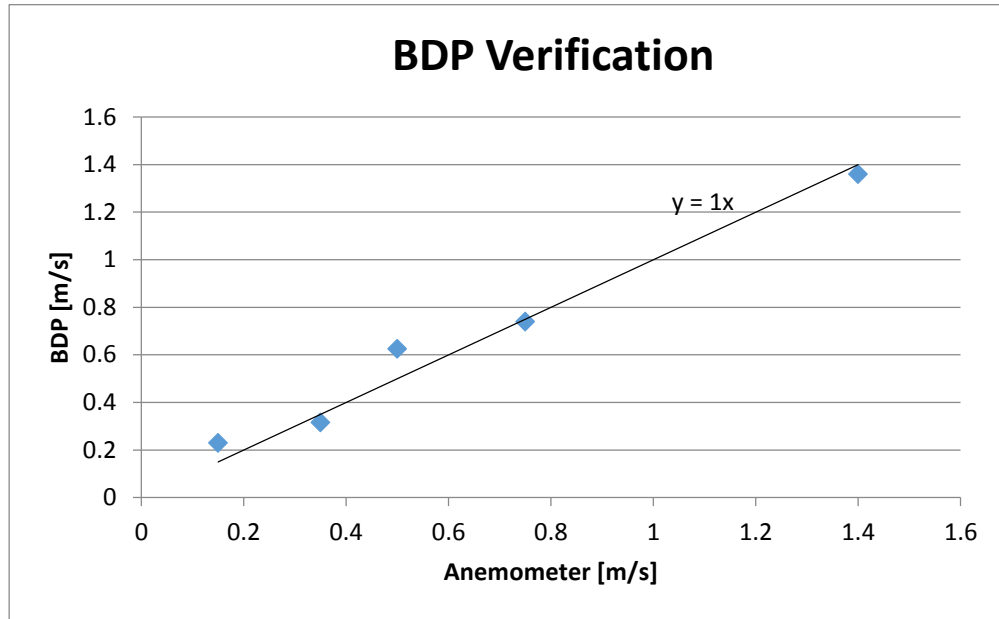


Figure 3: Velocity Data Verification

Figure 3 exemplifies the fact that the BDP measurements were extremely close to the HWA quantities. The $y=x$ line is used as a comparison tool because it represents 0% uncertainty for the measurements. If the probe and anemometer velocities were perfectly equal, then the points would coincide with the line. The data points are all relatively close to the comparative line, reinforcing that the BDP setup is working properly.

References

- [1] "Hot-Wire Anemometers: Introduction." (2006) eFunda.
- [2] "Differential Pressure Transmitter with Field Selectable Ranges." *Differential Pressure Transmitter with Field Selectable Ranges*. Omega Engineering Inc., n.d. Web. 26 Mar. 2014.
- [3] "Hot Wire Anemometer with Real-Time Data Logger." *Hot Wire Anemometer with Real-Time Data Logger*. Omega Engineering Inc., n.d. Web. 26 Mar. 2014

Appendix O: Calculation Procedure to obtain Velocities

Author: Camille Levy

1. Obtain ambient density (ρ , in kg/m^3) based on room temperature
2. Calculate Calibration Factor based on Differential Pressure Transducer settings:
 - Maximum Pressure: $\pm 12.5\text{Pa} = 25\text{Pa}$
 - Voltage Output Range: 0-5 V

$$CF = \frac{P}{V} = \frac{25\text{Pa}}{5\text{V}} = 5 \frac{\text{Pa}}{\text{V}}$$

3. Convert Voltage to Pressure by multiplying by the Calibration Factor:

$$P = V * C.F.$$

4. Calculate Pressure differential:

$$\Delta P = |P_1 - P_2|$$

5. Calculate Velocity:

$$Velocity \left[\frac{m}{s} \right] = \frac{1}{K} \sqrt{\frac{2\Delta P}{\rho}}$$

where $K=1.08$ [1]

References

[1] McCaffrey, B. J., G. Heskestad. (1976). "A robust bidirectional low-velocity probe for flame and fire application." *Combustion and Flame* 26: 125-127.